Structure and Critical Behavior

of

Polymer Gels

by

Yong Li

B.S., Peking University (1982)
M.S., College of William and Mary (1985)

Submitted to the Department of Physics on June, 1989,
in partial fulfillment of the requirements for the degree of

Doctor of Philosophy

at the

MASSACHUSETTS INSTITUTE OF TECHNOLOGY
JUNE 1989

Signature of Author _____

Department of Physics
June, 1989

Certified By _____

Toyoichi Tanaka
Thesis Supervisor

Accepted By _____

George F. Koster
Chairman, Departmental Committee

Structure and Critical Behavior of Polymer Gels

by

Yong Li

Submitted to the Department of Physics on June, 1989,

in partial fulfillment of the requirements for the degree of

Doctor of Philosophy in Phy.

ABSTRACT

Polymer gels undergo volume phase transition: they can discontinuously change their volume as much as 1000 times in response to infinitesimal environmental changes. Light scattering experiments have revealed the divergence of the network density fluctuation near the critical point. The purpose of this thesis is to experimentally determine the universality class to which the gel phase transition belongs.

For this purpose, we have studied the criticality of the N- isopropylacrylame gels by approaching the critical point along the isobar path. The techniques we have used include calorimetry, static and dynamic laser light scattering, and direct measurement of the volume of the gels. We obtained the critical exponents along the isobar path, α_π, ν_π, γ_π and δ. From these exponents, the conventionally defined exponents are calculated. The experimental results indicate that the gel system is an Ising-like system. This result can be understood by using the analogy between the gel phases and the liquid-gas phases.

We also studied the structure and the mechanical properties of the network system. The importance of the inhomogeneities of the network system was further revealed.

The work presented in this thesis will help us both in the theoretical understanding and practical application of the gel system.

Thesis Supervisor: Dr. Toyoichi Tanaka

Professor of Physics

Dedicated to My Parents

Li, Li-han Wang, Yu-zheng

ACKNOWLEDGEMENT

At the end of the four and one half years effort to complete the work of this dissertation, I want to recognize the people who helped me along the way. I benefited a great deal from the discussions with Dr. Sridhar Gorti, Dr. Yasuo Suzuki and Mr. Terrence Hwa and other colleagues and fellow students. Their generosity and friendship is greatly appreciated.

My friends Gerry Swislow, Alec Sandy, Mark Spector, Zibin Hu and many others have helped me in many ways. Their humor, encouragement and friendship will never be forgotten.

I wish to thank my Professor Toyoichi Tanaka for his enthusiastic guidance, encouragement and warm friendship during the course of this research. I thank him for his consistent support and many valuable insights into scientific problems occurred in my projects. Working with him has been a privilege and a pleasure. I am also grateful to him for the financial support in the form of research assistantship.

Last and most of all, I am very grateful to my parents, Li, Li-han and Wang, Yu-zheng for their unconditional support and encouragement. They gave me energy to continue when things were bad and added enjoyment when things were well. I wholeheartedly express my thanks my thanks to them. My wife, Jui-Lian Li, has contributed to this thesis from the beginning to the end in a very special way. The love she offered me in the past several years is more than words can express.

Contents

Chapter 1

Overview

1.1 Phase Transition and Critical Phenomena

1.1.1 Phenomenon

A thermodynamic system contains many particles. The behavior of the system is governed by the interaction among these particles and the entropy of the system. The entropy favors the disorder (well mixing). If the interaction is repulsive, then the system will stay well mixed and there will be no phase transition. But when the interaction is attractive, i.e, favoring ordered state, then the competition between the interaction energy and the entropy will determine the state of the system. Under proper conditions, the phase separation or phase transition can occur.

There are many systems exhibit phase transition and phase separation phenomena, like liquid-gas transition, binary liquid phase separation, spontaneous magnetization, etc. Figure 1.1 is a schematic description of the phase diagram of the ferromagnet system.

The phases before and after the transition is identified by a characteristic parameter m, called order parameter. The change of the order parameter during a phase

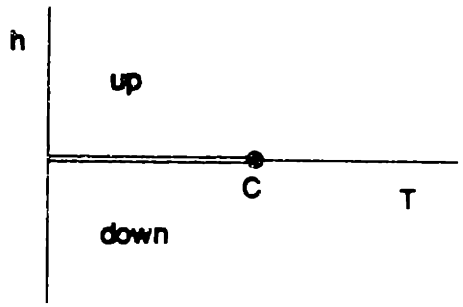

Figure 1.1: Schematic sketch of the phase diagram of the ferromagnet system.

transition can be either discontinuous or continuous. The discontinuous transition is called first order transition. The point that separates the continuous transition and the discontinuous transition is called critical point.

In general, the high temperature state is called disordered state, and the low temperature state ordered state. The order parameter m is related with the symmetry of the system. In the disordered state, the system has more symmetry than the ordered state, so the phase transition process is also called a symmetry broken process. The order parameter has the property of being single valued in the disordered state (often 0) and multivalued in the disordered state. For the ferromagnet case, the symmetry is the spin up-down. In the absence of the external field, when the temperature is very high, the macroscopic state (m = 0) of the system is the same if we flip all the up-spins down and down-spins up (up-down symmetry). But when the temperature is lower than the critical temperature (Curie temperature), there is a total non-zero spontaneous magnetization m *neq* 0. If we flip all the spins once, then the total magnetization will be -m, so the up-down symmetry has been broken. The order parameter m is zero above the critical temperature and double valued below the critical temperature. In the case of liquid-gas system, the order parameter is the den-

sity measured from the critical point, $\rho - \rho_c$. The symmetry is occupied-unoccupied symmetry.

The essence of the second order phase transition is that the competition between the interaction energy and the entropy is very close. Around the critical point, due to the nearly complete cancellation of these effects, the local property of the system can fluctuate around the mean value dramatically. It is exactly this fluctuation causes many macroscopic quantities to have singular behavior. Near the critical point, many response functions, like the heat capacity C_v, susceptibility χ, diverge by certain power. These powers are called critical exponents. It is very important to realize that although the choice of the order parameter is often obvious, there is no precise definition and standard ways of identifying it (Anderson 1981).

For a clear chronicle review of the classical phase transition study, see G. E. Uhlenbeck (1966)

1.1.2 Mean Field Theory

The earliest successful phase transition theory is the non-ideal gas (liquid-gas) theory by Van der Waals in 1873. Later Weiss developed the Weiss ferromagnet theory and explained the existence of the Curie temperature in 1907 (Stanley 1971). The binary alloy phase transition was explain by a theory developed by Bragg and Williams. All of these theories, including Landau's second order phase transition theory (L. D. Landau and E. M. Lifschitz 1959), are mean field theories. The basic assumption of the mean field theories is that each particle is affected by an average interaction provided by all the other particles. The interaction (average field) is in turn related with the average behavior of the particles. This is why the mean field theories are also called self-consistent theories. The mean field theory gives us a direct insight of the physics of the problem. Although the mean field theory can be solved exactly

around the critical point, because of its basic assumption, it does not describe the critical phenomena, in particular, the critical exponents well. Some of the exponents derived from the mean field theory are listed bellow.

$$C_v = |-t|^{\alpha}. \tag{1.1}$$

$$\delta\rho = (-t)^{\beta}. \tag{1.2}$$

$$\delta P = |\delta\rho|^{\delta}. \tag{1.3}$$

with $t = (T - T_c)/T_c$ and

$$\begin{cases} \alpha = 0. \\ \beta = \frac{1}{2}. \\ \delta = 3. \end{cases} \tag{1.4}$$

When the system is very far from the critical point, the mean field theory gives very satisfactory results. But since the mean field theory neglects the fluctuations of the density parameters in the system, which is absolutely essential for the critical behavior of the system, we do not expect it to give good result near the critical point. The criterion beyond which the mean field theories do not work is given by Ginzburg (1960). The idea is that in order for the mean field theory to work, the fluctuation of the density (order parameter) should be much smaller than the average value of it. In another word, the mean field theory fails when

$$\frac{<(\Delta m)^2>}{m^2} \gg 1 \tag{1.5}$$

1.1.3 Renormalization Group Theory

As more and more experiments were done on the critical phenomena, the discrepancy between the theoretical predictions of the mean-field theories and the experimental

results became more and more apparent (Heller and Benedek 1962). Many experimental results showed that the value of β is around 0.33, rather than 0.5, and the exponents α is a non-zero in many cases. These discrepancies led the very important discovery of the renormalization group theory (RG), which was first initiated by Kandanoff (1967) and further developed by Wilson (1971). The basic idea of the renormaliztion group theory is that when the critical point is approached, the correlation length of the system become very large. Since most of the thermodynamic variables are directly related with the correlation length, we can assume that the details of the system (molecular distance) is irrelevant. Based on this, we can group nearby particles together as an effective particle. The interaction among these new particles is related with the original (bare) interaction among particles. Then we can group these effective particles into even larger ones, etc. At the critical point, the correlation length is infinite, so each time after we have performed an grouping operation, the new system should behave the same as the old one. This means that the critical point is a fixed point of the renormalization group operation. It has been shown both theoretically and experimentally that the renormalization group theory is a very successful theory of critical phenomena.

Form the renormalization group theory, we understand that the important parameters that govern the critical behavior of a thermodynamic system are very few, among them, the dimensionality of the space d, the number of the components of the order parameter n and the symmetry of the system. The fine details, like the whether it is nearest neighbour or longer ranged interaction, is irrelevant. Although in the reality, arguably, the dimension of the space and the number of the components of the order parameter are always integers, it's been proven many times that it is beneficial when we treat them as continuous variables.

The existence of the universality class of the critical phenomena was one of the most important results of the renormalization group theory. The commonly encoun-

tered universality classes are d=3, n=1 (Ising), n=2 (X-Y) and n=3 (Heisenberg) classes. Most of the classical systems mentioned above (liquid-gas, binary mixture, ferromagnet, etc) are in 3-d Ising universality class. The exponents of the 3-d Ising universality class calculated by the RG theory is,

$$\begin{cases} \alpha &= 0.11, \\ \beta &= 0.35, \\ \delta &= 5. \end{cases} \tag{1.6}$$

1.2 Gels

The study of gel network system can be traced back to the rubber elasticity experiment done by Gouth in 1805 (Flory 1953). This experiment demonstrated the fact that the length of a stretched rubber string become shorter when the temperature is increased. This is exactly the opposite of the most of other materials. In 1920, Staudinger (1920) correctly pointed out that the polymers are flexible chains of covalently connected molecules. Based on Staudinger's finding, the elasticity of polymers and network systems were explained successfully. To emphasize the important mechanical property of the network system, a terminology *elastomer* was introduced to replace the term *rubberlike material.*

In 1941, James and Guth began developed the *Phantom Network Theory* to theoretically calculate the rubber elasticity (James and Guth 1943, 1947 and 1949 and James 1947). In this theory, the crosslinks fluctuate over time without being hindered by the neighbouring chains except for only a few network points on the surface are fixed to define the shape and the volume of the elastomer. The term *phantom* derives from the assumed ability of the crosslinks to move around regardless of the topological constraints by the network. Frederick Wall, Paul Flory, and John Rehner in 1942 and 1943 developed the alternative *affine network theory* (Flory 1953). According

to this theory, the coordinates of the crosslinkings are transformed linearly with the macroscopic deformation. Both of these theories gives similar result on the elasticity calculation.

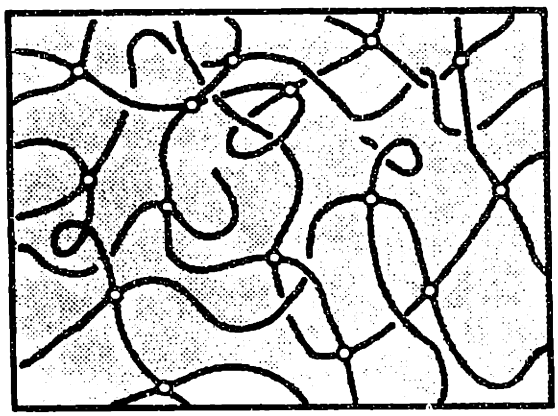

Figure 1.2: Schematic sketch of part of a typical gel network.

Gel is a 3-dimensional polymer network immersed in solvent (Fig.1.2). Mechanically, it is very similar to the natural rubber. It has very high deformability and nearly complete recoverability. Depending upon the solvent and other conditions, the network chains can either repel each other to be swollen or attract each other to be very compact. The first statistical mechanical treatment of this problem (aimed at the polymer solution then) were given independently by Flory (1942) and Huggins (1941).

The Flory-Huggins theory is a mean-field (molecular) theory which is very similar to that of the Van der Waals gas-liquid theory. The theory (for a handy reference, see appendix D) predicted a phase transition (do not be confused by the sol-gel transition) of the network system between the dense phase and dilute phase. In 1973, Tanaka, Hocker and Benedek observed the collective diffusion motion from gel network using dynamic light scattering spectroscopy. Since then, gels have been under intensive study. Tanaka (1979a) and Ilavsky (1982) later experimentally observed the

transition and showed the existence of the critical point in the gel network system (Hochberg and Tanaka 1979). The phase transition of gels have been found to be universal experimentally, i.e, the phase transition has been observed from variety of gels (Amiya and Tanaka 1987). The gel phase transition can be induced by many factors, for instance, temperature (Hirotsu and Tanaka 1987), solvent composition (Tanaka et al 1980; Ilavsky 1982; Hrouz et al 1981; Ilavsky et at 1982), pH (Tanaka 1981b), electric field (Tanaka et al 1982), external osmotic pressure (Hirotsu 1987; Y. Li, chapter 10) and mechanical external pressure (Y. Li, chapter 6), etc. Fig.1.3 bellow is a typical first order phase transition of N-isopropylacrylamide gels induced by the temperature.

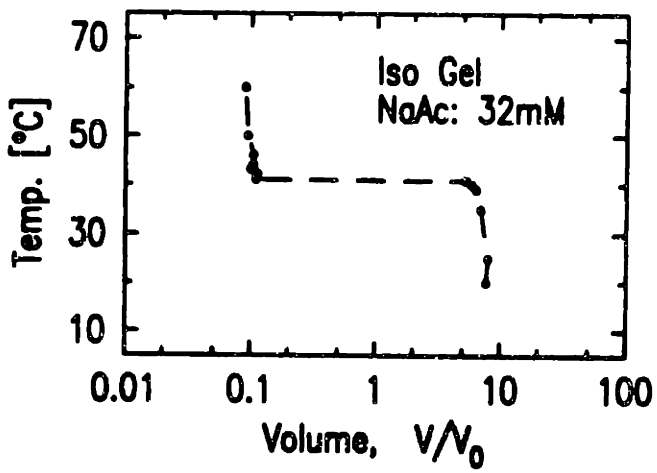

Figure 1.3: Phase transition of N-isopropylacrylamide gel with 32mM sodium acrylate. Notice that the volume change is about 100 times

The gels we have studies are mainly two kinds. One is acrylamide gel, and the other is N-isopropylacrylamide gel. They have different properties. In pure water, acrylamide gel is temperature insensitive near the room temperature and the N-isopropylacrylamide gel is temperature sensitive. Depending upon the experiment, we use one of them as our sample. These gels are formed by free radical copolymerization. For detailed information about out gel samples, see appendix A.

1.3 Motivation

Under proper conditions, the volume of a gel can change discontinuously by a factor as high as a thousand times. The change of volume corresponds to the change in density of gel network. Phenomenologically, the two phases of the gel can be identified as a dense and a dilute phase. These may correspond to the liquid and gas phases of a liquid-gas system. As we have mentioned before, there exists a second order critical point in the gel system, which is similar to that found in liquid-gas systems. Lee and Yang (1952) had shown that the lattice-gas system can be mapped onto the Ising system and vice versa (see also Huang 1965, chapter 16). Experimental results also strongly support the argument that the liquid-gas system is in Ising universality class (Heller 1967; Ma 1976). Hence, the similarity between the gel phase transition and the liquid-gas phase transition leads us to anticipate that near the critical point the gel will behave like a 3-d Ising system.

On the other hand, many properties of gel network can be understood by applying the polymer theories. But there are differences between polymer solutions and gels (e.g., the existence of the gel shear modulus). So one can ask to what extend the analogy between the polymer solution and the gel system exist and what are the effects of the differences between them.

The motivation of the first part of this thesis is to experimentally and quantitatively examine the critical behavior of the gel system. Although the analogy between the polymer system and the gel network system has helped us a great deal in understanding the behavior of the gel network, very little theoretical work has been done directly for the gels. It is not clear to us that how far can this analogy go and under what circumstances will the difference between them will appear. We wish our work can provide some helpful information in developing a network critical phenomenon theory.

The second part of this thesis is related with the structure of the network. The study of the gel structure is quite difficulty because the the gel system often is not well defined, in another word, many defects exist inside a network. We have probed the structure of the gel network by using several techniques.

1.4 Thesis Organization

This thesis mainly contains two parts. One is the study the critical behaviour of N-isopropylacrylamide gel. The other is the study of the network structure by laser light scattering and mechanical pressure techniques, and also by varying the ionic group concentration. Along the course of these studies, some interesting properties of the gel network system were discovered and studied. The fascinating oscillation of the scattered light intensity is especially worth mentioning.

The first part of the thesis includes chapter 2, 3, 4 and 5. The measurement of the critical exponents δ, α_π and ν_π and related topics are described in chapter 2, 3 and 4 respectively. Chapter 5 is a final summary and general discussion of the gel network criticality. From our experimental data, we concluded that the gel network system behaves like an 3-dimensional Ising system.

The second part of this thesis includes chapter 6, 7, 8, and 9. The major topics of this part is the structure of polymer network system. In chapter 6, the inhomogeneity of the gel system is studied by laser light scattering. The oscillation of the scattered light intensity from gels is discussed in chapter 7. Chapter 8 is devoted to the mechanical study of the network system. We directly measured the shear modulus, bulk modulus and indirectly measured the friction coefficient between the network and the solvent. In chapter 9, we discuss the property of the network as a function of the chemical composition by measuring the swelling ratio and other quantities.

Chapter 10 contains some of the unfinished experiments that we consider them

worth pursuing.

All the information related with our gel samples are given in the Appendix A. Some of the experimental setups are also described in appendix A. The critical behavior of the Flory-Huggins mean-field theory is presented in appendix B. We also calculated the stretching limit of a polymer chain in the appendix C. Finally, the kinetics of the volume relaxation of gels with certain geometry has been calculated in appendix D.

Chapter 2

Critical Isobar

2.1 Introduction

Although there are many ways to approach a critical point in the parameter space, due to the practical limitations, for different systems, often it is more natural to approach the critical point along one way than another. The conventional critical exponents are defined along the isochore (Fig.2.1a) (equivalent of the external field h=0 for the ferromagnet system). Along this path, the system goes from a two-phase co-existence state to a single phase state. For $T < T_c$, the system has two phases, as the temperature approaches the critical value, the densities of these two phases approach the critical point along the co-existence curve. For $T > T_c$, the density is equal the critical density ρ_c.

The following exponents are defined along the critical isochore,

$$C_v \sim |t|^{-\alpha}. \tag{2.1}$$

$$\delta\rho \sim (-t)^{\beta} \quad for\ T < T_c. \tag{2.2}$$

Another popular path is the critical isotherm (Fig.2.1b). Along this path, the system continuously goes from one phase to the other without any discontinuous

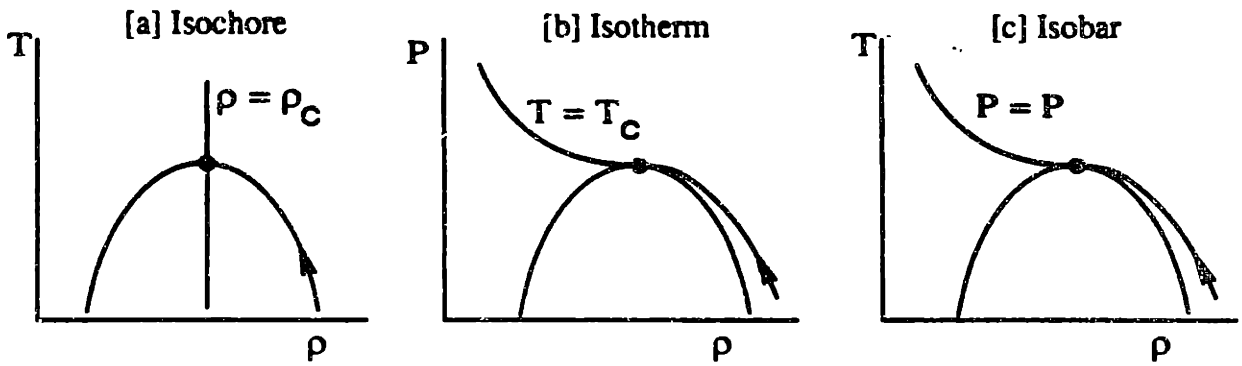

Figure 2.1: [a] Critical isochore path. For $T < T_c$, the system approaches the critical point along the co-existence curve. [b] Critical isotherm path. The critical exponent δ is defined along the path. [c] Critical isobar path. The exponent δ', which is equal δ in value, is defined along this path.

change in the density. The critical exponent δ is defined along this path.

$$\delta P = |\delta\rho|^{\delta}. \tag{2.3}$$

For a liquid-gas system, we can also approach the critical point along the critical isobar $P = P_c$. Along this path, we can define an exponent δ' similar to that defined along the isotherm.

$$\delta T = |\delta\rho|^{\delta'}. \tag{2.4}$$

Here $\delta\rho = |\rho - \rho_c|$ and $\delta T = |T - T_c|$. In general, the quantity $(\partial P/\partial T)_\rho$ is an analytic function of T and ρ. It has no singularity at the critical point. Near the critical point let us write

$$\frac{\partial P}{\partial T} = A. \tag{2.5}$$

Hence

$$\delta P = A\delta T, \tag{2.6}$$

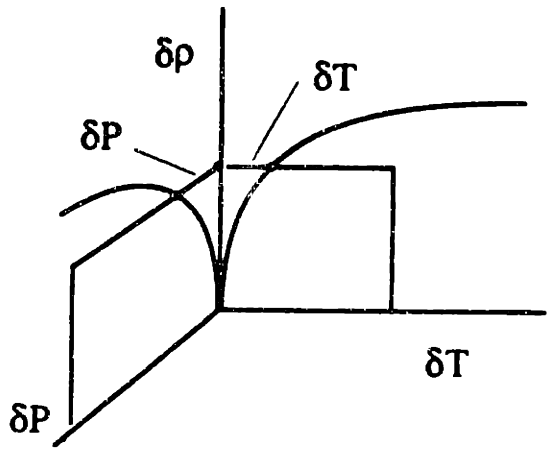

Figure 2.2: Relation between pressure δP and temperature δT for fixed density ρ. The relation is linear.

where A is a constant. Thus the intersection of the surface of the equation of state $f(\pi, \rho, T) = 0$ and the plane $\rho = constant$ is a straight line (figure 2.2). Substituting eq (2.6) into eq (2.4), we find immediately that the two exponents defined in eq (2.6) and eq (2.3) are the same. In later part of this thesis, we are not going to distinguish between δ and δ' unless it is necessary.

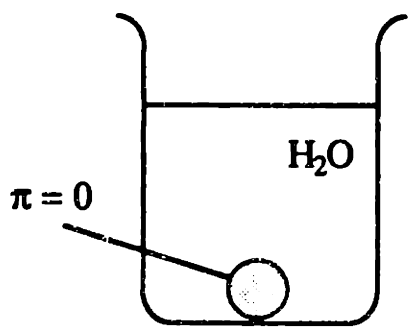

Figure 2.3: All experiments were done with the gels freely surrounded by water, i.e., the chemical potential of water molecules inside and outside the gels are the same. In other words, the osmotic pressure of the network is zero.

During all of our experiments, the gels were immersed in water (figure 2.3). In equilibrium, the total osmotic pressure of the gel network is zero. This fact makes

the isobar (i.e, osmotic pressure π kept constant) path the most natural experimental path. This experimental condition is different from those of the Ising systems like liquid-gas or binary liquid, which are usually examined under isothermal or isochoric conditions. This also makes it difficult to directly measure the conventionally defined exponents, like α, β and γ, which are measured along the isochoric path.

In general, the equation of state of a gel network system can be written as

$$f(\pi, V, T, \theta, \{y_i\}) = 0, \tag{2.7}$$

where π is the total osmotic pressure, V the volume, T the temperature, θ is the network-solvent interaction parameter, $\{y_i\}$ are the network structure parameters, including the polymer constituent concentration and the network cross-linker concentration. As we have mentioned before, in equilibrium the osmotic pressure π, as a function of V, T, θ and $\{y_i\}$, is zero. The critical isobar of the system is then determined by θ and $\{y_i\}$. Although it is common to vary the solvent (θ) to investigate phase transition of gels, in our experiment we have chosen to use water as our solvent and vary $\{y_i\}$ to achieve the critical point. The advantage of this is that the solvent is simple and stable. Compared with a complex solvent (mixture of more than one solvent), preferable absorption of solutes to polymers (see section 9.2), which usually depends on the temperature, is eliminated. The disadvantage is that many samples have to be made with varying chemical composition in order to find the gel that can reach the critical point.

2.2 Critical Exponents Along Isobar

The critical behavior of a thermodynamic quantity R can be expressed as

$$R_{sing} \sim A_{\pm}|x|^{-s} + \textit{higher order terms}, \tag{2.8}$$

where R_{sing} is the singular part of R, x is the path variable, A_- and A_+ are the amplitudes for $x < x_c$ and $x > x_c$ respectively, s is the critical exponent of R measured along the path x.

In general, the critical behavior of a thermodynamic quantity is path dependent, i.e, the critical exponents and the ratio of the amplitudes A_-/A_+ measured from different paths are different. But so long as the free energy of the system is analytic everywhere except at the critical point, the exponents measured from different paths are related.

First of all, we would like to point out that the ratio of the amplitudes A_-/A_+ is an universal constant within an universality class. For liquid-gas system, in the case of the specific heat, the ratio is: $A_-/A_+ \approx 1/2$. The ratio of the amplitudes is related with the fact that the available states for the fluctuations (excitations) of the order parameter are different for $x < x_c$ and $x > x_c$. Intuitively, it may be remembered as follows. Imagine a small amount of heat, δQ, is deposited in the system. For $T < T_c$, the δQ is shared by the two co-existence phases resulting a smaller δT (by a factor of 2), yielding a larger heat capacity. This kind of argument can be applied to other response functions like isotherm compressibility.

Along the critical isobar, however, the amplitude ratio A_-/A_+, is guaranteed to be the unity, i.e., the behavior is symmetric. This is primarily because that along the critical isobar, the system never enters the two phase co-existence region.

To derive relations among the exponents obtained from the critical isobar and the conventionally defined ones, we start from the scaling form of the free energy (Stanley 1971)(note[1]),

$$F(t, \rho) = t^{2-\alpha} g(\rho t^{-\beta}, 1), \tag{2.9}$$

where t and ρ are the reduced temperature $|T - T_c|/T_c$ and the reduced density

[1]This is a very natural result of the renormalization group theory.

$|\rho - \rho_c|/\rho_c$, respectively, α is the exponent of C_v along the isochore and β is the co-existence curve exponent. g(x, y) is a general homogeneous analytic function for finite x and y, and satisfies (stanley 1971)

$$\lambda g(x,y) = g(\lambda^a x, \lambda^b y), \tag{2.10}$$

where λ is an arbitrary number, a and b are the intrinsic properties of the function g, called the degrees of homogeneity of function g. Along the isobar, $\rho \sim t^{1/\delta}$. Since in general $1/\delta$ is smaller than β the first argument of the function g of eq. (2.9) is infinite at the critical point and the function is not well defined. It is, therefore, necessary to rewrite eq. (2.9). Choosing $\lambda = y^{-1/b}$ and $\lambda = x^{-1/a}$, we get two equations,

$$g(x,y) = y^{1/b} g(xy^{-a/b}, 1) = x^{1/a} g(1, yx^{-b/a}). \tag{2.11}$$

From eq. (2.11), eq. (2.9) can be rewritten as

$$F(t,\rho) = \rho^{\frac{2-a}{\beta}} g(1, t\rho^{-1/\beta}). \tag{2.12}$$

The heat capacity is then

$$\begin{aligned} C_v &\sim (\frac{\partial^2 F}{\partial t^2})_\rho \\ &\sim \rho^{\frac{-a}{\beta}} g''(1, t\rho^{-1/\beta}). \end{aligned} \tag{2.13}$$

Here g'' is the partial derivative of the function g(x,y) with respect to y. Along the critical isobar, $\rho \sim t^{1/\delta}$, $g''(1,0)$ is a finite constant,

$$C_v \sim t^{-\alpha/\beta\delta}. \tag{2.14}$$

The critical exponent of C_v along the critical isobar is defined as α_π,

$$\alpha_\pi = \frac{\alpha}{\beta\delta}. \tag{2.15}$$

By the same argument, the compressibility χ_T along the critical isobar can be calculated,

$$\chi_T \sim t^{-\gamma/\beta\delta}, \tag{2.16}$$

where γ is the compressibility exponent along the critical isochore. Thus we have the exponent of χ_T along the critical isobar,

$$\gamma_\pi = \frac{\gamma}{\beta\delta}. \tag{2.17}$$

If we define

$$\beta_\pi = \frac{1}{\delta}, \tag{2.18}$$

then, by using the scaling laws:

$$\alpha + 2\beta + \gamma = 2 \tag{2.19}$$

and

$$\alpha + \beta(\delta + 1) = 2, \tag{2.20}$$

we have the following scaling laws,

$$(\alpha_\pi + 2\beta_\pi + \gamma_\pi)\frac{\beta}{\beta_\pi} = 2, \tag{2.21}$$

and

$$[\alpha_\pi + \beta_\pi(\delta + 1)]\frac{\beta}{\beta_\pi} = 2, \tag{2.22}$$

Notice the similarity between eq. (2.19)-(2.20) and eq. (2.21)-(2.22).

If we know any two of the exponents above, we can calculate all the others. In our experiments, we measured α_π and δ, so we can determine other exponents:

$$\alpha = \frac{2\alpha_\pi\delta}{(\delta + 1 + \alpha_\pi\delta)}, \tag{2.23}$$

$$\beta = \frac{2}{(\delta + 1 + \alpha_\pi\delta)}, \tag{2.24}$$

$$\gamma = \frac{2(\delta - 1)}{(\delta + 1 + \alpha_\pi\delta)}. \tag{2.25}$$

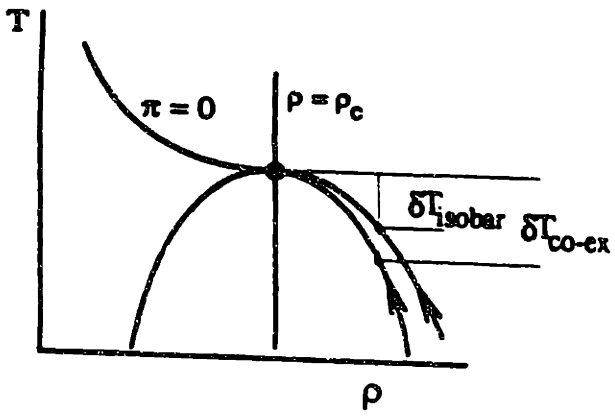

Figure 2.4: δT_{co-ex} and δT_{isobar} measured along co-existence curve and the critical isobar. For fixed density, there is a scaling relation between them.

Another way of deriving the above results is schematically described in figure 2.4. The relation between the density $\delta\rho$ and the temperature δT has different power along the coexistence curve and the critical isobar,

$$\delta\rho \sim (\delta T_{co-ex})^{\beta}, \quad along\ co-existence\ path \tag{2.26}$$

$$\delta\rho \sim (\delta T_{isobar})^{1/\delta}, \quad along\ isobar\ path. \tag{2.27}$$

For fixed density $\delta\rho$,

$$\delta T_{co-ex} \sim (\delta T_{isobar})^{1/\beta\delta}. \tag{2.28}$$

The physical meaning of eq (2.28) is quite clear. Along the critical isobar, the distance from the critical temperature, δT_{isobar} is closer than that along the co-existence curve. In another words, the distance has been scaled by power $1/\beta\delta$. The specific heat diverges as

$$\begin{aligned} C &\sim (\delta T_{co-ex})^{-\alpha} \\ &\sim (\delta T_{isobar})^{-\alpha/\beta\delta}. \end{aligned} \tag{2.29}$$

So we have the same result as we had before

$$\alpha_\pi = \frac{\alpha}{\beta\delta}. \tag{2.30}$$

The same argument will give eq (2.17) and eq (2.18).

2.3 Measurement of the Exponent δ

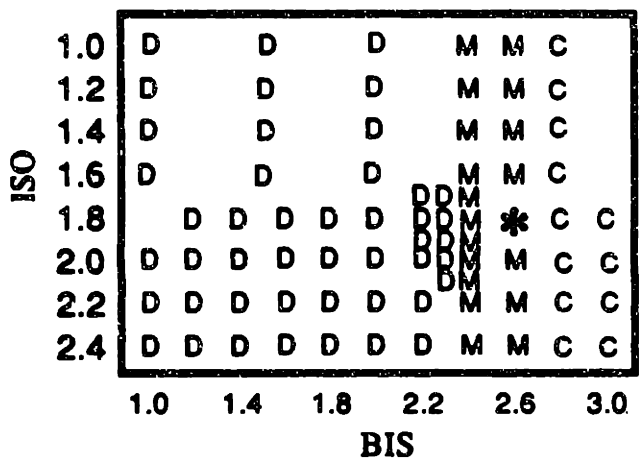

Figure 2.5: Isobar behavior of the gels. D stands for discontinuous volume transition, C stands for continuous transition and M stands for marginal transition (hard to tell).

In this experiment, we measured the density of the gels as function of temperature by measuring the swelling ratio of the samples. Cylindrical N-isopropylacrylamide (NIPA) gels with different chemical composition were made inside micropipettes at 0 °C. The concentration of the network main chain components, N-isopropylacrylamide (ISO), varied from 78mg/cc to 203mg/cc by 16mg/cc increments. The cross-linking molecules, N,N-methylenebisacrylamide (BIS), varied from 1.33mg/cc to 4mg/cc by 0.27mg/cc increments. The inner diameter of the micropipettes was 0.508 mm. After being taken out of the micropipettes, the gels were kept in water for several days before they were used for the experiments. Then these gels were cut into $\sim$ 1.5mm

long segments and transferred into a temperature controlled transparent cell which can hold 24 samples. The temperature of the cell was controlled to within 0.5 mK and was stable over many hours. The diameter of the gels was measured with a microscope. For each chemical composition three segments were measured and the average was taken. Near the critical temperature the increment in temperature was 10mK. The density of the gels was calculated by knowing the pre-gel solution concentration of the network constituent (7.8%) and the equilibrium gel diameters.

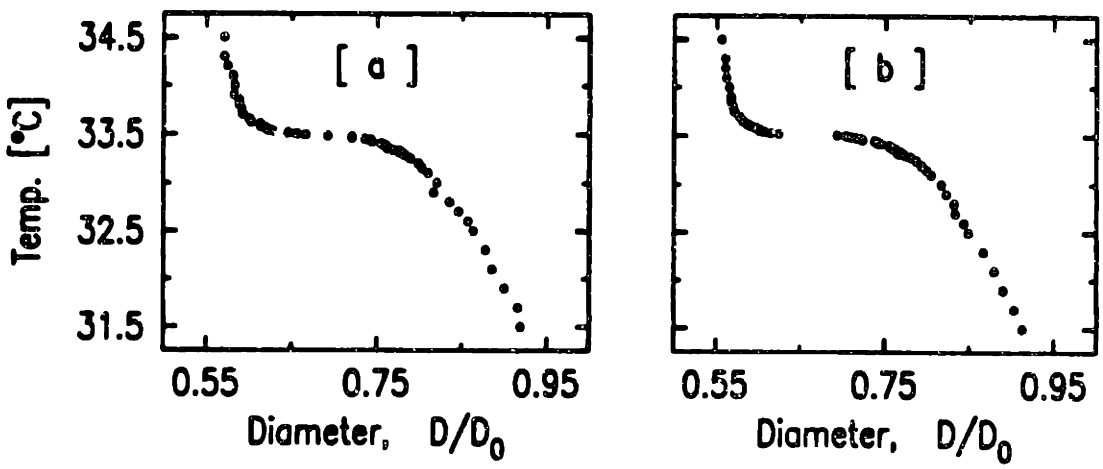

Figure 2.6: Nearly critical isobars. [a]. Chemical composition: ISO 156mg/cc, BIS 3.45mg/cc. [b]. Chemical composition: ISO 140mg/cc, BIS 3.45mg/cc.

From these diameter (D) and temperature (T) measurements, D-T curves were plotted. Some of these curves are continuous and some are discontinuous. Fig.2.5 is a map of the isobar behavior of the gels with different chemical composition. All the gels with BIS concentration less than or equal to 3.20mg/cc were discontinuous, whereas all the gels with BIS concentration greater than or equal to 3.7mg/cc were

continuous. The critical isobar is identified as the curve that is the closest to the curve which has the smallest discontinuity. Fig.2.6 are the two D-T curves that are the closest to the critical isobar from the ordered and the disordered phase side. In Fig.2.6, sample-a is continuous and sample-b is weakly discontinuous. We chose the sample-b to be the critical sample. The chemical composition of this gel is ISO 140mg/cc, BIS 3.45mg/cc in water. The technical aspect of the sample preparation can be found in the appendix A.

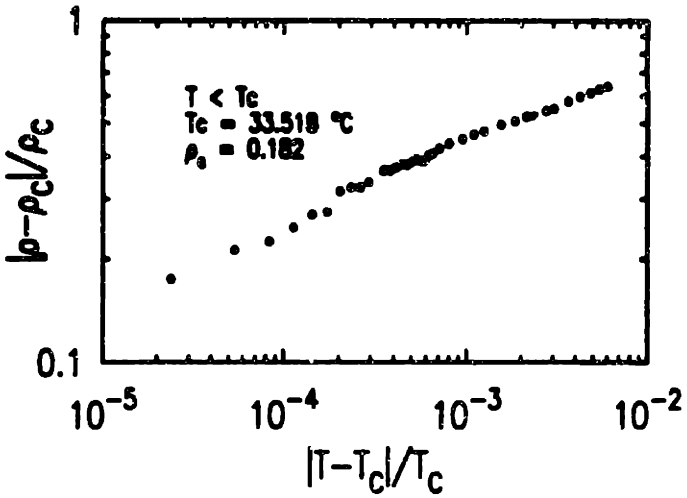

Figure 2.7: Log-log plot of the critical isobar. The inverse of the slope is the exponent δ.

Fig.2.7 is generated from Fig.2.6.b. The critical point is determined such that the $T > T_c$ part of Fig.2.6 is parallel with the $T < T_c$ part. The numerical value of T_c and ρ_c are, 33.518 and 0.182, respectively. Fitting the $T < T_c$ part of the data in Fig.2.6 with a straight line with a 95% confidence limit a slope 4.2 ± 0.5 is obtained. This is the exponent δ. The value of δ for the gel agrees with other measurements on 3-D Ising systems. We did not fit the $T > T_c$ part of the data because the errors associated with those points were much larger.

2.4 Summary

- Derived the relations among the isobar exponents and the conventionally defined ones.
- Measured the exponent δ, $\delta = 4.2 \pm 0.5$.

Chapter 3

Measurement of the Specific Heat C_v

3.1 Introduction

In this section, we shall emphasize the universal properties of the n-vector systems. It is very important to realize that there are only very few material dependent parameters in these problems (often 2, see Aharony and Hohenberg 1976). The elimination of these material dependent parameters by combination of other thermodynamic quantities yield universal (material independent) constants within the universality class.

Ever since the celebrated establishment of the renormalization group (RG) theory (Kadanaff 1966, 1967; Wilson 1971, 1983), we have gained tremendous amount of insight of the critical phenomena. In the past fifteen years, the study of the critical behavior of the specific heat has been particularly intense. The calculation of the critical properties of the n-vector systems has reached high precision (Guillou and Zinn-Justin 1977; Bagnuls and Bervillier 1985a; Bagnuls et al, 1987). Table 3.1 lists some of the results obtained by Bagnuls and Bervillier (1985a) and Bagnuls et al (1987). They are in excellent agreement with experimental results.

Table 3.1: Numerical calculations of the critical properties (Bagnuls and Bervillier 1985). The numbers in the parenthesis are error bars of the calculation.

n	ν	γ	α	Δ	$R^+_{B_{cr}}$
1	0.6298(7)	1.2407(12)	0.1106(21)	0.496(5)	-0.7081(5)
2	0.6689(10)	1.3160(20)	-0.0066(30)	0.524(4)	-1.057(22)
3	0.7047(9)	1.3864(28)	-0.1142(27)	0.5501(3)	-1.3785(41)

The general critical behavior of the specific heat C can be expressed as

$$C = A_{\pm}|t|^{-\alpha}\left[1 + D_{\pm}|t|^{\Delta}\right] + B_{cr} + B_{bg}. \tag{3.1}$$

Where Δ is the correction-to-scaling exponent, D_+ and D_- are the amplitudes for $T > T_c$ and $T < T_c$ respectively, B_{cr} is a non-trivial constant coming from the four-point correlation function (Bagnuls and Bervillier 1985b; Nicoll and Albright 1986), B_{bg} is the experimental value of specific heat C measured far from the critical point. The value of Δ is both theoretically (Saul and Jasnow 1975; Bagnuls 1985a, 1987) and experimentally (Beysens and Bourgon 1979; Bourgon and Beysens 1981) known to be very close to 0.51 ± 0.01 (varies from model to model and sample to sample).

Many combinations of the amplitudes, A_+, A_-, D_+, D_-, etc, have been proven to be universal constants within an universality class (see table 3.1). An interesting result has been obtained relating A_+/A_- with the specific heat exponent α (Barmatz, Hohenberg and Kornblit 1975; Aharony and Hohenberg 1976; Chase and Kaufman 1986) (figure 3.1)

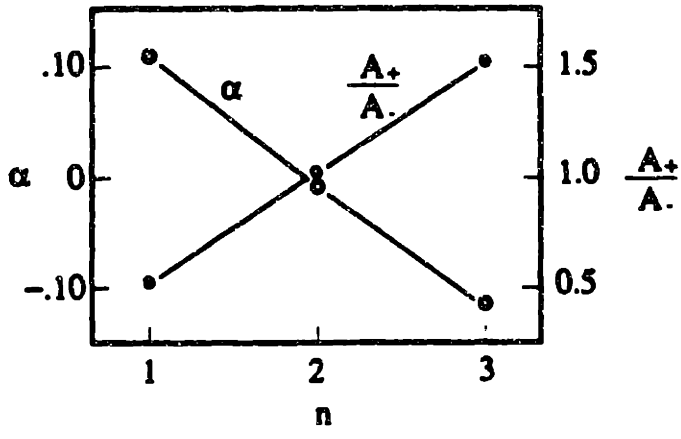

Figure 3.1: Relation among the amplitude ratio A_+/A_-, the exponent α and the number of components n of the order parameter (experimental results).

$$A_+/A_- \approx 1 - P\alpha + O(\alpha^2), \tag{3.2}$$

with $P \approx 4$. The ratio of A_+/A_- is very interesting since it must be exactly equal to unity when $\alpha = 0$ (the critical singularity becomes logarithmic). Hence $n = 2$ ($\alpha = -0.008$) is very close to n_0 at which the value of α vanishes. The ϵ expansion yields (Bervillier 1986) $n_0 = 1.942 \pm 0.026$.

n	A_+/A_-	D_+/D_-
1	0.524(10)	1.25
2	1.029(13)	1.172
3	1.521(0.022)	1.13

Table 3.2: Ratio of the specific heat leading amplitudes A_+/A_- (Bervillier 1986) and the correction-to-scaling amplitudes D_+/D_- (our Padè calculation based on the result of Chang and Houghton 1980)

The ratio of the correction-to-scaling amplitudes are also universal constants(Aharony

and Ahler 1986)

$$D_i/D_j = \frac{\lambda_i - \lambda_i^0}{\lambda_j - \lambda_j^0} + O(\epsilon), \tag{3.3}$$

where D_i is the amplitude of a thermodynamic quantity with critical exponent λ_i and mean field exponent λ_i^0, $\epsilon = 4 - d$ with d the dimensionality of the space. For the same thermodynamic quantity, we have

$$D_+/D_- = 1 + O(\epsilon). \tag{3.4}$$

Although the accurate value of D_+/D_- is not known, one thing we know well is that the ratio is a positive value. Table 3.2 lists some of the theoretical results. To the best of our knowledge, there is no reliable experimental result of D_+/D_- at this stage.

The constant B_{cr}, can also be used to construct universal constants (Bagnuls and Bervillier 1985; Nicoll and Albright 1986)

$$R^{\pm}_{B_{cr}} = \frac{A_{\pm}|D_{\pm}|^{\alpha/\Delta}}{\alpha B_{cr}} \tag{3.5}$$

Some of the calculated value of $R^{\pm}_{B_{cr}}$ are also listed in table 3.1.

3.2 General Discussion

Because the gel system constitutes mainly water (solvent), the effective mass is very small (The singular part of the heat capacity comes from the network and a very thin

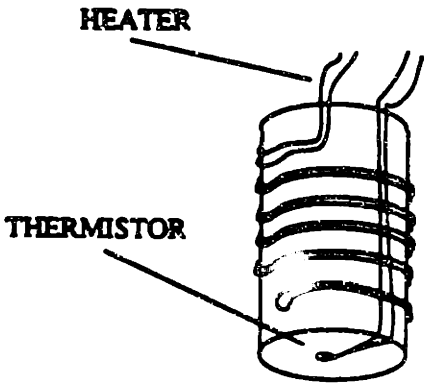

Figure 3.2: Specific heat sample cell. The mass of the empty cell is 1.8970mg. The capacity is 220μl. The effective resistance of the heater is 32Ω (total 37Ω, 1.2Ω/in). The δQ deposited in the holder is 6.704mJ.

layer of the surrounding solvent). In general, the total mass of a specific heat sample is

$$m_{total} = m_{cell} + m_{solvent} + m_{network}. \tag{3.6}$$

Where m_{cell} is the mass of the sample container, $\sim 2000mg$; $m_{solvent}$ is the mass of the solvent, $\sim 220mg$. The mass of the network $m_{network}$, which is primarily where we are getting the signal from, is only about 10% of the mass of the solvent, $\sim 20mg$. This mass is only about 1% of the total mass. In other words, in order to be detected, the singular part of the specific heat of the network has to be much larger than that of the container and the solvent.

Now we wish to do some theoretical discussion about the heat capacity measurement process (figure 3.3). Assuming we have a perfect thermal conducting sample with heat capacity C, the insulating material has thermoconductivity K (very small), then we can derive the temperature response function $\delta T(t)$ of the system. The result is

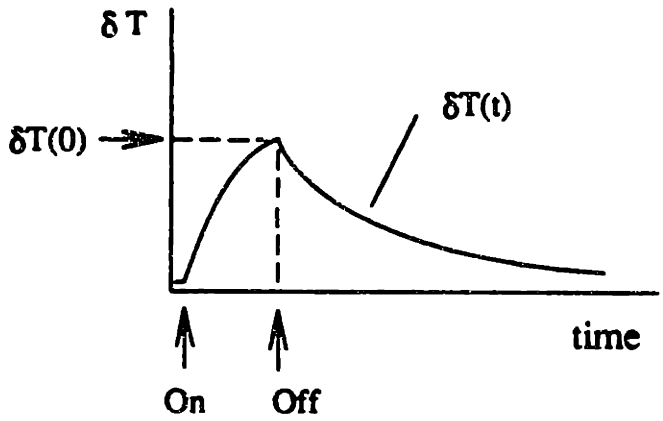

Figure 3.3: Ideal $\delta T(t)$. The heater is turned on at $t = 0$ and turned off at $t = t_0$.

$$\delta T(t) = \begin{cases} \frac{\delta Q}{K}(1 - e^{-\frac{K}{C}t}) & \text{for } 0 < t < t_0 \\ \\ \frac{\delta Q}{K}(1 - e^{-\frac{K}{C}t_0})e^{-\frac{K}{C}(t-t_0)} & \text{for } t_0 < t < \infty. \end{cases} \tag{3.7}$$

Where K and C are the thermoconductivity of the insulator and the heat capacity of the sample, respectively. The heater is turned on at $t = 0$ and off at $t = t_0$. This result is plotted in figure 3.3. In the case of $t_0 \ll \tau = C/K$, we have

$$\delta T(t) = \begin{cases} \frac{\delta Q}{C}\frac{t}{t_0} & \text{for } 0 < t < t_0 \\ \\ \frac{\delta Q}{C}e^{-\frac{K}{C}(t-t_0)} & \text{for } t_0 < t < \infty. \end{cases} \tag{3.8}$$

At $t = t_0$, we have $C = \delta Q/\delta T(t_0)$. For a real sample, the thermal conductivity is finite, then the plot in figure 3.3 will be smeared (in our experiment, $t_0 = 20$ seconds, $C/K \sim 400$ seconds).

In principle, the heat capacity measured this way is always an average of the heat

capacity from T to $T + \delta T$. This gives a natural limit of the experiment. In other words, the width of the heat capacity peak will have a lower bound = δT, which is about 3mK in our experiment. The portion of the peak within $T_c \pm \delta T$ will be smeared.

Another limiting factor is the response of the instrument. Due to the finite size (and mass) of the thermistor, there is a time delay between the actual temperature of the system and the temperature indicated by the thermistor. In our experiment, the delay is about 2 seconds. Because this instrument is developed on the try-and-improve basis, there are certain room for future improvement (for instance, using better thermistor).

3.3 Experimental

In this study we measured the specific heat C_v of the critical gel along the critical isobar path. Figure 3.4 is a schematic description of the experimental procedure. The calorimeter used in the experiment was computer-controlled. The gel was brought slowly to equilibrium at temperature T. Then a small amount of heat, δQ, was deposited into the system and the temperature increment, δT, was measured. The heat deposited, δQ, was fixed at 6.7mJ. The temperature jump, δT, which was around 2 ~4mK, was obtained by fitting temperature response of the system, $\delta T(t)$, to an exponential function and extrapolating the fit to the t = 0 point. Figure 3.5 is a typical measurement of $\delta T(t)$.

Data were collected three hours after the equilibrium temperature had been set. Three response functions were taken at each temperature point, with a thirty minute time interval between each run. The long time (24hrs) temperature stability of the sample holder was around ±0.5mK, the short time (2hrs) stability was better than ±0.2mK. The temperature increment rate decreased from 50mK/5hrs to 3mk/5hrs

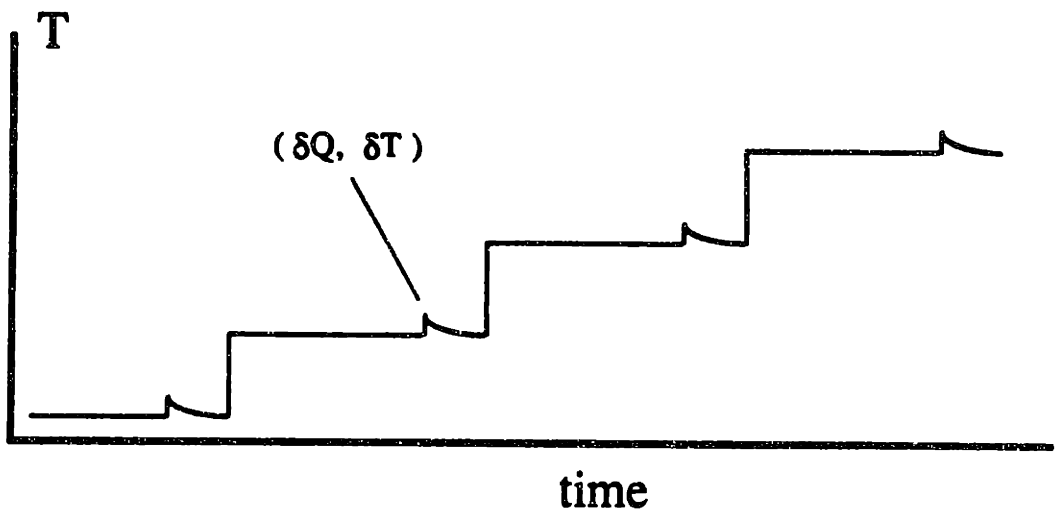

Figure 3.4: Schematic description of the experimental procedure. The system is brought to equilibrium slowly, then a small amount of heat, δQ, is deposited in to it. The temperature response of the system is measured and analyzed by fitting to a single exponential function. The temperature jump is obtained by fitting the response process to a single exponential function.

as the critical point was approached. The mass of the sample was about 240mg. The mass of the sample container (with heating coil, thermistor, leads, etc) was about 1.9g. The sample consisted of hundreds of small pieces of gel of linear size ~ 0.7 mm. The small sample size was needed to enhance the equilibration speed. These pieces were prepared by pressing a bulk gel through a fine sieve mesh twice. Then they were shrunken by heating to 30 °C and the excess water was removed to increase the sample network volume fraction. The raw data was processed to obtain the specific heat, C_v. This involved subtracting the heat capacity contributed by the sample container and the background water according to the the following formula:

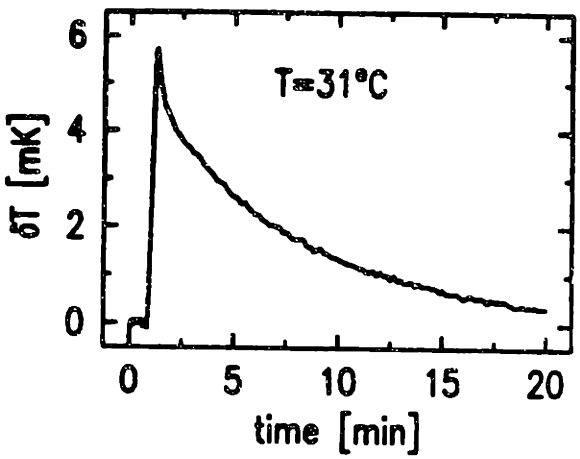

Figure 3.5: A typical temperature relaxation process measured at T = 31 °C. The heater was turned on at t = 50 seconds, turned off at t = 70 seconds.

$$C_v = \frac{1}{rm}[C_{total} - C_{cell} - (1-r)C_w m]. \tag{3.9}$$

Where C_{total} is the total heat capacity, $\delta Q/\delta T$, C_{cell} is the heat capacity of the empty sample container, C_w is the specific heat of water and r is the ratio of the mass of the gel network to the total mass of gel, m. The parameter r is estimated to be 0.1. The specific heat of water (blank sample) was measured to be $4.53JK^{-1}g^{-}1$. This is 8% higher than the known value 4.18 $JK^{-1}g^{-1}$. Since the temperature relaxation process near time zero is multi-exponential rather than just a single exponential, this discrepancy could be due to the definition of δT. In eq. (4.1) we used the specific heat value $4.53JK^{-1}g^{-1}$ to ensure consistent data analysis. The systematic error in the measurement of the specific heat can be large probably due to the lack of detailed information about the chemical reaction efficiency (estimate of r) and the effective resistance of the heating coil. We believe, however, that these factors only add a slow background contribution to the data. The observed critical behavior of the system

should not be affected by them. Fig.3.6 is the specific heat of the sample with the critical chemical composition along the critical isochore.

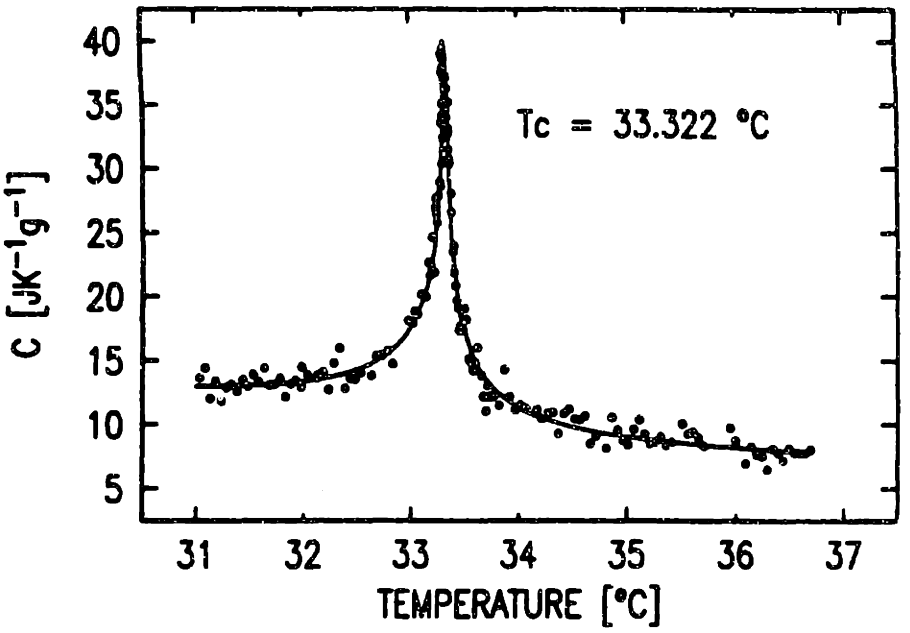

Figure 3.6: Specific heat of N-isopropylacrylamide gel along critical isobar. The solid curve is the fitted result.

For more detailed information about this instrument, see appendix B.

3.4 Equilibrium

G. Sanchez, M. Meichle, and C. W. Garland (Sanchez 1983) pointed out that heat capacity data of a non-equilibrium system may exhibit hysteresis between warming and cooling measurements. In our experiment, however, no hysteresis was observed (figure 3.7). We also compared the data taken three hours and four and one half hours after the temperature had been set (figure 3.8). We summed over the differ-

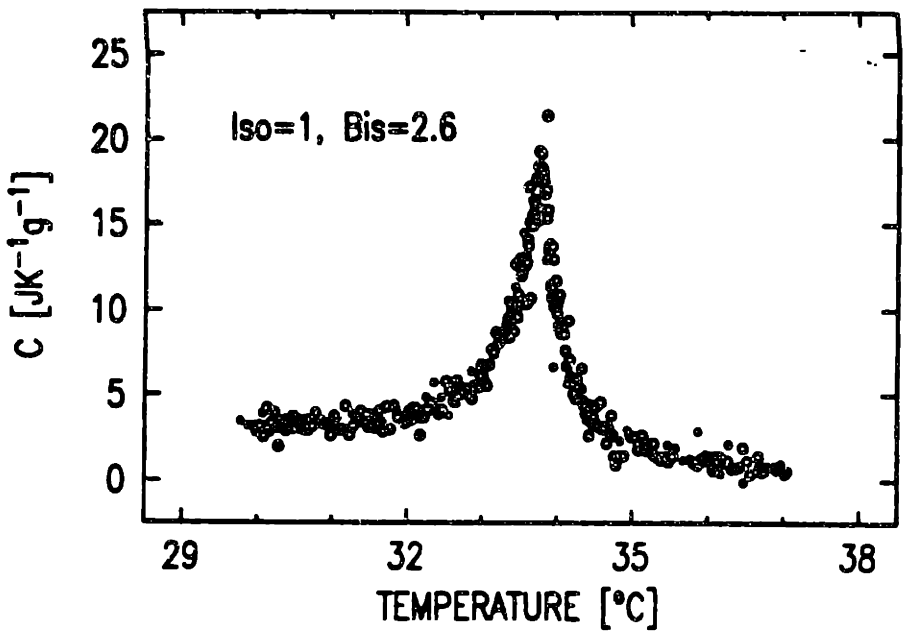

Figure 3.7: Specific heat of ISO gel with Iso=700mM, Bis=8.6mM. Open circles and the solid dots are the data collected in the heating and cooling processes respectively. We have detected no hysteresis.

ences of the δT's at each point and compared with the average of δT, we found that the difference is less than 1%. All these indicate that the data were taken under equilibrium conditions. This experiment was repeated on another sample with very similar chemical composition. All the experimental results reported here were fully reproducible.

Finally, we would like to point out that although the experiment was done along the $\pi = \pi_c$ (isobar) path, we can consider the volume as a constant during each measurement. This is because the temperature relaxation time, which is approximately 400 seconds, is much smaller than the volume relaxation time, which is approximately

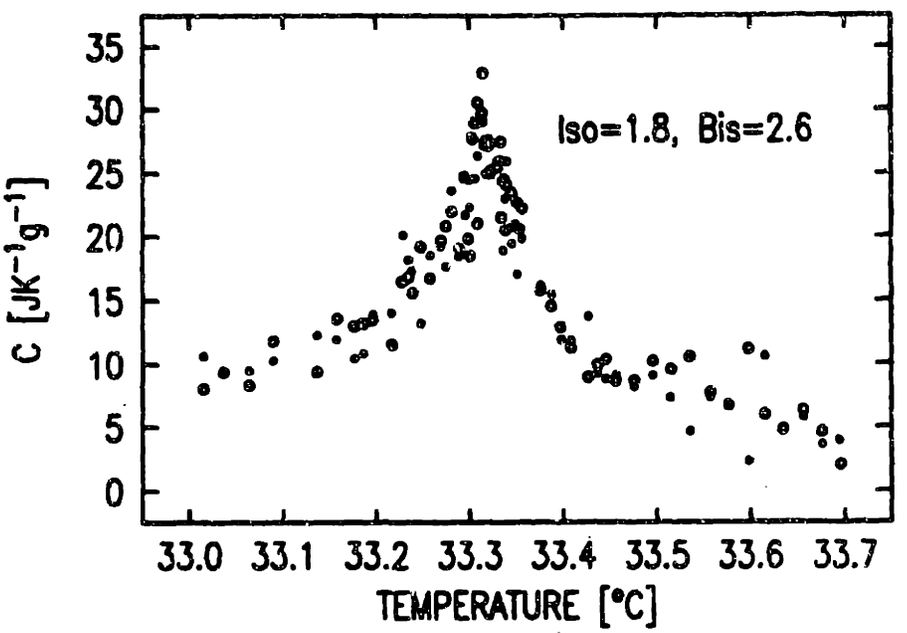

Figure 3.8: Specific heat measured 3 hours after the temperature had been set and 4.5 hours after. The difference is found to be less than 1%.

10^4 seconds (Tanaka 1979b).

3.5 Exponent α_π

Theoretically, one of the important aspects of the specific heat singularity along the critical isobar is that it is totally symmetric. This is because along the isobaric path, the system never enters the two-phase region (more details later in this section). This is different from that of the isochoric path, which generally is not symmetric (Chase 1986; Bervillier 1986). In that case the system goes from the ordered state to the

disordered state, or vice-versa.

We fit the data in figure 3.6 to the following function:

$$C_v = A|t|^{-\alpha_\pi}\left[1 + D|t|^{\Delta}\right] + B + c(T - T_c). \tag{3.10}$$

The correction-to-scaling (Bervillier 1986) exponents, Δ , was fixed at 0.5 (known both theoretically and experimentally). The data above and below T_c were fitted simultaneously by a least-squares fit with all the data point weighted equally. The fitting was carried out for $|t| > 3.3\times10^{-5}$ only. This was done to avoid the fitting error caused by the finite response of the instrument at the singular point. The quality of a fit is indicated by the χ^2 value. We first fit all the parameters to the whole temperature range of the experiment. Then smaller temperature ranges were fitted with the parameter c fixed at the whole range value. All the fitted parameters were found to be very stable for all the ranges we tried except when $|T - T_c|$ was less than 0.5 °C. When $|T - T_c| < 0.5$ °C the tail of the data was too small to allow a reasonable fit. We also performed the F-test on the exponent α with 95% confidence limit. The distribution of χ^2 is presented in Fig.3.9. From Fig.3.9, we find that error on α_π with a 95% confidence limit is -0.05 ± 0.13. The large error bar here is probably due to the fact that our sample is a mixture of small pieces of gel and water. The thermal conductivity of the sample as a whole is not homogeneous, and the spatial distribution of the thermal conductivity changes as the gels change their size. Since the thermal conductivity affects the temperature relaxation time, the change of the thermal conductivity can change the value of the temperature jump. Using much smaller gel pieces could be the solution to this problem.

For Ising system, in general, $\beta\delta > 1$, so $\alpha_\pi < \alpha$. This indicates that α_π is a lower

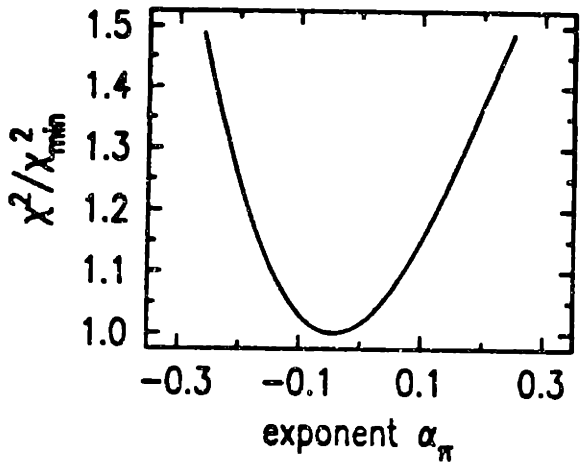

Figure 3.9: Normalized χ^2 distribution of the exponent α.

bound on α. After the exponent renormalization (see part C of this section) we have $\alpha_\pi \sim 0.05$, which is indeed smaller than the expected Ising value for α. The numerical values of the conventional exponents are calculated by using eqs. (2.15)-(2.17) and are listed in table 3.3.

Now come back to the symmetry feature of the specific heat. To have a quantitative result, we fitted the data to eq (3.1) (with the independent amplitudes for both $T < T_c$ and $T > T_c$), the results are

$$\begin{cases} \frac{A_-}{A_+} = 0.99 \\ \\ \frac{D_-}{D_+} = 0.90. \end{cases} \tag{3.11}$$

This result is exactly what we expected for the heat capacity measured along the critical isobar.

3.6 Temperature Relaxation and Fisher Renormalization

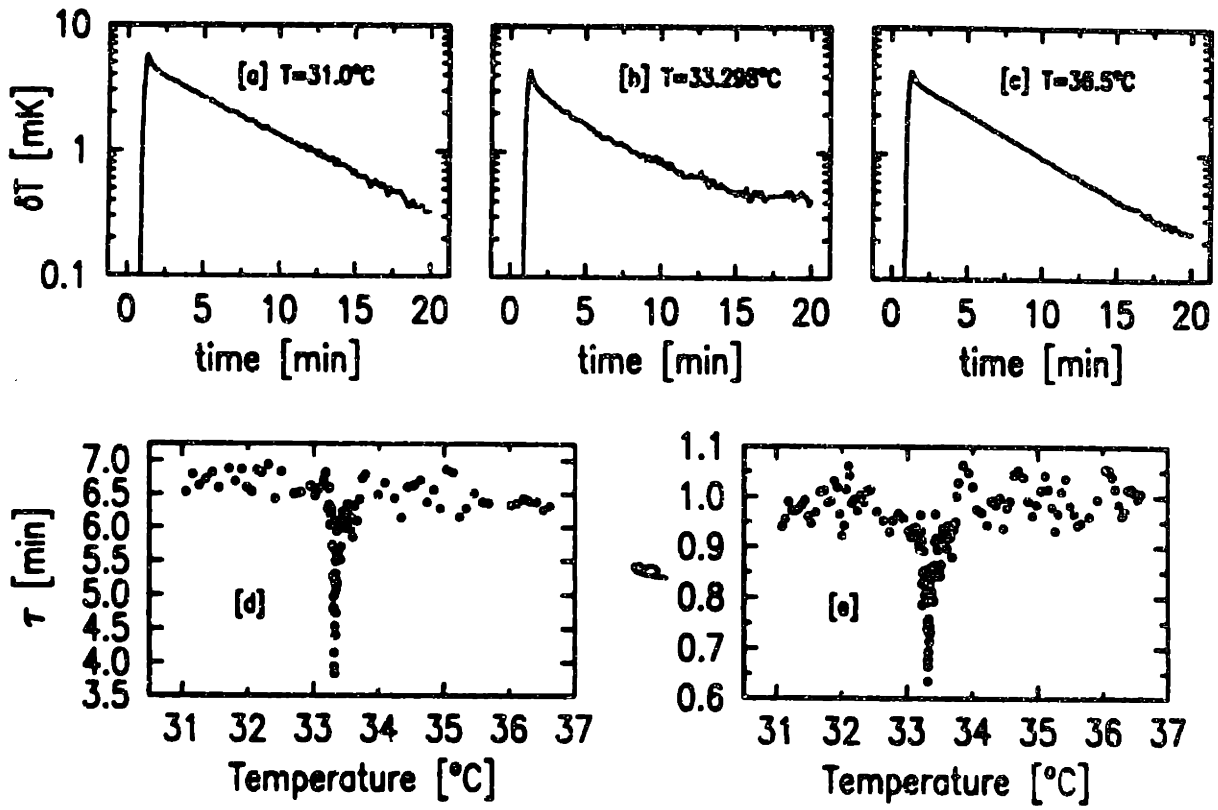

Figure 3.10: Relaxation process. [a] $T \ll T_c$; [b] $T \sim T_c$; [c] $T \gg T_c$; [d] William-Watts decay time. [e] William-Watts exponent.

Recently, S. T. Sun, Y. Li, E. Sato-Matsuo and T. Tanaka (Sun 1989) have investigated the inhomogeneities of gels and their critical behavior by light scattering. They found that gels have inhomogeneities embedded inside the network. Depending upon the gelation conditions, the inhomogeneities can be very large. They also found that

when the critical point is approached, that not only does critical opalescence exist, but also that the intensity of light scattered from the inhomogeneities diverges as well. The inhomogeneities seem to appear during the temperature relaxation process (see figure 3.10a-c). In our experiment, we also analyzed our temperature relaxation data, $\delta T(t)$, by the William-Watts relaxation form (Palmer 1984; Lindsey 1980):

$$\delta T(t) = \delta T(0) exp\left[-(t/\tau)^{\beta}\right]. \tag{3.12}$$

Where β is the William-Watts parameter. In general, when a relaxation process can be well fitted by eq. (4.3), the process can be explained as a multiple relaxation process, and the parameter β is related with the width of the distribution of the relaxation times τ (Palmer 1984). The smaller the value of β, the broader the distribution will be. Fig.3.10d and Fig.3.10e are the fitted parameter β and τ as a function of temperature. Clearly the relaxation process is very different when the critical point is approached. Adopting the argument of Ref.(10), we see that near the critical point the relaxation process becomes multi-relaxation process. Despite the large background contributions to our data by water, which constitute 90% of our sample, and the massive container, we found that the change of the value of β is surprisingly large. In comparison, the decay time of the pure exponential fit in Part A of this section is constant within $\pm 5\%$ for the entire temperature range including the critical temperature. So the critical slowing-down was not observed.

The anomaly in the temperature relaxation process may be an intrinsic property of the second order phase transition, in which case it will be universal and should be observed in other systems. On the other hand, it could be related with the inhomogeneity divergence at the critical point. Near the critical point the density difference between the static inhomogeneous domains is very large. Domains of different size will have different relaxation times and thus multiple relaxation processes will be

observed.

Fisher (Fisher 1968, 1970) pointed out that the critical exponent renormalization phenomenon may be observed when there exists a hidden variable in the system. The renormalized exponents can be expressed as

$$\alpha_R = -\frac{\alpha}{1-\alpha}, \tag{3.13}$$

$$\beta_R = \frac{\beta}{1-\alpha}, \tag{3.14}$$

$$\gamma_R = \frac{\gamma}{1-\alpha}, \tag{3.15}$$

where the subscript R indicates the value expected to be observed experimentally when the system has a hidden variable., called the renormalized parameters. Notice the minus sign in front of the α_R expression. The fisher critical exponent renormalization phenomenon has been observed in many experiments (for instance, Garland, Rouch, et al, 1988)

In the case of gel, the hidden variable may be the structural inhomogeneity. Following Fisher's argument, the experimental exponents are in fact the renormalized exponents. By using eq. (3.13)-(3.15), we get the intrinsic exponents α, β and γ. They are listed in the last row of table 3.3 below.

α	β	γ
-0.08±0.19	0.40±0.08	1.3±0.4
0.09±0.16	0.36±0.07	1.2±0.3

Table 3.3: Critical exponents calculated from experimental value α_π and δ. The last row takes the Fisher renormalization into account.

3.7 Summary

- Measured the specific heat of N-isopropylacrylamide gel along critical isobar.
- The specific heat is symmetric with respect to the T_c along the critical isobar.
- The direct fit yields an exponent $\alpha_\pi = -0.05 \pm 0.13$.
- We observed the critical temperature relaxation anomaly.

Chapter 4

Light Scattering Study of the Gel Criticality

This chapter is intimately related with chapter 6 and chapter 7, *"Light Scattering Study of the Network Structure"* and *"Oscillation of the Scattered Light Intensity"*.

4.1 Introduction

The scattering of light by a media is caused by the interaction between photons and the media. Given a media, there are many degrees of freedom for each particle of the media. The light scattered from each degree of freedom of the particles will give information about that degree of freedom. For instance, Raman scattering provides information about the energy spectra of molecules. In general, the absorption of ultraviolet, visible, infrared, and microwave radiation can provide detailed information about electronic, vibrational, and rotational energy levels of molecules. The scattering related with the translational degree of freedom of molecules is commonly called Rayleigh or Brillioun scattering. In this thesis, we only concentrate on the Rayleight scattering.

The Rayleight scattering of light by a media is caused be the inhomogeneities of

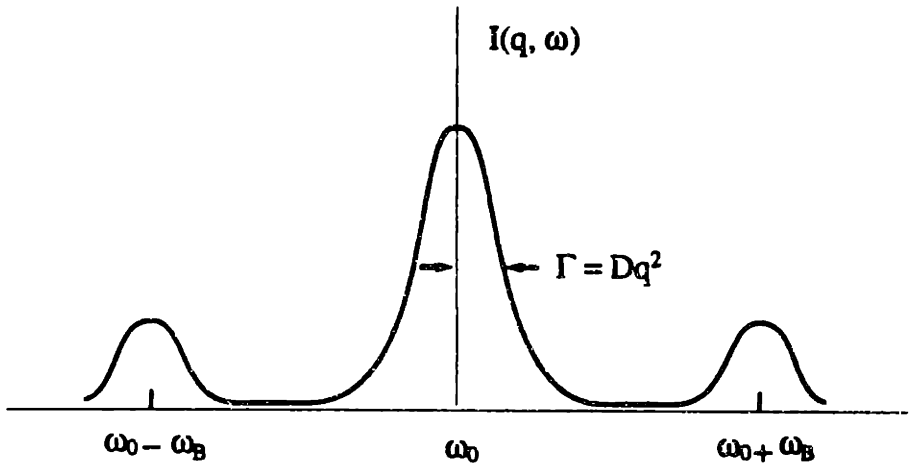

Figure 4.1: A generic light scattering spectrum. The x-axis is the frequency of the scattered light, ω_0 is the frequency of the incident light. The central peak is the Rayleigh scattering (quasielastic light scattering) and the other two peaks are the Brillioun doublets (Doppler shifts).

the optic index of the media, or the fluctuation of the dielectric constant. There are many ways of introducing fluctuations in the media, some of them are, for instance, the thermal fluctuation of the particles in the sample, impurities (or mixture of different substances), etc. Among them, the thermal fluctuation is the most frequently encountered one. Because of the interaction among the particles in the sample, there is a correlation among the behavior of the particles. Within the correlation distance, the particles are strongly correlated, but beyond this distance, they are virtually independent to each other. The correlation length, ξ, defines the size of the objects that will scatter light in a coherent way. When the critical point of a system is approached, the correlation length becomes larger and larger, and eventually reach the size of the order of the incident light wavelength, λ, when this happens, tremendous amount of

light will be scattered. This phenomenon is called critical opalescence.

The dynamic laser light scattering technique can be dated back to 1914, when Leon Brillouin predicted the doublet, now known as Brillouin-doublet, of the scattered light spectrum from a thermally excited density fluctuations in an isotropic body (Brilliuon 1914, 1922) (figure 4.1). The doublet symmetrically spaced around the incident frequency with frequency shift ω proportional to the sound velocity c in the medium and the propagation vector length q of the density fluctuation giving rise to the scattering:

$$\omega = \pm cq, \tag{4.1}$$

with q related to the wave length λ of the light and the scattering angle θ

$$q = \frac{4\pi}{\lambda} \sin(\theta/2). \tag{4.2}$$

So the Brilliuon scattering is essentially the Doppler shift of the incident light by sound waves propagating inside the sample. The width of the brillioun peak is the lifetime of the sound wave.

The first experimental demonstration of frequency distribution was made by Gross (Gross 1930, 1932). In addition to the doublet, he also observed a central line (Rayleight -line). The central line was explained successfully by Landau and Placzek (1934) (also Kadanoff and Martin 1963, Mountain 1966 for the complete derivation of the final formula. also see Stanley 1971) as the scattering from non-propagating density fluctuations caused by the entropy field at a constant pressure field. According to their theory, the Brilliuon doublet originates from density fluctuations produced by propagating fluctuations of pressure at constant entropy (adiabatic sound wave). A prototype light scattering spectrum is given in figure 4.1. In all of the experiments we did, we had only concentrated at the central peak, i.e., quasi-elastic light scattering.

Figure 4.2 is a schematic description of a typical laser light scattering setup. There are two types of scattering related with the central peak of figure 4.1. One is called

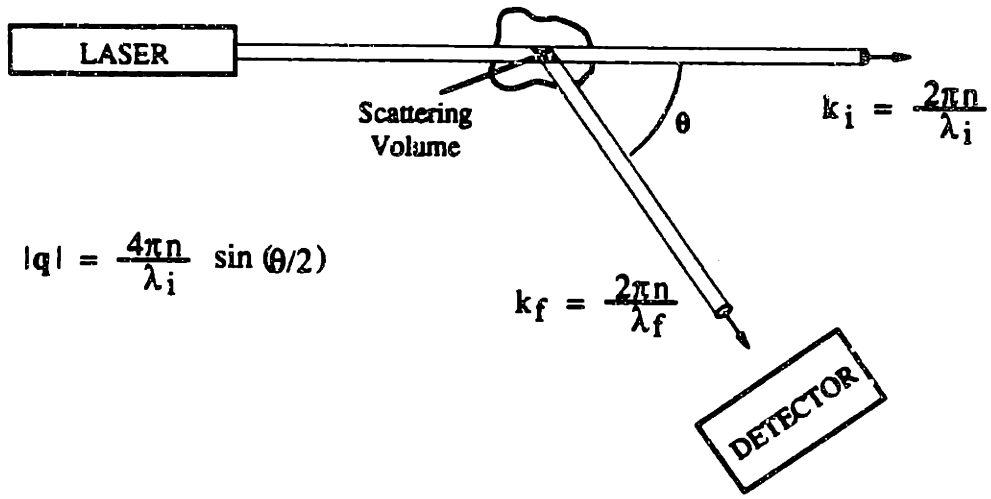

Figure 4.2: A schematic representation of the laser light scattering experiment

elastic light scattering, which measures the total scattered light intensity at a fixed angle, $I(\mathbf{q})$, (equivalent of integrating the central peak over frequency ω), the other is the quasi-elastic (or dynamic) light scattering, which measures the spectrum by either passing the scattered light through a spectrometer (frequency domain, $I(\omega, \mathbf{q})$) or measure the auto-correlation function of the scattered field (time domain, $I(t, \mathbf{q})$).

The dynamic light scattering measures the scattered electric field auto-correlation function $g_1(t)$ from the sample,

$$g_1(t) \equiv \langle E_s^*(t) E_s(0) \rangle. \tag{4.3}$$

Where E_s is the scattered electromagnetic field. The direct measurement of the $g_1(t)$ can be achieved by either the interference between the scattered field and a reference beam (heterodyne) or the interference between the scattered field only (homodyne). Because of the fact that only the scattered intensity is detectable by most

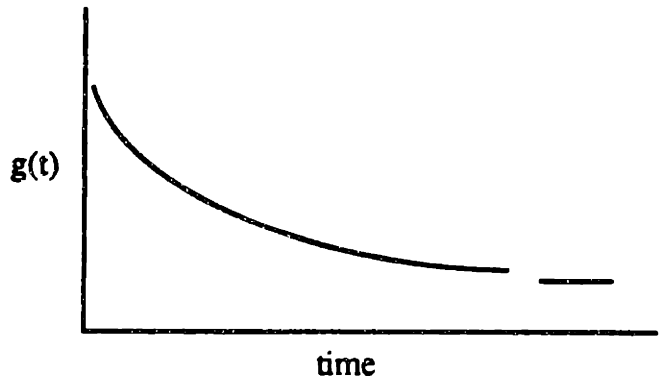

Figure 4.3: Quasi-elastic dynamic auto-correlation function. The small tail is the delayed baseline for reference.

of the detectors, the heterodyne measurement yields,

$$\begin{aligned} g(t) &= \langle E_L^*(t)E_s(t)E_L(0)E_s^*(0)\rangle, \\ &= \langle E_L^*(t)E_L(0)\rangle\langle E_s^*(0)E_s(t)\rangle \\ &= Const \cdot g_1(t). \end{aligned} \tag{4.4}$$

Where E_L os the field of the reference beam (local oscillator). The last step is obtained by using the fact that the reference beam is always correlated.

The homodyne technique measures the scattered intensity correlation function $g_2(t)$.

$$\begin{aligned} g_2(t) &= \langle I_s(t)I_s(0)\rangle, \\ &= \langle E_s^*(t)E_s(t)E_s^*(0)E_s(0)\rangle, \\ &= Const[1 + |g_1(t)|^2]. \end{aligned} \tag{4.5}$$

The last step is obtained by assuming the sample fluctuation is a gaussian process and the scattered field obeys the gaussian statistics.

Figure 4.3 is a generic curve of the correlation function measured by the laser light scattering. Usually the heterodyne correlation function can be fitted by a single

exponential function,

$$g(t) = Ae^{-Dq^2t} + B, \tag{4.6}$$

where A is the amplitude and B the background signal. The coefficient D is called *Collective Diffusion Constant* in the case of gel. There will be a factor of 2 in front of the D if the homodyne method is used.

4.2 Critical Behavior of D and I

In 1973, Tanaka, Hocker and Benedek (Tanaka 1973) developed a theory describing the behavior of the scattered light from a gel sample. The basic equation from which they started their analysis is the most general equation of the motion of the gel network (Newton's second law)

$$\rho\frac{\partial^2\mathbf{u}}{\partial t^2} = \nabla\cdot\tilde{\sigma} - f\frac{\partial\mathbf{u}}{\partial t}. \tag{4.7}$$

Where $\mathbf{u}$ is the displacement vector of the network element, ρ the density of the network, f the friction coefficient between the network and the solvent, $\tilde{\sigma}$ is the stress tensor. The auto-correlation function of the polarized and depolarized scattered light they obtained are, respectively,

$$\begin{aligned} g_1(t,\mathbf{q})_{pol} &= \frac{I_0}{c}\left(\frac{\omega_0}{c}\right)^4\frac{sin^2\phi}{4\pi R^2}\left(\frac{\partial\epsilon}{\partial\rho}\right)_T^2\rho^2\frac{LkT}{K+4\mu/3}exp\left(-\frac{K+4\mu/3}{f}q^2t\right), \quad (4.8)\\ &\sim A_{pol}exp\left(-D_lq^2t\right) \end{aligned}$$

$$\begin{aligned} g_1(t,\mathbf{q})_{dep} &= \frac{I_0}{c}\left(\frac{\omega_0}{c}\right)^4\frac{sin^2\phi}{4\pi R^2}\left(\frac{\partial\epsilon_D}{\partial u_{xy}}\right)_T^2\frac{LkT}{\mu}exp\left(-\frac{\mu}{f}q^2t\right), \quad (4.9)\\ &\sim A_{dep}exp\left(-D_tq^2t\right). \end{aligned}$$

Where A is proportional to the scattered intensity and D the collective diffusion constant. They are,

$$\begin{cases} A = \frac{kT}{K+4\mu/3}, \\ \qquad\qquad \text{polarized light scattering,} \\ D = \frac{K+4\mu/3}{f}, \end{cases} \tag{4.10}$$

$$\begin{cases} A = \frac{kT}{\mu}, \\ \qquad\qquad \text{depolarized light scattering.} \\ D = \frac{\mu}{f}, \end{cases} \tag{4.11}$$

These results relate the light scattering quantities with other basic properties of the network system. By measuring the polarized scattered intensity and the decay time, we can obtain $(K + 4\mu/3)$ and f.

We can also relate these quantities with the density-density correlation function of the network $g(\mathbf{r}) = (1/\phi)\,\langle\Delta\phi(\mathbf{r})\Delta\phi(0)\rangle$ (Tanaka 1985),

$$K^{-1} = \frac{1}{kT}\int g(\mathbf{r})d\mathbf{r}, \tag{4.12}$$

$$f^{-1} = \int \frac{g(\mathbf{r})}{6\pi\eta_s r d\mathbf{r}}. \tag{4.13}$$

Using the Ornstein-Zernike formula

$$g(\mathbf{r}) = C\,\frac{r_0}{r} exp(-r/\xi), \tag{4.14}$$

we have

$$D = \frac{kT}{6\pi\eta\xi}, \tag{4.15}$$

$$K = \frac{kT}{4\pi C r_0 \xi^2}. \tag{4.16}$$

Where ξ is the density-density correlation length. Near the critical point

$$\xi \sim |t|^{-\nu}. \tag{4.17}$$

So the collective diffusion constant D and the scattered light intensity I have the behavior

$$D \sim |t|^{\nu}, \tag{4.18}$$

$$I \sim |t|^{-2\nu} \equiv |t|^{-\gamma}. \tag{4.19}$$

So we see that by measure the critical behavior of D or I, we can obtain the exponent ν_π and γ_π (by definition, K^- is proportional to the isotherm compressibility).

In the above, we have used the assumption that the critical behavior of the shear modulus is similar of stronger (bigger exponent) than that of the bulk modulus. Our assumption is justified by the following,

- Near the critical point, the local network density fluctuates. The elastic property of the network is determined by the dilute parts of the network (weaker areas). So near the critical point, both K and μ goes to zero.

- Our critical temperature measured during the critical isobar, specific heat, and the collective diffusion constant are 33.52 °C, 33.32 °C, and 33.52 °C respectively. Within the experimental error, these values are essentially the same. This is in contradictory with the basis of Onuki's assumption (He used the result that there is $1°C$ difference in the critical temperatures measured by isobar and the light scattering, which we believe was due to the fact that the experiment was not conducted under equilibrium).

4.3 Experimental Results

The sample we used is the same as the ones used in the experiments in chapter 2 and 3 (they all come from one big gel). The sample, with linear size of 8mm, was immersed in water in a quartz optical cell with side $\sim 10mm$. The cell temperature is

regulated down to a fraction of 1mK. The details about the control of the temperature is described in appendix A.

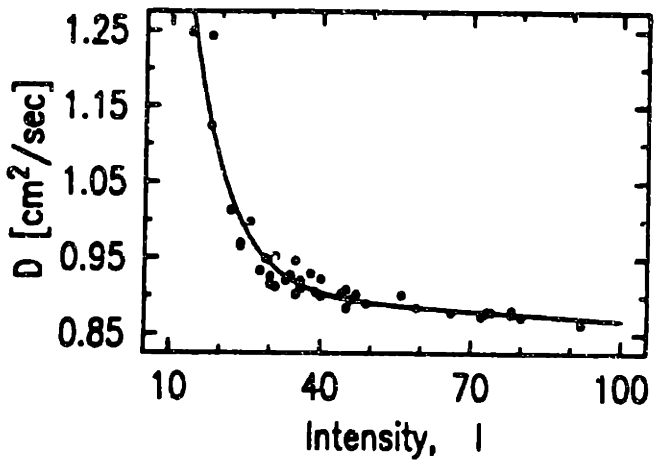

Figure 4.4: Relation between the collective diffusion constant and the scattered light intensity.

We have shown recently that there are inhomogeneities inside the gels (Sun 1989, also chapter 6 of this thesis). The intensity of the scattered light is position dependent. During the experiment, we discovered that the diffusion constant D is closely related with the scattered light intensity. Figure 4.3 shows the relation between them (the details can be found in chapter 6). This relationship can be explained satisfactorily by assuming the inhomogeneities behaves as local oscillators. So the correlation function is a heterodyne function with the reference beam intensity position dependent. The lowest value of D corresponds to the 'pure' heterodyne correlation function. So the way we measured the diffusion constant D is by measuring many D's at different position, take the smallest D as our experimental result. The temperature dependence of the D obtained this way is plotted in figure 4.5. The average waiting time between two temperature points is 4.2 days to ensure the equilibrium.

From figure 4.4, we find that the critical behavior of D started much further away from the critical point compared with the specific heat behavior. We have fitted the

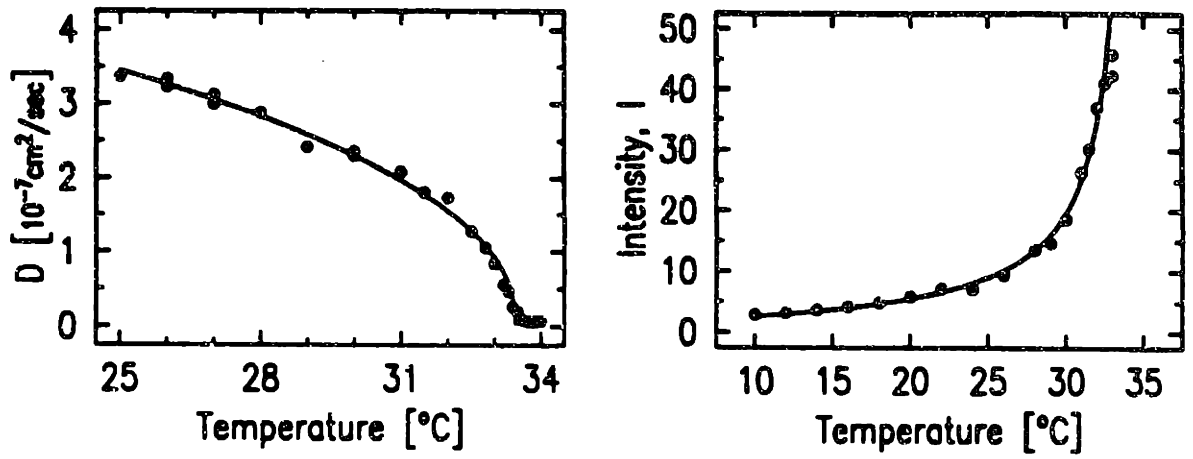

Figure 4.5: [a] Collective diffusion constant D and [b] scattered intensity I as a function of temperature.

data by a simple function

$$D = \begin{cases} A + B(1 - T/T_c)^{\nu_\pi} & \text{for } T < T_c \\ A & \text{for } T > T_c. \end{cases} \tag{4.20}$$

Our result is

$$\nu_\pi = 0.45 \pm 0.07. \tag{4.21}$$

Similar procedure performed on the scattered intensity data resulted

$$\gamma_\pi = 0.90 \pm 0.25. \tag{4.22}$$

Using the value of the critical exponents β and δ we have obtained in chapter 2 and 3, we find

$$\nu = 0.67, \tag{4.23}$$

$$\gamma = 1.3. \tag{4.24}$$

These are in good agreement with other known Ising systems.

4.4 Summary

- Collective diffusion constant D had been measured as the critical point is approached. From this experiment, we obtained the correlation length exponent $\nu_\pi = 0.45 \pm 0.07$.
- Intensity of the scattered light diverges as we approached the critical point. The isotherm compressibility exponent $\gamma_\pi = 0.9 \pm 0.25$.
- From D and I, we find that the friction coefficient f goes to zero at the critical point with an exponent ~ 0.45 along the isobar.
- Our results indicates that the critical behavior of the shear modulus μ is similar to that of the the bulk modulus. This is in contradictory with Onuki's assumption.

Chapter 5

Summary of the Gel Criticality

α_π	δ	ν_π	γ_π
-0.05±0.13	4.2±0.5	0.45±0.07	0.9±0.25

Table 5.1: Critical exponents of N-isopropylacrylamide gel measured along the critical isobar path.

In table 5.1, we summarized all of the exponents we measured from N-isopropylacrylamide gel network system. These exponents are measured along the critical isobar curve (hence the subscript π), which is different from the conventional path. The critical isobar path was achieved by choosing the gel that has the critical point right on the $\pi = 0$ path.

Table 5.2 compares the the conventionally defined critical exponents of the gel systems derived from table 5.1 with other known Ising systems. Can we conclude that the gel system is in the Ising universality class ? To answer this, we have to know how can one decide if a system in certain universality class or not.

system	α	β	γ	Δ
3-d Ising	0.11	0.31	1.25	5
Co_2	0.12	0.3447	1.2	4.2
Xe	0.08	0.344	1.203	4.4
Gel	-0.05	0.4	1.3	4.2
Gel	0.09	0.36	1.3	4.2

Table 5.2: Numerical calculations of the critical properties (Bagnuls and Bervillier 1985).

Within each universality class, there are many universal quantities, including some exponents, ratio of some amplitudes, combination of amplitudes and exponents, etc. Ideally, if one can experimentally show that all the measured universal quantities are the same as the corresponding quantities of a known universality class, then we say the system belongs to this universality class. Another way is to approach the problem from the theoretical point of view. If one can show that the Hamiltonian of two systems are virtually identical (can be mapped on to one another with simple variable change), or the flow diagrams have the same behavior, then we can also conclude that the two systems are in the same universality class. One example of this is the mapping between Lattice-Gas and Ising system demonstrated by Lee and Yang (1952).

Table 5.3: Numerical calculations of the critical properties (Bagnuls and Bervillier 1985; Bervilier 1986).

n	α	β	γ	δ	A_+/A_-
1	0.1106(21)	0.3243	1.2407(12)	4.826	0.524
2	-0.0066(30)	0.3453	1.3160(20)	4.811	1.029
3	-0.1142(27)	0.3639	1.3864(28)	4.810	1.521

Table 5.3 are the numerical results obtained by Bagnuls and Bervillier for a n-vector system (n=1, Ising; n=2, X-Y; n=3, Heisenberg). Considering the experimental errors one usually encounter, the most sensitive quantities (arguably) are the exponent α and the amplitude ratio of the specific heat, which varies from -0.11 to 0.11 and 2 to 0.5 respectively. fortunately our experimental result of α_π has a big error and no information can be obtained from the amplitude ratio along the isobar path (guaranteed to be unity).

There is another important factor in determining the universality class of a system, that is, the identification of the order parameter. In the case of gel, the phase transition is characterized by the volume fraction (density) of the network. So the order parameter is a scalar. Based on this observation and our experimental exponents, we conclude that the gel system is an Ising like system.

There are many factors that contribute to the error bars of our results. In the case of the specific heat experiment, the small filling factor of the sample probably contributes the most.

Chapter 6

Gel Inhomogeneities

6.1 Introduction

The inhomogeneities of the gel network system has been noticed and studied for more than a decade. It has been very bothersome from the light scattering experiment point of view. But it is very important from both the theoretical and application point of view to understand the cause of the inhomogeneities. In this chapter, we discuss the inhomogeneities of the gel network structure. The content of this chapter is directly related with the measurements presented in chapter 4. The understanding of the inhomogeneities may help us to understand the oscillation of the scattered light intensity which will be presented in the next chapter.

Using a further simplified model derived from the hetero-structured network model shown in figure 6.1, Weiss, van Vliet and silberberg successfully explained the permeability of acrylamide gel as a function of chemical composition (Weiss and Silberberg 1975; Weiss, van Vliet and Silberberg 1979). Hsu and colleagues examined the effects of inhomogeneities of polymer network on the swelling equilibrium of acrylamide gels and on the diffusion of water molecules within the gels (Hsu 1983). The ring structures and intramolecular chemical reactions during gelation were studied by Standford

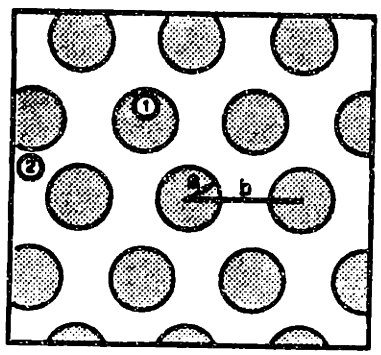

Figure 6.1: Two-phase structure of heterogeneous gel (schematic). The spheres are high concentration regions (both in monomer units and crosslinkers). The flow path is mainly in the dilute region.

and Stepto (Standford and Stepto 1981). They found that the shear moduli of the polyester and polyurethane gels were reduced markedly in the presence of elastically inefficient network loops. Funke reviewed several different polymer networks with non-uniform cross-links (Funke 1983). Recently Martin and Wilcoxon (1989) had studied the spatial correlations and the growth in dilute gels near the sol-gel transition and also encountered the inhomogeneity problem. They concluded that the cause of the inhomogeneity as quenched randomness produced by the reaction of diffusion clusters. To obtain good quality data, they found that it was necessary to average over 50 scattering volumes to average out the inhomogeneity effect. S. T. Sun, Y. Li, T. Tanaka and E. Sata-matsuo also studied the inhomogeneities of gels far above the sol-gel transition in N-isopropylacrylamide and acrylamide gels (1989). They concluded that the inhomogeneities of the gel network with concentration far above the sol-gel threshold (Bansil and Gupta 1980) are caused by the thermal fluctuation and phase separation of the pre-gel solution.

Our study presented here is a further study of the gel inhomogeneities. In this chapter, we will discuss the temperature and chemical composition dependence of the inhomogeneities of gels. We will also discuss the dynamic aspect of the inhomogeneities probed by dynamic laser light scattering spectroscopy, which agrees with the model proposed by Weiss and colleagues (figure 6.1). We also report another

proper way of obtaining information from a gel network light scattering spectroscopy (instead of averaging over 50 scattering volumes). The use of this method is demonstrated by our measurement of the critical exponents ν_π and γ_π presented in chapter 4 of this thesis.

This work was initiated by Dr. Shao-Tang Sun several years ago. He observed the dependence of the inhomogeneities of the network on the gelation temperature. We continued this work and more information about the network inhomogeneities have been obtained. The samples we have used here are mainly N-isopropylacrylamide gels, which is different than Sun's (acrylamide gel). The author of this thesis is very grateful to Dr. Sun's permission of using all the data freely.

6.2 Experimental Method

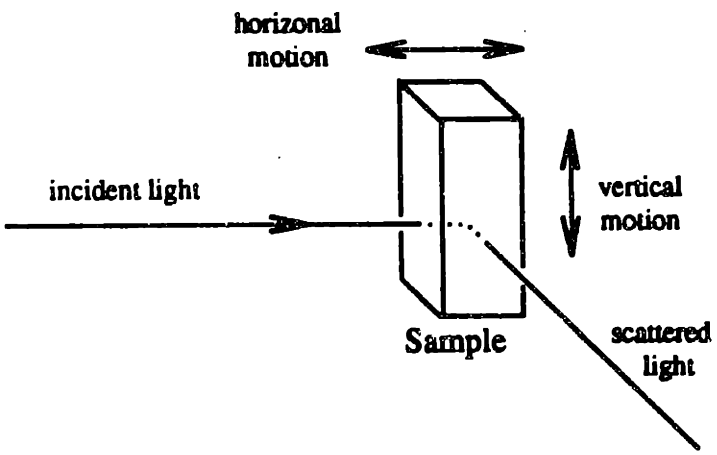

Figure 6.2: Schematic experimental setup. The sample can be moved either parallel with the incident beam or be moved vertically. The experimental results from these two movements are the same within the experimental resolution.

In our experiment, the basic setup is the same as the one described in chapter 4 and in the appendix A. Figure 6.2 is a schematic representation of our experimental method. Figure 6.3 demonstrates the scattered intensity as a function of position. There are two spectra in this figure. The intensity is collected while the sample is moved step

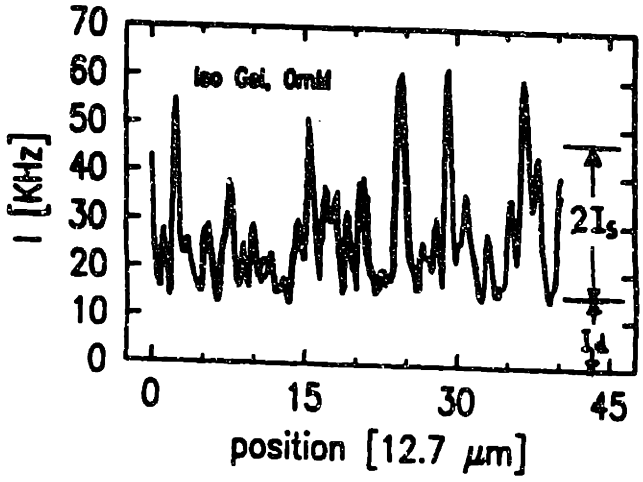

Figure 6.3: The scattered light intensity from an ISO gel. The measurement temperature is 10 °C. The reproducibility of this phenomenon is obvious.

by step by the translator (half turn every five seconds). The second spectrum in figure 6.3 was taken right after the first one had finished. The reproducibility of the spectrum is obvious. We also can move move the sample by a syringe pusher with a continuously variable speed. The intensity was read by the computer every one second.

The scattered intensity can be decomposed into two parts, as shown in figure 6.3. One is scattered from the dynamic thermal fluctuation of the network, which give rise to the minimum non-zero intensity I_d. The other, I_s, is scattered by the static inhomogeneities, responsible for the up and down intensity fluctuations. Experimentally, I_s is the variance of the intensity, I_d is the average of the minima of the spectrum (I_d can also be defined as the difference between the mean and the variance).

6.3 Temperature Dependence of the Inhomogeneity Amplitude

The temperature dependence of the scattered light intensity (inhomogeneity amplitude) is illustrated in Fig.6.4. There are two temperatures enter this problem. One

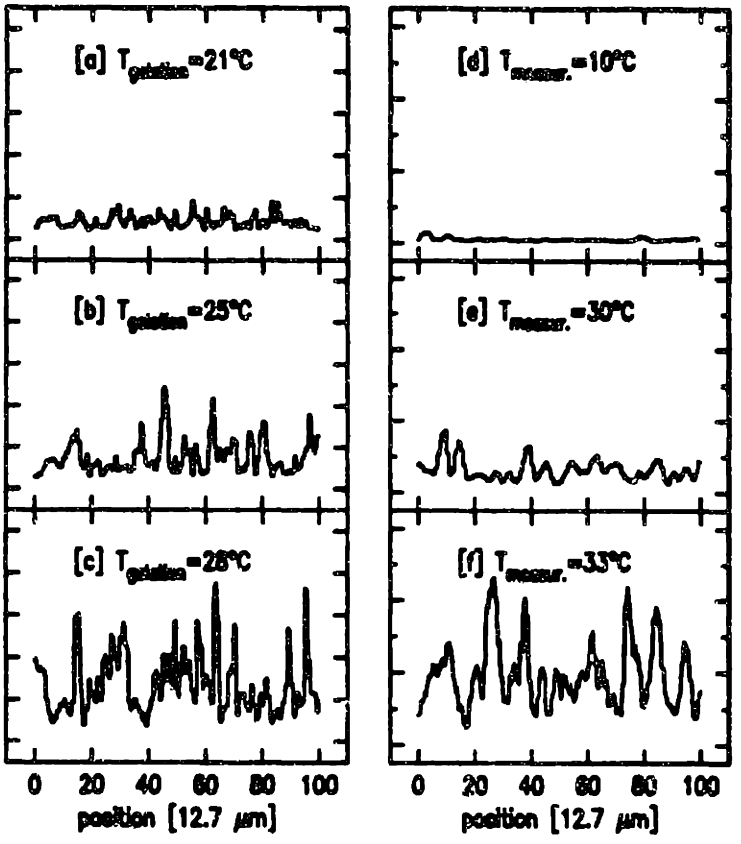

Figure 6.4: Position dependence of the scattered light intensity from an N-isopropylacrylamide gels are shown as a function of gelation temperature (a, b and c). The measurement temperature was 10 °C. On the right side (d, e and f), the position dependence are shown for different measurement temperatures, but for the gelation temperature of 0 °C.

is the gelation temperature (the temperature at which the gel is made) and the other is the measurement temperature.

6.3.1 Gelation Temperature

In our experiment, the gelation temperature is controlled by water circulator with temperature stability ±0.05 °C. Because of the fact that the gelation process of the ISO gel is an exothermal process (releases heat), in principle, the gelation temperature will be higher than the temperature regulator used to regulate the gelation temperature. However, with rectangular cells as thin as 0.7mm, and gelation process as slow as 10 minutes, we still observed the total opacity (white) of all the gels formed at

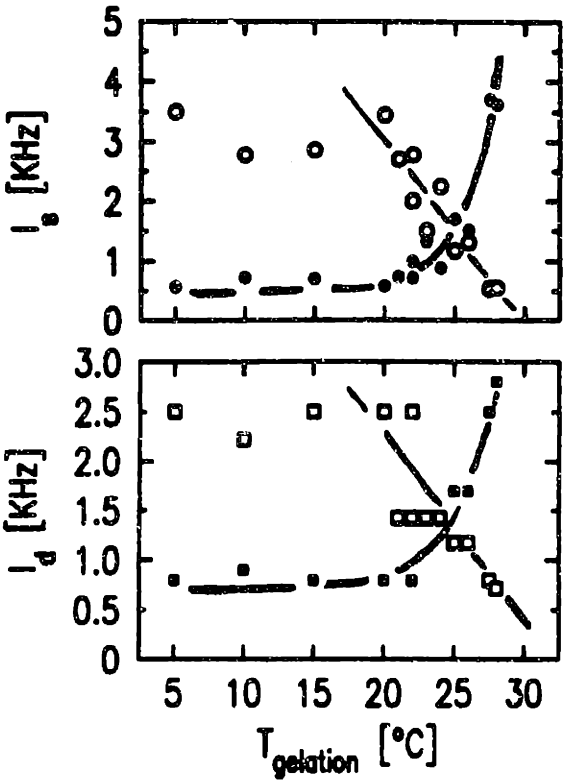

Figure 6.5: Gelation temperature dependence of the scattered light intensity from the static inhomogeneities (I_s) and dynamic fluctuations (I_d) of the network.

temperature higher than 28.5 °C. This indicates that the critical temperature of the late-stage pre-gel solution is several degrees lower than that of the bulk gel (33.5 °C). We shall call this temperature the critical temperature of the pre-gel solution.

The measurement was performed at 10 °C. From figure 6.3a, 2b and 3c, it is apparent that the scattered intensity is strongly gelation temperature dependent. These results can be interpreted as due to the thermal fluctuation and phase separation of the pre-gel polymer solution.

The gelation temperature dependence of the gel inhomogeneity can be understood as follows. When the gelation temperature is far from the pre-gel solution critical temperature, the fluctuation of the pre-gel solution is very small, giving fairly homogeneous network as the final product. On the other hand, when the gelation temperature is very close to the pre-gel solution critical temperature, in the later stage of the gel-formation process, many big polymers and small network pieces ex-

ist. The critical temperature of these big polymers (and network pieces) is very close to the gelation temperature, resulting big fluctuations in the polymer distribution. The final result is a highly inhomogeneous gel network.

The average intensities of the scattered light intensity I_d and I_s are shown in figure 6.5. Because of the formation of the inhomogeneities, we expect the dynamic fluctuation of the network will also be affected. Indeed, in figure 6.5, we find that the dynamic fluctuation grow larger near the critical point as well.

6.3.2 Measurement Temperature

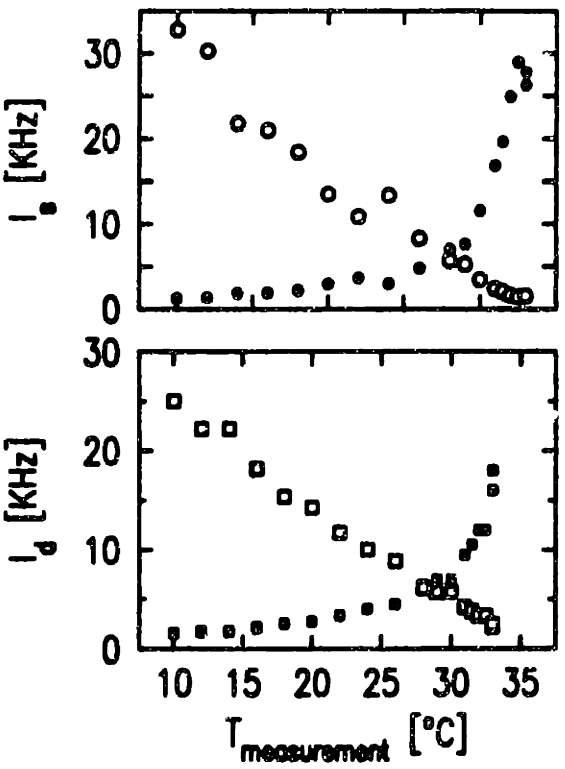

Figure 6.6: Measurement temperature dependence of the scattered light intensity from the static inhomogeneities (I_s) and dynamic fluctuations (I_d) of the network.

The measurement temperature dependence of the scattered light intensity is shown in figure 6.4 (d, e and f) and summarized in figure 6.6. The sample was made at 0 °C (ice water). As the measurement temperature approaches the critical temperature, both the intensities scattered from the static inhomogeneities, I_s, and the dynamic thermal fluctuations, I_d, diverge. The divergence of I_d can be understood as the

critical fluctuation of the network. The divergence of the light intensity scattered by the frozen inhomogeneity, I_s, however, is not trivial. In general, the scattering from the inhomogeneities, impurities, etc, does not have critical behavior. The fact that the scattered light intensity from the frozen inhomogeneities diverges at the critical point indicates that the structural inhomogeneities are very much 'alive'.

The critical behavior of the I_s indicates that the basic nature of the inhomogeneities is the same as the rest of the network. They can not be due to things like dusts or sparkles.

6.4 Temperature Dependence of the Spatial Distribution

From figure 6.3 and 6.4, we noticed that there is a characteristic width and average distance between two peaks of the scattered light intensity. This width and distance is usually several times larger than the biggest steps of the motion of the sample, which is $12.7\mu m$ (0.5 mil). So this width can not be due to the limitation of the motion or the light beam size. We have also tried to vary the pin hole in front of the detector, but found no appreciable difference. From these observations, we conclude that the width and the rage distance of the peaks reflect the domain size of the inhomogeneities. These linear dimensions may correspond to the dimensions in Weiss's model shown is figure 6.1. It is very important to understand the origin of these dimensions to have a thorough understanding of the network structure.

6.4.1 Gelation Temperature

The way we analyzed the scattered light spatial spectra is by calculating the correlation function $C(r)$,

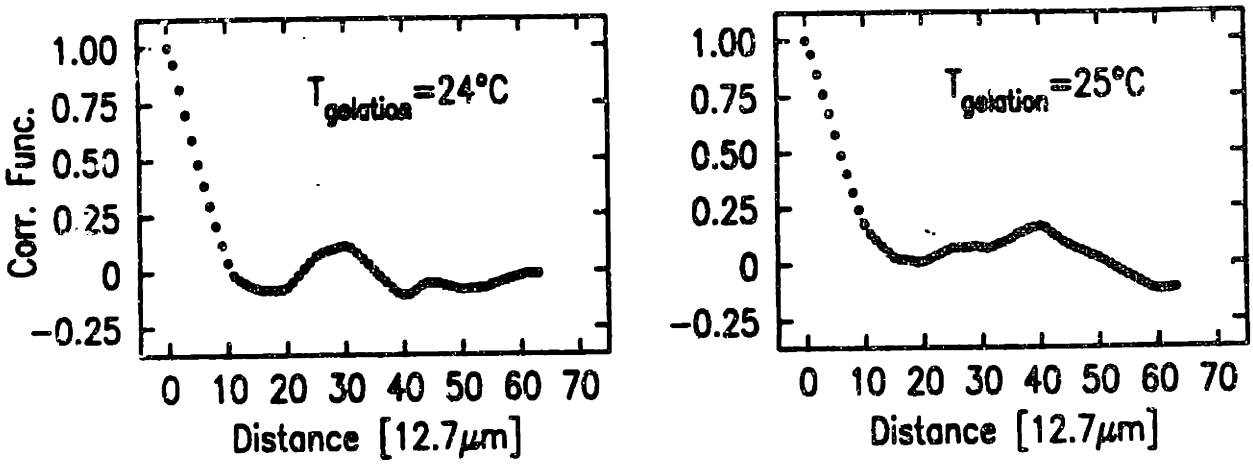

Figure 6.7: Two typical correlation functions of 1000 channels spectra with window width 64 channels wide. They are the samples made at 24 and 25 °C, respectively. The details in the tail is due to the randomness of the inhomogeneities.

$$C(r) =< I(r)I(0) >, \tag{6.1}$$

where r is the distance between two points, brackets <> represents the ensemble average. The correlation function is calculated by a computer program (not an electronic correlator). We defined the correlation length here as the distance corresponds to the half height value of the correlation function. The position of the base line of the correlation function is often quite apparent. For a spectrum with peaks randomly distributed, the width of the correlation function reflects the half width of the average peaks.

Two typical correlation functions are given in figure 6.7. The details of the tails of these correlation functions are totally random. The gelation temperature dependence of the correlation length is plotted in figure 6.8. From this figure, we find that, unlike the amplitude of the scattered light intensity, the spatial distribution of the

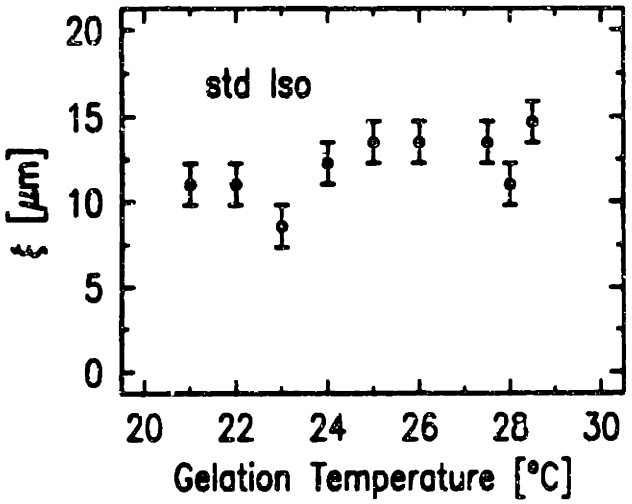

Figure 6.8: Correlation length as a function of gelation temperature.

inhomogeneities is insensitive to the gelation temperature. The correlation length from figure 6.8 is about $25\mu m$. The error here is very big, because we did not have enough statistics.

6.4.2 Measurement Temperature

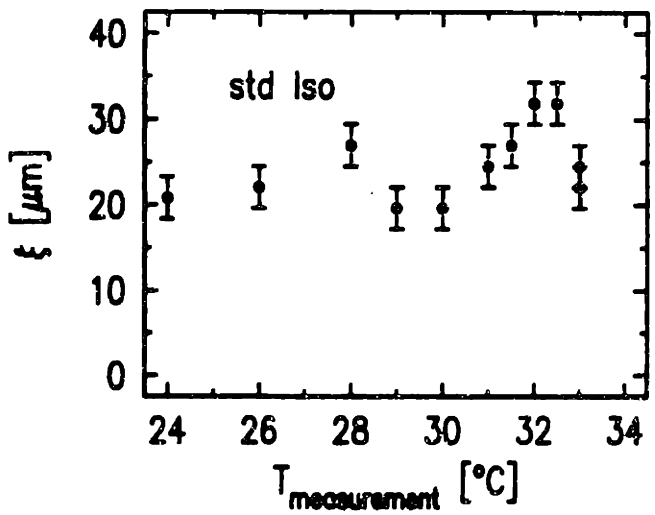

Figure 6.9: Correlation length as a function of measurement temperature.

The temperature dependence of the correlation length has been extracted in the same way as has been described above. The result is plotted in figure 6.9. The experimental value of the correlation length plotted in figure 6.8 and 6.9 are similar.

Obviously more average is need to achieve better results.

6.5 Chemical Composition Dependence of the Spatial Distribution

Am	Bis	AP	Temed
$0.58 \sim 2$	$0.05 \sim 1$	$0.5 \sim 2$	$1/128 \sim 1$

Table 6.1: Variation of the chemical components. When one chemical is varied, all the others are kept at their standard concentration.

The chemical components effect of the inhomogeneities are also studied. In this experiment, we varied all the chemical components. Table 6.1 is a list of what we have done.

6.5.1 Bis dependence

The result here is obtained in collaboration with Terence Hwa, a co-student of the thesis author. The bisacrylamide dependence of the correlation length is plotted in figure 6.10.

In this experiment and the ones that below, we used a gear box to push the sample slowly and continuously. The speed of the gear box was set at $5.9\mu m/sec$ in this experiment. For each sample, twenty spectra were taken. Each point in figure 6.10 is obtained from a correlation function which is the average of twenty individual correlation functions.

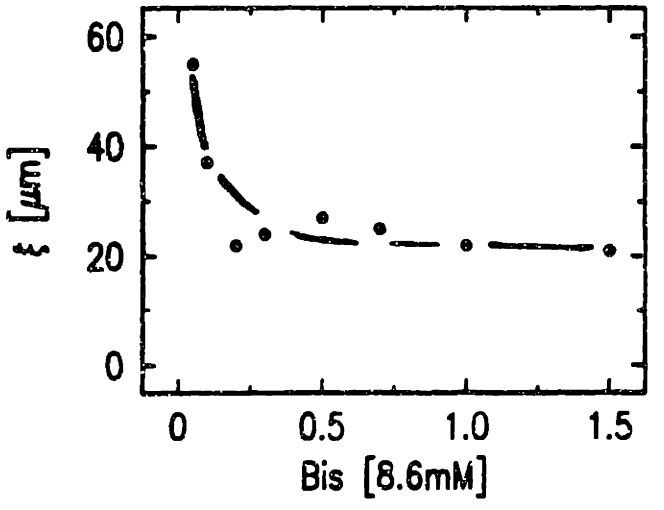

Figure 6.10: Correlation length as a function of the cross-linking molecules concentration.

From figure 6.10, we noticed that the correlation length diverges at the gelation threshold, which is well known (for instance, de Gennes 1979). Away from the threshold, however, the correlation length is almost independent of the concentration of the cross-linking molecules. The average correlation length far from the gelation threshold is about $23\mu m$.

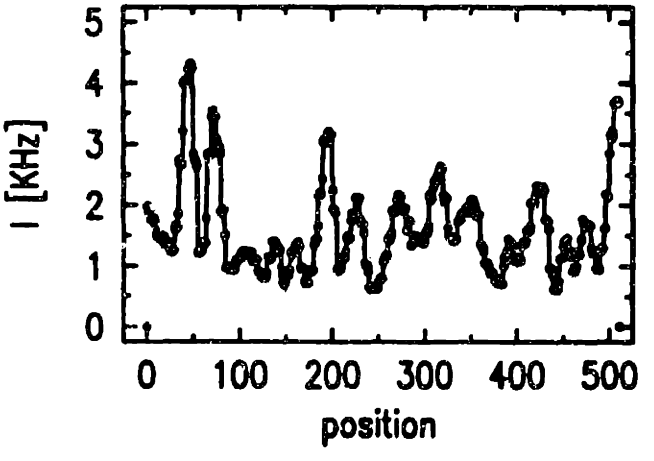

Figure 6.11: Original spectrum (curve) and the spectrum calculated from the spectrum of the fourier transformation. Just for testing purpose.

We also performed Fast Fourier Transformation on our data (figure 6.11). The correlation function and the fourier transformation is related,

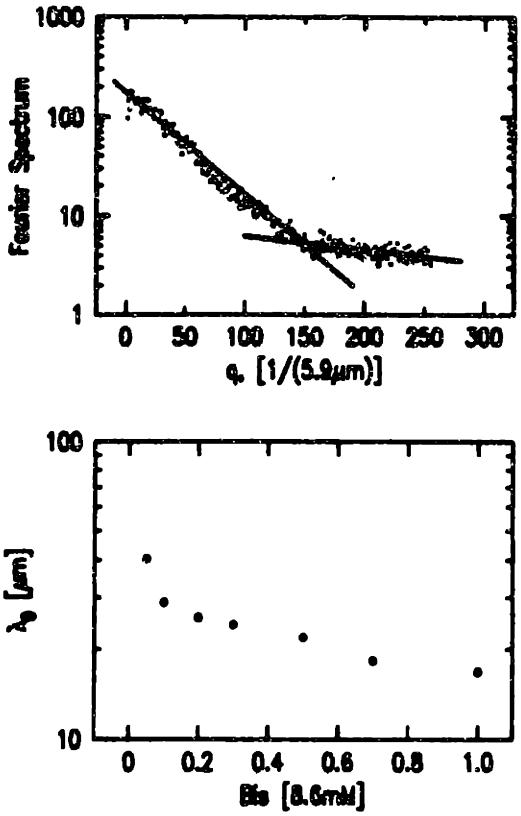

Figure 6.12: [a] Fourier spectrum of the sample with bis=0.86mM. [b] Cross-over length λ_0 as a function of cross-linking molecules.

$$C(r) = \int dq |I(q)| e^{-iqr}, \tag{6.2}$$

where q is the spatial wavevector (not to be confused by the scattering wavevector).

Figure 6.12a is a typical fourier spectrum. We observed double exponential type behavior. The cross-over length λ_0 is plotted in figure 6.12b.

Figure 6.12 may be explained as follows. Intuitively, we expect that the smallest structure corresponds the width of the peaks, the fourier spectrum should be fairly flat in the region smaller than the peak width. On the other hand, since the peaks are randomly distributed, we expect the intensity of the fourier spectrum decreases as the frequency (q in this case) increases. These are exactly what we have in figure 6.12a. The corss-over wavelength λ_0 corresponds the width of the peaks. As we expected , λ_0 increases as the gelation threshold is approached.

6.5.2 Other Chemicals

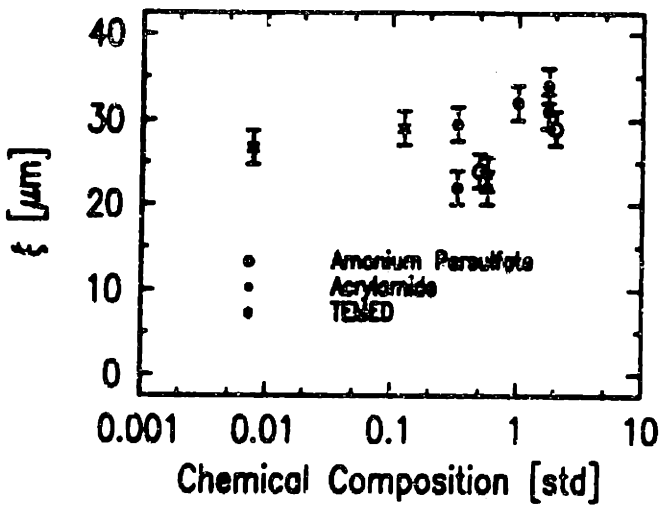

Figure 6.13: Correlation length dependence on other chemicals, including monomers (acrylamide), free-radical initiators (amonium persulfate), and the reaction accelerator (TEMED).

The chemical dependence of the correlation length on other chemicals are plotted in figure 6.13. We find that the correlation length is not sensitive to any of the variations of the chemical composition. This may be largely due to the lack of the enough statistics.

6.6 Dynamic Aspect of the Inhomogeneities

6.6.1 Experimental

The study of the dynamic aspect of a system can often provide important information about the system. We have study the inhomogeneities of the network system by dynamic laser light scattering spectroscopy. Figure 6.14 shows that not only the static quantity I, the scattered intensity, is a function of the position of the scattering volume, but also the dynamic quantity D, the collective diffusion constant. In figure 6.14, the scattered intensity and the auto-correlation function were measured simultaneously. The sample is a N-isopropylacrylamide gel. The measurement temperature was 33°C and the measurement was conducted after the sample has reached

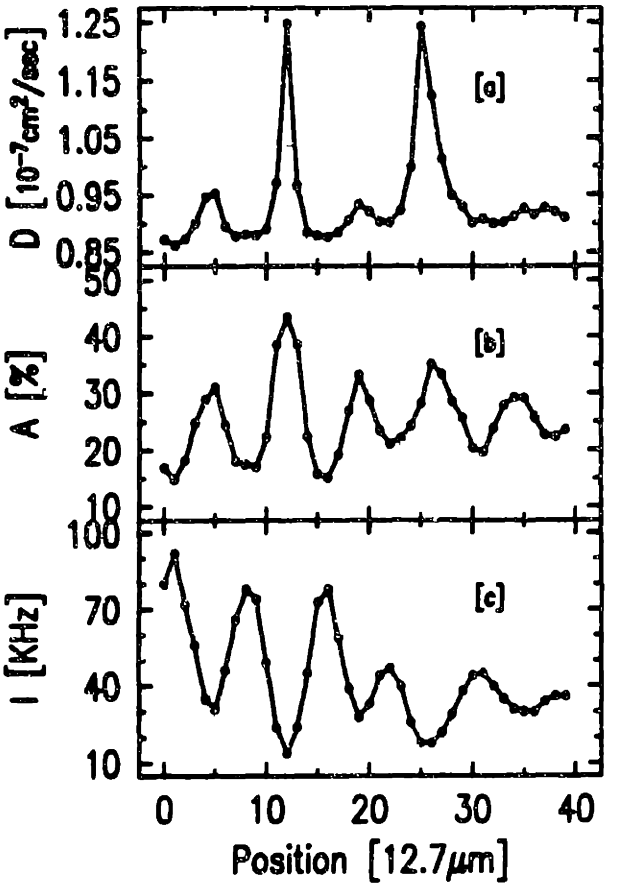

Figure 6.14: Demonstration of the inhomogeneity effects. The sample was moved parallel with the incident light, $12.7\mu m$ per step. (a) Collective diffusion constant D from single exponential fit. (b) Signal to background ratio A. (c) Total scattered intensity from the sample.

equilibrium. During each data measurement, the intensity of the scattered light varied more or less, but all the data point were taken in long enough time so that the actual average was taken. A single exponential function was fitted to the correlation functions,

$$G(t) = G_0(1 + Ae^{-Dq^2t}). \tag{6.3}$$

Where A is the signal to background ratio. The quality of the fit is indicated by the maximum residual R, defined as

$$R = max\left\{\left|\frac{G_{data} - G_{fit}}{G_{data}}\right|\right\}. \tag{6.4}$$

Fig. 6.14a is the spatial distribution of the local collective diffusion constant. Notice the fact that the value varies by as much as 50%. The Fig. 6.14b is the auto-

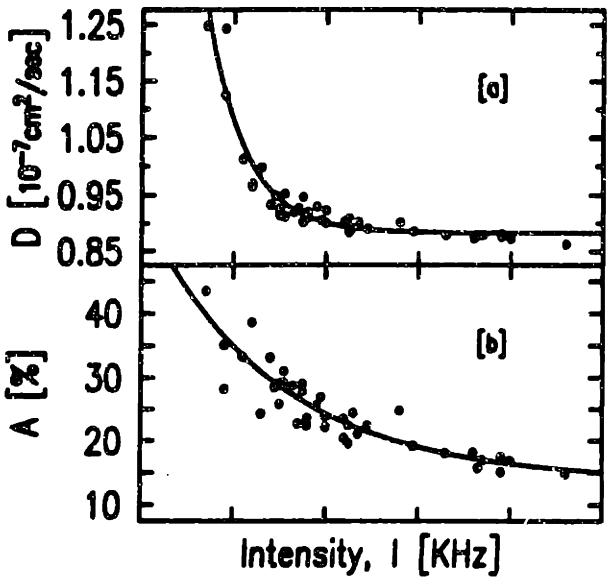

Figure 6.15: Relation of the signal to background ratio A and the collective diffusion constant D with the scattered light intensity I.

correlation signal to background ratio A, which varies by as much as a factor of 2. Fig.6.14c is the scattered intensity. It is not hard to notice that whenever there is a peak in the intensity, the D and A are in their minimum. Fig. 6.15 is a replot of Fig. 6.14. It is clearly shown that the relations among these quantities are very well defined.

6.6.2 Analysis

First, we noticed that the spatial separation of these peaks are about $\sim 50\mu m$, or in another words, there are domains within the gels with linear size $\sim 50\mu m$. This is a very large number compared with the length scale of the network pore size $\sim 10^{-2}$–$10^{-1}\mu m$, which can be estimated from the chemical ingredient of the network. Within each domain, there are roughly 10^8 network chains (defined as the piece connecting two adjacent crosslinkers). In Sun's paper (1989), the inhomogeneities were argued as caused by the pre-gel solution thermal fluctuation and phase separation. We

checked the gels made at different temperatures and found no significant domain size difference. (The domain sizes stay almost the same as the measurement temperature is changed. This is because within the measurement temperature range, the size of the gel changes only by a small amount). This result does not support the argument given by Sun, et al. Maybe this is because our temperature range is not wide enough. Here, we propose another possible reason for the cause of the domains. Started from some seeds, branched polymers started to grow and form some local isolated network. These networks grow bigger and bigger and eventually will be in contact with each others. Two things can happen, provide given enough monomer units. One is that the networks just keep growing and penetrate into each other and become structurally connected, the other is that the live ends of different networks meet and become chemically connected. We consider the first gelation mechanism to be the dominate mechanism. Depending upon the amount of monomers given, various kind of domains can form. If the amount is such that the networks just barely touch each other, then the domains are basically just the networks themselves. If the amount is big enough to allow deep penetrations of the chemically individual networks, then the gel should be more homogeneous. In between these two limits, situations can be complex. At this stage, due to the limitation of detailed knowledge about the gelation process, it does not make sense to try to get into the details.

According to Weiss (1979), the variation of the relative network substance in the two phases (figure 6.1) is fairly small, about a factor of 2 (more in the dense region). The ratio of the dense domain to the dilute domain is $2^{1/3}$, or 1.26, which is comparable within our experimental error. This maybe the reason why we did not observe any chemical composition dependence of the correlation length.

This domain assumption above does not exclude Sun's argument. In fact, if we adopt both argument, we can explain both the intensity dependence and the domain size independence on the gelation temperature. As each individual network

forms, the thermal fluctuation and phase separation effects freezes into the network. These fluctuations within each network has a smaller length scale and is temperature dependent, reflected by the laser light scattering results.

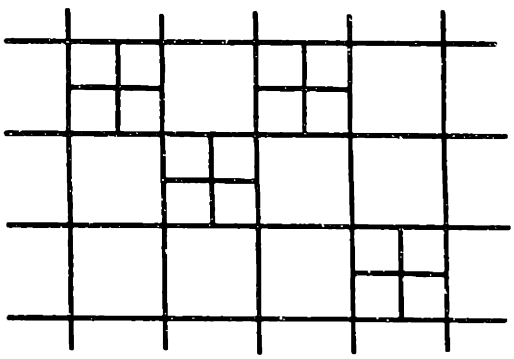

Figure 6.16: Grid simplification of the gel network structure.

We know that for the same incident light intensity and the scattering angle, the intensity of the scattered light depends solely on the fourier component of the density fluctuation corresponding the scattering angle. This component in turn is contributed by two factors. One is the phase structure of the density fluctuation, the other is the overall density (or the total number of the scatterers) of the scattering volume element, which appears as a multiplication factor. So there are two possible reasons for the scattered light to reach a maximum. But the collective diffusion constant is independent of the phase of the local fluctuation and is dependent on the structure of the network. The strong correlation between the scattered intensity and the collective diffusion constant tell us that the cause of the spatial variation of these quantities can only be the density variation. We are going to adopt a simplified picture to illustrate the basic structure of the network. Replace the polymer chain by a straight line, we picture the network as a 3-d square grid with different grid sizes from place to place(Fig.6.16). Now let us make the following assumptions,

1) Inside the network, there exist 'dead' spots that act like local oscillators;

2) There are much more of these spots in the denser regions than in the diluter regions.

With these assumptions, we can explain the results in Fig.6.14 and Fig.6.15. To understand these results, we should go back to the basics of the auto-correlation of the scattered light. In general, there are two types of auto-correlation techniques. One is the homodyne mixing, the other is heterodyne mixing (Berne and Pecora 1976). In the case of homodyne correlation, scattered light correlate with itself, whereas in the case of heterodyne correlation, the scattered lights correlate with a portion of the unscattered light (reflected by local oscillator). Because of the existence of the local oscillators, the light intensity correlation function should be written as

$$G(t) =< |E_L(0) + E_S(0)|^2 |E_L(t) + E_S(t)|^2 > . \tag{6.5}$$

Where E_L and E_S are the scattered electric field from the local oscillators and the network, respectively. Notice that in the limit of $E_L = 0$, we get a pure homodyne correlation function. The equation 6.5 above has 16 terms in it. Among them, 10 are zeros.

Define

$$g_1(t) = < E_S(t) E_S^*(0) >, \tag{6.6}$$

$$g_2(t) = < E_S(t) E_S^*(t) E_S(0) E_S^*(0) > . \tag{6.7}$$

Then equation 6.5 can be written as

$$\begin{aligned} G(t) &= {I_L}^2 + 2 I_L I_S + 2 I_L I_S g_1(t) + {I_S}^2 g_2(t) \\ &= (I_L + I_S)^2 + 2 I_L I_S g_1(t) + {I_S}^2 {g_1}^2(t). \end{aligned} \tag{6.8}$$

Where I_L and I_S are the light intensities. The above equation is obtained by using

$$g_2(t) = 1 + {g_1}^2(t). \tag{6.9}$$

Assume

$$g_1(t) = e^{-Dq^2t}, \tag{6.10}$$

then we can write

$$G(t) = (I_L + I_S)^2 + 2I_L I_S e^{-Dq^2t} + {I_S}^2 e^{-2Dq^2t}. \tag{6.11}$$

From eq. (6.11), we know that in general the correlation function is a multi-exponential function. In the limit of $I_L \gg I_S$, we have a heterodyne correlation function

$$G(t) = {I_L}^2(1 + 2\frac{I_S}{I_L}e^{-Dq^2t}), \tag{6.12}$$

and in the limit of $I_S \gg I_L$, we get the homodyne correlation function

$$G(t) = {I_S}^2(1 + e^{-2Dq^2t}). \tag{6.13}$$

From the above two equations, we know that the apparent diffusion constant from the homodyne mixing is bigger than that from the heterodyne mixing by a factor of 2. When the scattered light from the local oscillator is large, the total scattered intensity will be large, and the second term will dominate over the third one, so we get a smaller effective diffusion constant, as we have observed in Fig.6.14a.

The signal to noise ratio A defined in eq.(6.3) can be written as

$$A \equiv \frac{2I_L I_S + {I_S}^2}{(I_L + I_S)^2}. \tag{6.14}$$

When the scattered light from the local oscillator is large compared with I_S, the signal to background ratio decreases. This is exactly what we have observed in Fig.6.14b.

From Fig.6.14b, the value of A varies from about 50% to 15%. As A decreases from 50% to 15%, we expect to have a better and better single exponential fit to the correlation function. Fig.6.17 is the maximum residual of the fit plotted against the signal-to-background ratio A.

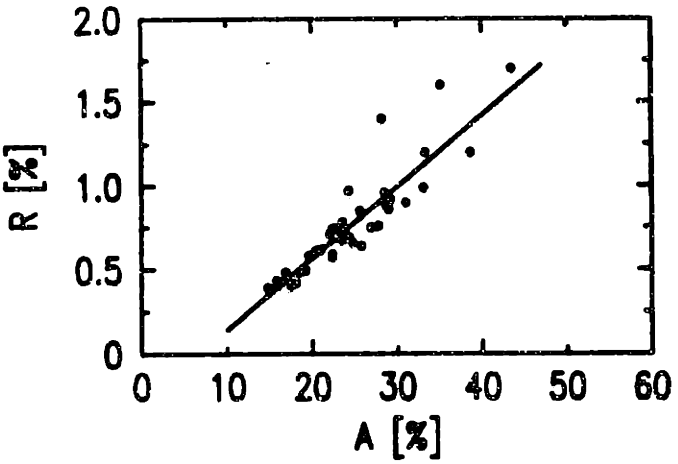

Figure 6.17: Maximum residual of the single exponential fit against the signal to background ratio A

6.7 Other Gels

The chemically cross-linked agrose gels and the gelatin gels have been studied as well (for sample preparation, see Amiya and Tanaka 1987). Although the agrose polymer gel is opaque and become polymer solution at high temperature, the chemically crosslinked agrose gel is clear for the whole experimental temperature range.

The inhomogeneities were also observed in these gels even at high temperatures (above the corresponding polymer gel melting temperature). At low temperature (say, room temperature), the inhomogeneities are reproducible. However, at high temperature (50 - 70°C), the scattering is very weak, the inhomogeneities are not reproducible. The scattered intensity changes with time for fixed sample position. We believe that these observations are caused by the dilute chemical crosslinks. At low temperature, the helical structure of the polymers enhances the crosslinks, make the network more strongly formed. When the temperature is above the melting temperature, the helical crosslinks disappear, leaving only the dilute chemical crosslinks. The network now is very mobile locally, due to the lack of enough crosslinks.

6.8 Conclusion

We did not observe any significant dependence of the correlation length on temperature and chemical composition. Much better statistics is needed to do so.

We have further confirmed the existence of the inhomogeneities of the gel network system. These inhomogeneities are domains with different density. The domain size is about $\sim 50\mu m$. The properties of each domain, like the collective diffusion constant D, longitudinal elastic modulus, the friction coefficient f, are different. We have attempted to argue that these domains are related with the individual networks formed in the early stage of the gelation process. A simplified grid picture was introduced to help visualize the network structure.

Finally, we would like to comment on the impact of the structure of the gel network on the laser light scattering spectroscopy. From the results we have presented above, we know that the data obtained from the laser light scattering on gels will have big variations from place to place. The proper way to extract meaningful information is to collect many data points from different portion of the sample under the same condition, then plot them as a function of scattered light intensity. The value obtained by extrapolating up to the scattered intensity equal infinite is the value you would obtain if the experiment were done by ideal heterodyne mixing technique. From our experience, the convergence of the data behaves well on the high scatted light intensity side.

Chapter 7

Oscillation of the Scattered Light

7.1 Introduction

In the course of studying the critical behavior of the gel system using light scattering technique, we noticed that the intensity of the scattered light from the sample fluctuates with very large amplitude as a function of time. A comparison with the scattered intensity from a polystyrene solution, confirmed the fact that the fluctuation was caused by the gel. Further study of this phenomenon revealed the richness of the information inside the fluctuation. We found that the scattered intensity not only fluctuates, but also oscillates and beats, with a wide range of periods, which are astonishingly slow. In fact, they were so slow that the attempt of explaining them by the known mechanical property of the gel was totally out of the question.

We still do not have a satisfactory explanation for this phenomenon. In this chapter, we will present in detail the experimental phenomenon and results. A tentative explanation will be given in the last section of this chapter.

For demonstration purpose, figure 7.1 is a typical result of the oscillation of the scattered intensity. Figure 7.1a and 7.1b is the intensity and the Fourier spectrum of the intensity, respectively. The sample here is a ISO gel with size smaller than the

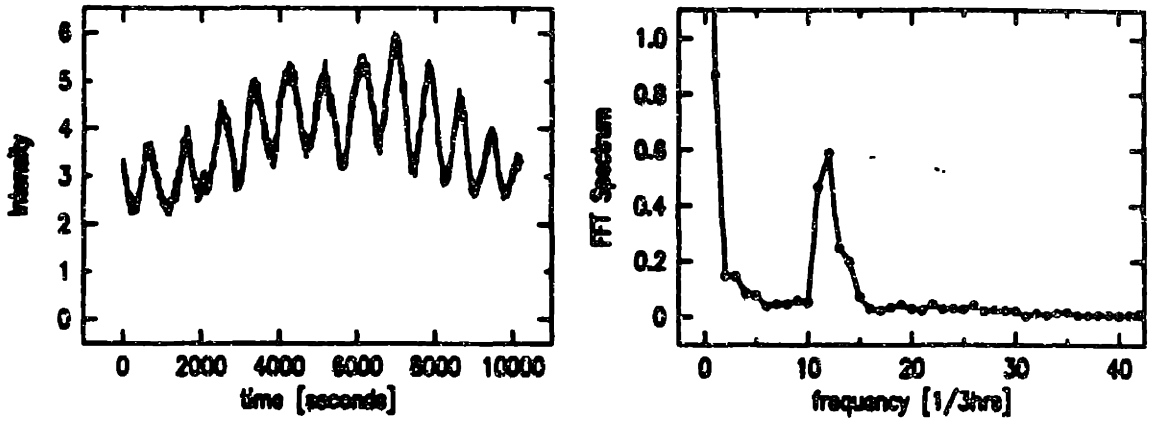

Figure 7.1: [a] The oscillation of the scattered light intensity as a function of time. [b] the Fast Fourier Transformation of the scattered intensity on the left.

optical cell that contains it (free of the wall constraint). The period of the oscillation in figure 7.1a is 13 minutes, or, the frequency is 1.3×10^{-3}Hz.

We would like to point out here that the oscillation can be observed when the temperature is far from the critical point. This indicates that the oscillation is not a critical phenomenon.

7.2 Experimental Observations

The experimental setup used in the experiments described in this chapter is the same as we have described in chapter 4 and chapter 6. The intensity of the scattered light is either collected by a flow chart recorder (in early experiments) or by a computer. All of the data were collected at 90° scattering angle. The temperature was controlled within a fraction of 1 mK per day (this is not very essential).

7.2.1 Basic Observation

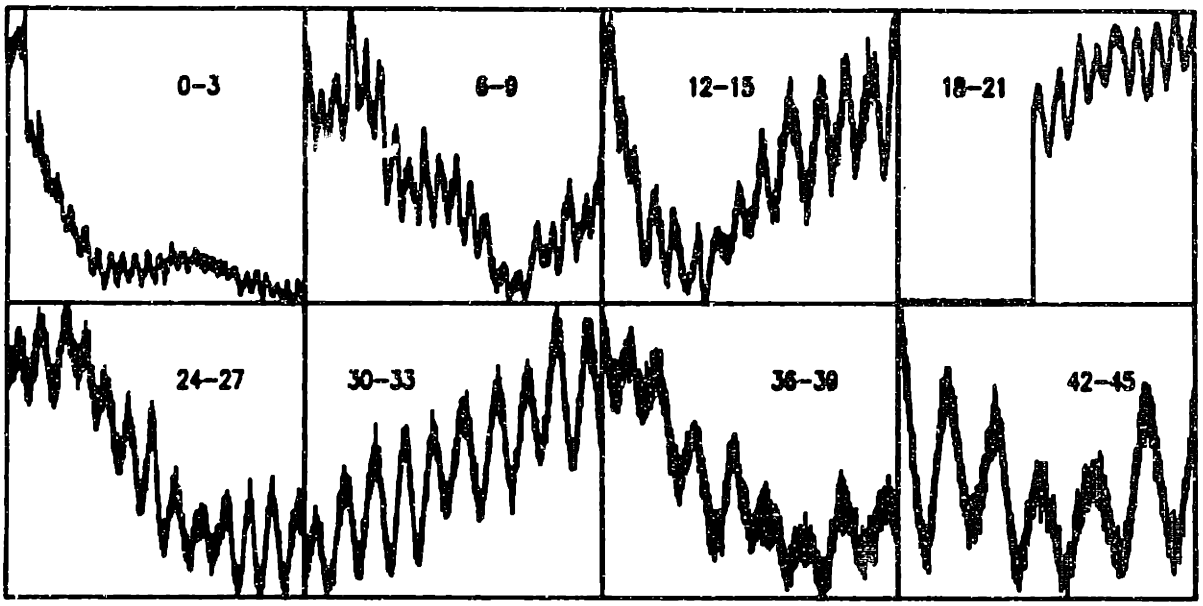

Figure 7.2: Typical scattered light intensity as a function of time for a long period. The temperature of the sample was changed from 25 °C to 26 °C at $t = 0$. The time interval of each frame is indicated by the numbers in the frame.

Figure 7.2 is a typical result of the scattered light intensity in a long time period after the temperature been changed at $t = 0$ from 25 °C to 26 °C. The time interval of each frame is indicated by the two numbers in the frame. Each frame is three hours long. The zero intensity is the fourth frame was due to the power off of the laser. The samples were made in a cylindrical tube first. Then was transferred in to a optical cell filled of water. The diameter of the gel in the experimental temperature range was always smaller than the inner diameter of the cell, so it is free from the wall constraint. The temperature of the sample container is changed at time zero. At the beginning, the scattered light intensity varies very fast, of the order of seconds, then becomes slower and slower. Eventually stops. We noticed that sometimes the variation is almost a perfect sinusoidal curve, and other times a noise-type with certain

peridicity, and yet other times with no peridicity at all.

7.2.2 Frequency Domain

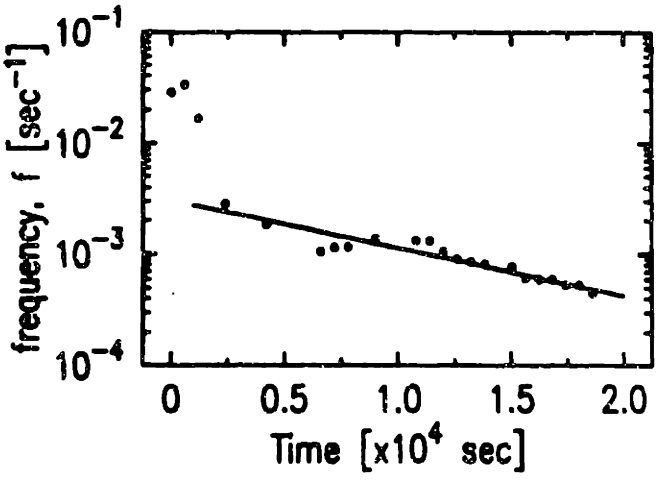

Figure 7.3: Frequency of the oscillation as a function of time. The data is obtained by processing figure 7.2

Figure 7.3 is a plot of the frequency of the oscillation as a function of time. From figure 7.3, we find that the frequency relaxation process is a exponentially decay process (except at the very begining).

7.2.3 Decreasing Temperature

The data we have presented above are collected after the temperature was increased at $t = 0$. In other words, the data was collected from a shrinking process. In figure 7.4, we present the data collected in a swelling process, i.e., the temperature was decreased at $t = 0$. From this figure, we know that the oscillation occurs in both swelling and shrinking processes. This is very important because it eliminates some of the theories we have thought about.

7.2.4 Beatings

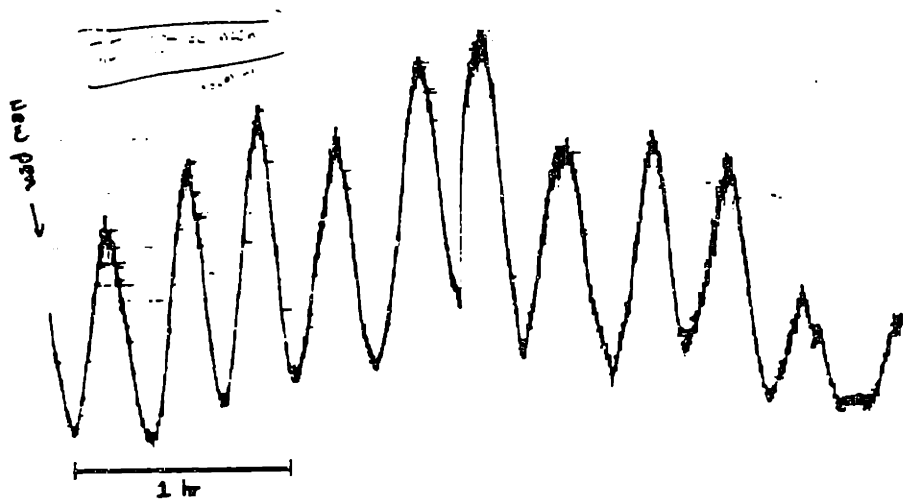

Figure 7.4: Scattered light intensity after the temperature was decreased at $t = 0$. The gel swells when the temperature is decreased.

Figure 7.5 demonstrates the beating phenomenon we observed in the scattered light intensity. This type of behavior appears quite often.

7.2.5 Wall Confinement

In this experiment, we used a gel which was made in the optical cell and was never taken out. Very surprisingly, we found that when the temperature is below 30 °C, the intensity is very stable; above this temperature, the intensity starts to oscillate (Fig. 7.6). The data above can be explained readily if we notice that the temperature at which the intensity starts to oscillate is the same as the temperature at which the swelling ratio of the sample is equal unity, i.e., $V/V_0 = 1$(Fig. 7.7). Below this temperature, the gel is confined by the wall of the cell (free gel would swell). Above this temperature, however, the swelling ratio is less than unity, the gel separates from the wall. At this point, the confinement no longer exist, the gel behaves the same as we have described in the first several subsections.

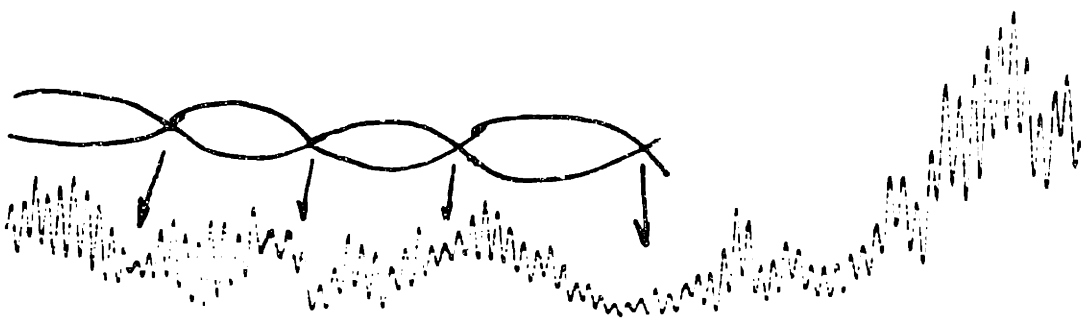

Figure 7.5: Beating of the scattered light intensity. The two frequencies are nnnnHz and nnnnHz, respectively.

7.2.6 Frequency Localization

In order to understand if the oscillation is propagating within the sample, we used two PMT detectors simultaneously, one at 90° scattering angle and the other at 70°. The results are in figure 7.8a. There was no correlation observed. We have also tried to change the distance between the two scattering volumes, but still no correlation between the two intensity signals was ever observed. This experiment directly shows that the oscillation within the sample is totally local. The frequency is a local quantity. This also tells us that the oscillation is not due to a globally propagating wave.

In figure 7.8b, we find that the oscillation of one scattering volume stopped while the other is still oscillating. The oscillation is a local behavior, independent of the neighbours. This confirms the observation presented in the previous subsection.

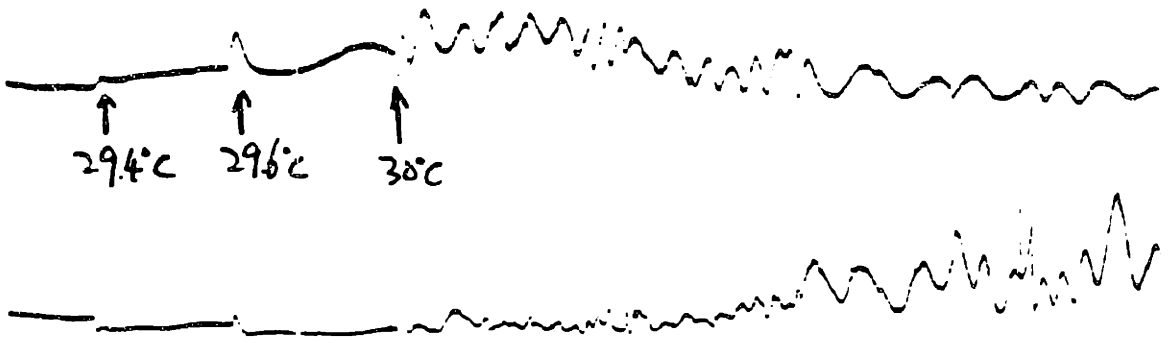

Figure 7.6: Effect of the wall confinement on the oscillation of the gel made in the optical cell. The oscillation only happens when the temperature of the sample holder is above 30 °C. Below this temperature, the gel is confined by the wall of the optical cell.

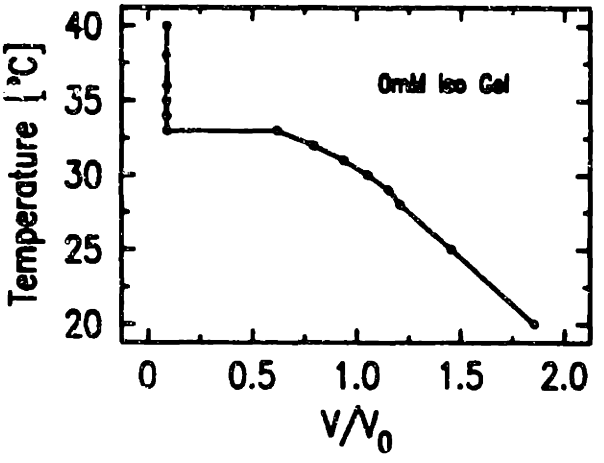

Figure 7.7: Swelling ratio of 0mM iso gel as a function of temperature. At ~30 °C, the ratio is equal unity.

7.3 Theoretical Considerations

7.3.1 What is Oscillating

What the scattered intensity measures is the Fourier components of the dielectric constant ϵ,

$$I(\mathbf{q}) = < |\delta\epsilon(\mathbf{q})| > . \tag{7.1}$$

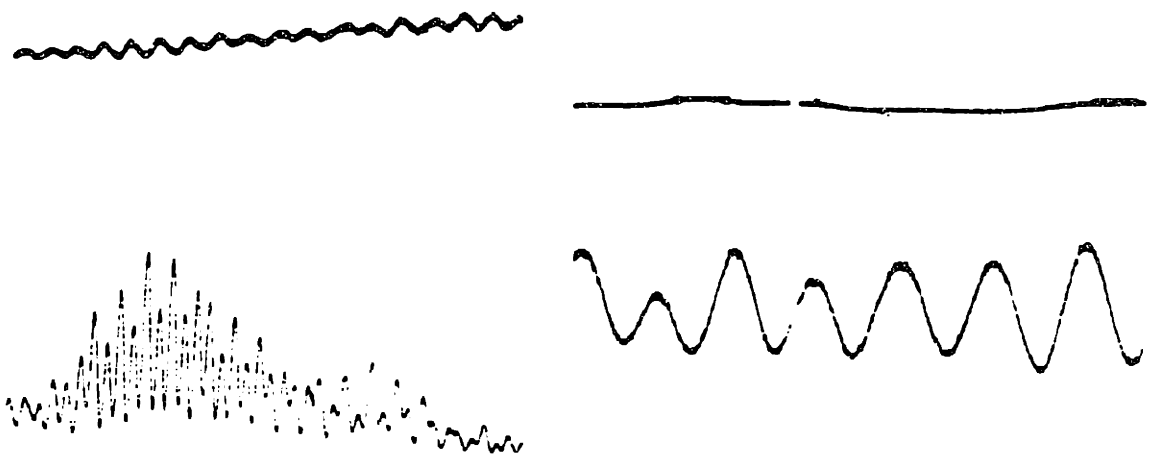

Figure 7.8: Double detector result. [a] The behavior of the scattered intensity from these two scattering volumes has no correlation. The frequency is a local quantity. [b] The oscillation of one position stopped long before the other.

So it has to be the dielectric constant that is oscillation. This is the same as to say that the density of the network is oscillating.

7.3.2 Indeed Very Slow

In order to appreciate how slow this is, let us do some exercise. Assume the scattering volume is about $20\mu m$, which is reasonable from chapter 6. A typical oscillation period of the scattered intensity from a gel is about 1000 seconds. These give us a speed which is about $200\mathring{A}$/sec, or 4mm/day, or 1.5m/year !

From another point of view, assume the intensity oscillation comes from the sound wave of the network. Then the frequency is related with the modulus G and the

density ρ of the system,

$$f \sim \sqrt{\frac{G}{\rho}}. \tag{7.2}$$

From chapter 8, $G \sim 5 \times 10^4$ $dynes/cm^2$, the density of the network ρ is about 0.05 g/cm^3. Plug these numbers in eq (7.2), we get $f \sim 10^3$ Hz. Our experimental value, which can be $\sim 10^{-3}$ Hz, is 10^6 times smaller than this. If we take the experimental frequency and the density of the network as given, then we will need a modulus which is ten orders of magnitude smaller than what we have obtained experimentally (chapter 8).

From the double-detector experiment, we know that the propagating wave type of theory will not work because the oscillation of the scattered light is localized.

So we find that it is impossible to understand the oscillation by means of the mechanical quantities we have measured. A totally different mechanism is governing the phenomenon.

7.3.3 Inhomogeneities ?

Brenner, Gelman and Nossal (1978) and Nossal and Brenner (1978) had shown that for soft gels, an external oscillator coupled to the system can force the gel to oscillate with resonance frequency. They detected the slowest frequency of this oscillation by means of light scattering. The primary sample they used was agrose gels with concentration varied from 0.25% to 1%. With the optical geometry similar to the ones we have used in our experiment, they found that the fundamental (slowest) frequency is 46Hz for agrose gel with 2% concentration is $1 \times 1 \times 4$ cm cuvette. This wave corresponds to the fundamental standing wave in the cuvette.

Experimentally the modulus of gel network and the friction coefficient between the network and the solvent varies with the concentration of the network by similar power. This is supported by the fact that the collective diffusion constant of the

network system has only a weak dependence on the concentration of the network compared with the power dependence of the modulus and the friction coefficient. So we do not think to the first order approximation, there is a big difference between the soft gels (0.5%) and regular gels (10%). The result of Nosssal et al may be explained to better satisfactory as due to the strong external modulation.

7.3.4 Possible Mechanism

We have noticed that started at the time when the temperature of the sample was changed, the oscillation of the scattered intensity continues for several days. This time scale is similar to that of the volume equilibration process, which is the same as the internal osmotic pressure relaxation time. From this, we postulate that the oscillation is directly related with the stress field inside the sample created by the change of the temperature. This stress field cause the network to move in such a fashion that the scattered light intensity oscillates with an extremely slow frequency.

Since the relaxation time for the oscillation is similar to that of the stress (osmotic) field, we can use the stress field as our natural variable.

The stress field will cause the local network move collectively, causing the solvent to convect. The convection of the solvent in turn will affect the motion of the local network and the neighbours. This is a highly non-linear effect. The velocity of the solvent flow is directly related with the strength of the local osmotic pressure, and will become zero when the osmotic pressure field becomes a constant.

We know there are inhomogeneities in the gel network (chapter 6). The clusters that are weakly connected with the neighbours will be able to drift with the flow of the water to certain degree with very small effective friction. The oscillation of the scattered light may be due to the motion of the clusters caused by the flow.

7.4 Future Experiment

- Jump size dependence.
- Chemical composition dependence.
- Position dependence.
- Good statistics.

Chapter 8

Mechanical Study of Gels

8.1 Introduction

In the case of a liquid-gas system, the external pressure, p, plays an important role. It is the same for the gel network system, except now it is the osmotic pressure that is doing the job. Osmotic pressure of a network system can be defined as the energy needed to expand the network by unit volume. Following this, the external osmotic pressure can be defined as the contribution to the osmotic pressure by the sources other than the interaction among the network and solvent molecules. Some of the examples of the external osmotic pressure, for instance, can be the network in a high molecular weight polymer solution (chapter 11; Hirotsu, 1986), ionic gel in electric field (Tanaka, 1982). In this chapter, we shall concentrate on the mechanically applied pressure only.

From the application point of view, it is very important to understand the mechanical properties of the material. Especially when we consider the potential applications of gels in mechanical devices such as artificial muscles, switches, actuators, etc., this becomes apparent.

The mechanical study of elastomers started from the study of the rubber elastic-

ity. The discovery of the phenomenological Mooney-Rivlin equation (Monney 1940; Rivlin 1947) marked another beginning of the study. The extensive study of the elastomer mechanical properties has lead a much better understanding of these materials. The analogy among the elastomer elasticity and the quantities of other systems is remarkable (de Gennes 1976). Many experimental methods have been developed to study the mechanical properties of the elastomers, as we will see later in this chapter. Most of these techniques measures the shear modulus only. In this chapter, we will demonstrate a way of measuring both the shear and bulk modulus.

8.2 Theory of Elasticity

This section provides a quick review of the theoretical aspects of the shear and bulk modulus. The theory of the elasticity is valid usually only under the continuum (hydrodynamic) limit. For a good reference, see Landau and Lifshitz (1986), " *The Theory of Elasticity* ".

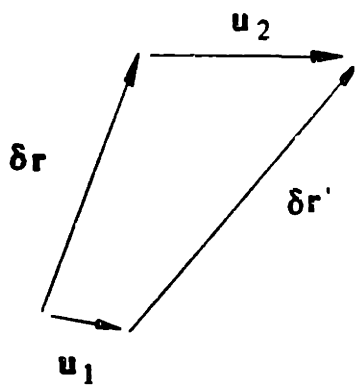

Figure 8.1: A vector before and after the deformation.

Under small deformation, the volume element at position $\mathbf{r}$ will be shifted to a new position $\mathbf{r}'$. Define the displacement vector $\mathbf{u}(\mathbf{r})$ as

$$\mathbf{u}(\mathbf{r}) = \mathbf{r}' - \mathbf{r}. \tag{8.1}$$

Now consider a small distance vector $\delta\mathbf{r}$ (Fig.8.1). After the deformation, both the head and tail of the vector will be displaced by $\mathbf{u}_1$ and $\mathbf{u}_2$. Write $d\mathbf{u} = \mathbf{u}_1 - \mathbf{u}_2$, we can write down the distance vector after the deformation, $\delta\mathbf{r}'$,

$$\delta\mathbf{r}' = \delta\mathbf{r} + d\mathbf{u}. \tag{8.2}$$

With the Einstein summation convention, the change of the distance squared $\delta\mathbf{r}^2$ is

$$\begin{aligned} \delta\mathbf{r}'^2 &= (\delta\mathbf{r} + d\mathbf{u})^2 \\ &= \delta\mathbf{r}^2 + 2u_{ik}dx_i dx_k. \end{aligned} \tag{8.3}$$

Where u_{ik} is the strain tensor defined as

$$u_{ik} = \frac{1}{2}\left(\frac{\partial u_i}{\partial x_k} + \frac{\partial u_k}{\partial x_i}\right). \tag{8.4}$$

The trace of the the tensor u_{ll} is nothing but the divergence of the displacement vector $\mathbf{u}$, so it represents the local fractional volume change. By definition, this is the hydrostatic compression,

$$\begin{aligned} u_{ii} &= \nabla \cdot \mathbf{u}(\mathbf{r}) \\ &= \frac{\delta V' - \delta V}{\delta V}. \end{aligned} \tag{8.5}$$

The strain tensor can be separated into two parts, pure shear and pure hydrostatic compression,

$$u_{ik} = \left(u_{ik} - \frac{1}{3}\delta_{ik}u_{ll}\right) + \frac{1}{3}\delta_{ik}u_{ll}. \tag{8.6}$$

The free energy F of the deformation is

$$F = \mu \left(u_{ik} - \frac{1}{3}\delta_{ik} u_{ll} \right)^2 + \frac{1}{2} K {u_{ll}}^2, \tag{8.7}$$

where μ and K are the shear and bulk modulus respectively. The first term is the contribution from the shear deformation, and the second term comes from hydrostatic compression. Related with the deformation, the stress tensor σ_{ik} can be defined by

$$dF = -SdT + \sigma_{ik} du_{ik}, \tag{8.8}$$

or,

$$\sigma_{ik} = \left(\frac{\partial F}{\partial u_{ik}} \right)_T. \tag{8.9}$$

So, we have (using $\delta_{ik}[u_{ik} - \frac{1}{3}\delta_{ik} u_{ll}] = 0$),

$$\sigma_{ik} = K u_{ll} \delta_{ik} + 2\mu \left(u_{ik} - \frac{1}{3}\delta_{ik} u_{ll} \right). \tag{8.10}$$

The strain tensor can also be expressed in terms of the stress tensor,

$$u_{ik} = \frac{1}{9K}\delta_{ik}\sigma_{ll} + \frac{1}{2\mu}\left(\sigma_{ik} - \frac{1}{3}\delta_{ik}\sigma_{ll} \right). \tag{8.11}$$

Eq (8.10) and (8.11) relate the experimental quantities u_{ik} and σ_{ik} by the mechanical properties of the material, K and μ.

8.3 Experimental Methods

The basic experimental setup is shown in Fig.8.2. The weight of mass m is applied to the gel via the light weight support rod A. The The tube B, which has a slightly larger inner diameter than the diameter of the tube A, is used to keep the tube A stay upright.

When the weight m is placed on the rod A, a pressure p is applied vertically to the gel. By measuring the change of the height and the diameter of the gel, we can obtain the moduli K and μ.

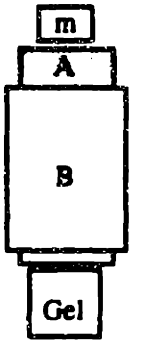

Figure 8.2: The schematic sketch of the setup for the mechanical study of the gel network system. The temperature of the sample can be controlled with stability $\pm 0.05^{o}$C.

In this experiment, the deformation is homogeneous, that is, the strain tensor u_{ik} is a constant throughout the system. This tells us that the stress tensor σ_{ik} is a constant too. Because of this, the stress constant can be determined by the boundary conditions. Since there is no external force on the side of the gel, therefore $\sigma_{ik}n_k = 0$. Because the normal unit vector n is perpendicular to z-axis, i.e. $n_z = 0$, it follows that all the components σ_{ik} are zero except σ_{zz}. On the end of the gel $\sigma_{zi}n_i = p$, or $\sigma_{zz} = p$. The strain tensor can be obtained using eq (8.11)

$$u_{rr} = u_{xx} = u_{yy} = \frac{1}{3}\left(\frac{1}{3K} - \frac{1}{2\mu}\right)p, \tag{8.12}$$

$$u_{zz} = \frac{1}{3}\left(\frac{1}{3K} + \frac{1}{\mu}\right)p. \tag{8.13}$$

From these two equations, we can find the shear and bulk modulus

$$\mu = \frac{p}{2}\frac{1}{u_{zz} - u_{rr}}, \tag{8.14}$$

$$K = \frac{p}{3}\frac{1}{u_{zz} + 2u_{rr}}. \tag{8.15}$$

The *Poisson's* ratio, σ, is defined as

$$\sigma = -\frac{u_{xx}}{u_{zz}}, \tag{8.16}$$

from eq (8.12) and (8.13)

$$\sigma = \frac{1}{2}\frac{3K - 2\mu}{3K + \mu}. \tag{8.17}$$

Since K and μ are always positive, Poisson's ratio σ can vary between -1 (for $\mu = \infty$) and 1/2 (for $K = \infty$). Using Poisson's ratio, eq (8.14) and (8.15) and the ratio μ/K can be written

$$\mu = \frac{p}{2(1+\sigma)}\frac{1}{u_{zz}}, \tag{8.18}$$

$$K = \frac{p}{3(1-2\sigma)}\frac{1}{u_{zz}}, \tag{8.19}$$

$$\frac{\mu}{K} = \frac{3(1-2\sigma)}{2(1+\sigma)}. \tag{8.20}$$

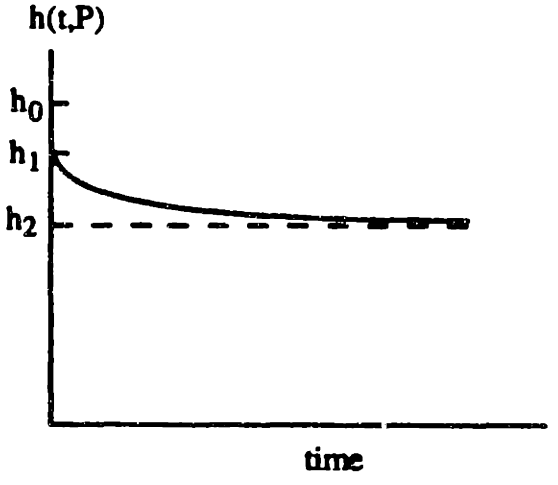

Figure 8.3: Definition of the experimental quantities. h_0 is the initial height of the sample. h_1 is the height right after the external pressure is applied. h_2 is the height at time $t = \infty$. Similar quantities are defined fro the radius.

Fig.8.3 is a schematic plot of a typical experimental result. Denote the initial height and radius by h_0 and r_0 respectively, As soon as the external pressure is applied to the sample, the height and radius will be changed into h_1 and r_1, with the volume unchanged $h_0 {r_0}^2 = h_1 {r_1}^2$. After the sample has reached its final equilibrium, the height and radius are denoted by h_2 and r_2, respectively. At any other time, the

relaxation functions are defined,

$$\delta h(t) = h(t) - h_2, \tag{8.21}$$

$$\delta r(t) = r(t) - r_2. \tag{8.22}$$

The change of the gel dimension is measured with a microscope, with resolution 0.05mm. The samples are either polyacrylamide or isopropylacrylamide gels made in Kimble test tubes with inner diameter $\sim$ 8.5mm, with the standard recipe. The final equilibrium diameter after the gel has been taken out of the test tube is $\sim$ 9.7mm. A $\sim$ 9.5mm long segment of the gel was used for the experiment.

We also have an alternative design which is essentially the same as that in figure 8.2 except the gel holder can hold nine samples at the same time (a later one can hold 19 gels). The device is immersed in a transparent water tank with the temperature been regulated by a water circulater with stability $\pm 0.05°C$.

We will describe two experimental methods in the following. One is used under the the gel equilibrium condition, from which both K and μ can be obtained. The other is under the quasi-equilibrium condition, from which only the shear modulus μ can be obtained. The instantaneous response method has been used for many years without a solid theoretical justification. So later in this chapter, we will discuss the validity of this method.

8.3.1 Instantaneous Response Method

In this method, what is measured is the instant response, h_1, of the gel under the uniaxial pressure (see figure 8.3). Because the gel volume relaxation time is much longer than the time scale involved in this method, we can assume the volume of the gel is a constant. This tells us that $d_1^2 h_1 = constant$. For a small pressure, we have

$$u_{zz} = -\frac{h_1 - h_0}{h_0}, \tag{8.23}$$

$$u_{rr} = -\frac{u_{zz}}{2}. \tag{8.24}$$

The conventional argument for obtaining the shear modulus is by using eq (8.14) directly. This gives

$$\mu_1 = \frac{p}{3}\frac{h_0}{h_0 - h_1}. \tag{8.25}$$

The physical justification of this derivation is the following. The moduli of the system comes from two parts. One is the solvent, the other is the network. The solvent is incompressible, yielding incompressibility of the whole system. However, there is no shear modulus associated with the solvent, so the shear modulus measured comes from the network solely.

Here we propose another way of thinking. Under the constant volume condition, from eq (8.10),

$$\sigma_{ik} = 2\mu_1 u_{ik}. \tag{8.26}$$

When the uniaxial pressure p is applied to the gel, a hydrostatic pressure p_h is created. This is a uniform pressure in all directions. Under these two pressures, the gel deforms. So we have

$$p + p_h = 2\mu_1 u_{zz}, \tag{8.27}$$

$$p_h = 2\mu_1 u_{rr}. \tag{8.28}$$

From these two equations,

$$\mu_1 = \frac{p}{3}\frac{h_0}{h_0 - h_1}, \tag{8.29}$$

$$p = -3p_h. \tag{8.30}$$

The first result here is the same as the one obtained by the conventional argument. The ratio of the shear moduli μ_1 to μ_2 (by measuring h_2) is

$$\frac{\mu_1}{\mu_2} = \frac{2(1-\sigma)}{3}\frac{h_0 - h_2}{h_0 - h_1}. \tag{8.31}$$

Since the Poisson's ratio varies from -1 to 1/2, the first factor is always less than unity unless the bulk modulus K is infinite. The second factor, on the other hand, is always larger than unity unless the bulk modulus K is infinite.

From the definition of these two shear moduli, we find that they should be equal in value. The large value of the friction coefficient provides us a easier way of measuring the shear modulus (μ_1).

8.3.2 Equilibrium Response Method

By equilibrium, we mean that the gel shape and size is independent of time. Then what we have measured are two pairs of dimensions, (h_0, d_0) and (h_2, d_2) (see figure 8.3). So we have

$$u_{zz} = -\frac{h_2 - h_0}{h_0}, \tag{8.32}$$

$$u_{rr} = \frac{d_2 - d_0}{d_0}. \tag{8.33}$$

The shear and bulk modulus can be directly calculated by using eq (8.14) and (8.15).

8.3.3 Kinetics

The swelling of a spherical gel with negligible shear modulus was studied by T. Tanaka and D. J. Fillmore (1979). Peters and Candau (1986, 1988) studied the the swelling kinetics of sphere, long cylinder and large disc gels with arbitrary shear modulus. In their calculation, however, the length of the cylinder and the diameter of the disc are fixed (hence pure two dimensional problems). But it is more common experimentally to have long gels with free ends and large discs with free rim. We have calculated the kinetics of the freely immersed gels for the case of long cylinders and large discs in appendix D. We can treat our samples in this chapter as infinitely long cylinders

because of the experimental geometry shown in figure 8.2. Notice that both ends of the sample is in touch with large flat surface. There is no solvent can be transported in the z-direction. This is the same as a infinitely long cylinder.

From appendix D, the kinetics of the gel shape relaxation process is described by

$$u(t) = \sum_{n=0}^{\infty} B_n e^{-D_e q_n^2 t} J_1(\alpha_n), \tag{8.34}$$

with the $\alpha_n \equiv a q_n$ determined by

$$\alpha_n J_0(\alpha_n) + \frac{1+\sigma}{1-\sigma} J_1(\alpha_n) = 0. \tag{8.35}$$

So the kinetics is a combination of other quantities. According to appendix D, the kinetics we measured should be about 3/2 times slower than if the gel were freely immersed in the solvent.

8.4 Data Analysis

8.4.1 Study of NIPA gel

In this study, we measured both the instantaneous response and equilibrium deformation of the gel, and also the kinetics of the relaxation process. THe sample used were standard acrylamide gels made in pipettes with inner diameter equal $8.5mm$. The experiment were performed on the swollen gels. The swollen diameter of the gels were $9.7mm$

Figure 8.4 is the instantaneous response result. From this figure, we find

$$\mu_1 = (3.09 \pm 0.30) \times 10^4 dynes/cm^2. \tag{8.36}$$

Fig.8.5a and 8.5b is the experimental result of u_{zz} (which is $(h_0 - h_2)/h_0$) and u_{rr} (which is $(d_0 - d_2)/d_0$) as a function of the uniaxial pressure P, respectively. Within

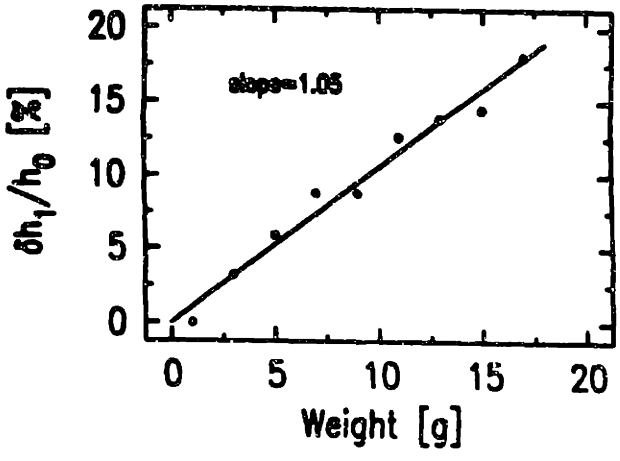

Figure 8.4: Instantaneous response deformation as a function of the applied pressure (weight). The volume of the gel is the same as that before the deformation.

this pressure range, the elasticity is in the linear range. From these two figures, we find

$$\sigma = 0.40 \pm 0.12 \tag{8.37}$$

$$\mu_2 = (2.51 \pm 0.43) \times 10^4\ dynes/cm^2. \tag{8.38}$$

$$K_2 = (11.7 \pm 1.6) \times 10^4\ dynes/cm^2. \tag{8.39}$$

All of the errors are given by 95% F-test method. First, we noticed that the two shear modulus measured above are the same within our experimental error. Secondly, the bulk modulus K is larger than the shear modulus by a factor of four.

Using $\sigma = 0.4$ and eq (8.35), we find that $\alpha_1 = 3.0$. The time constant of the process is (using a = 0.5cm)

$$\begin{aligned} \tau_1 &= \frac{a^2}{D_e \alpha_1^2} \\ &= 1.85 \times 10^{-7}\ f\ cm^4/dynes. \end{aligned} \tag{8.40}$$

Figure 8.6a is a typical measurement of the kinetics. Figure 8.6b is the relaxation

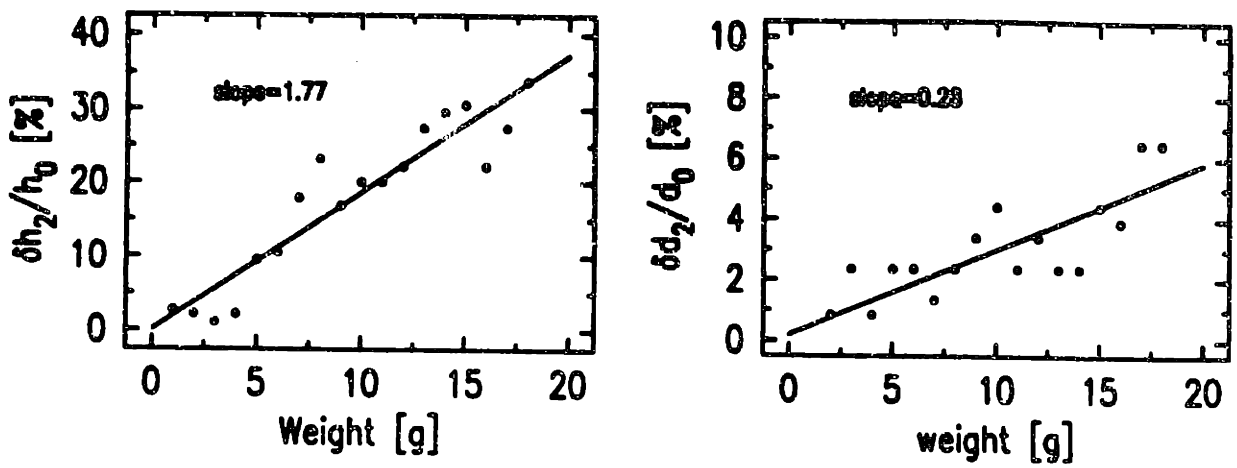

Figure 8.5: Equilibrium deformation as a function of the applied pressure (weight). [a] change of the height; [b] change of the diameter.

tir ıe of the gels with different weight on top of them. The average relaxation time is

$$\tau = 32 \pm 5 \; hours. \tag{8.41}$$

From this, we can obtain the friction coefficient f,

$$f = 6.2 \times 10^{11} dynes\, sec/dynes\ . \tag{8.42}$$

This number is comparable with the value of f obtained from the light scattering data by Tanaka, Hocker and Benedek, which is around 2.2×10^{11} (Tanaka 1973).

8.4.2 Crosslink Effect

We studied the moduli dependence on the concentration of the cross-linking molecules (figure 8.7a and 8.7b). Only the instantaneous response method was used. In a wide range, the power law dependence is observed. Then the dependence saturates beyond the concentration bis_s. From these data, we find

$$\mu \sim bis^{0.7}, \tag{8.43}$$

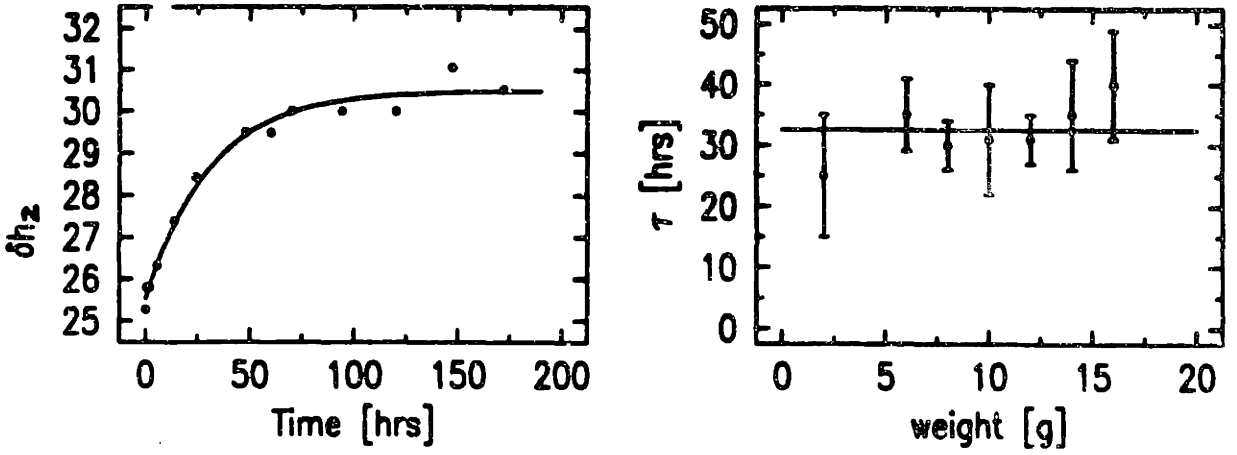

Figure 8.6: [a] is a typical measurement of the kinetics. [b] is the relaxation time of the gels with different weight on top of them.

where *bis* is the concentration of the crosslink molecules.

The rigidity of the gel network is related with the elasticity of it. From Flory's argument, under uniaxial deformation (elongation), the retractive force τ of the network per unit initial area can be written as

$$\tau = \frac{\nu kT}{V}\left(\alpha_F - \frac{1}{\alpha_F{}^2}\right), \tag{8.44}$$

where ν is the total number of chains in the sample, V is the volume, α_F is the deformation ratio defined as

$$\begin{aligned} \alpha_F &= \frac{r}{r_0} = \frac{r_1}{r_0}\frac{r}{r_1} \\ &= \alpha_0\alpha. \end{aligned} \tag{8.45}$$

Where r_0 is the reference state in Flory's calculation and $\alpha_0 = r_1/r_0$. The r_0 is the radius of gyration of a free gaussian chain. The r_1 is the radius of gyration of a chain when the gel was made, which satisfies the following relation

$$\nu(2r_1)^3 = V. \tag{8.46}$$

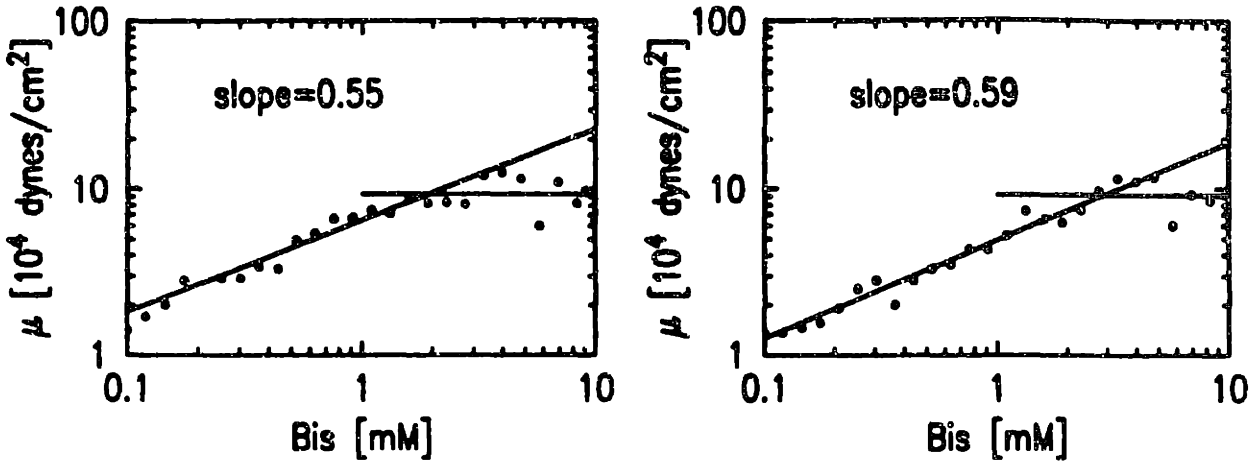

Figure 8.7: Shear modulus of acrylamide gel with different crosslink molecules in the pre-gel solution. The unit of the x-axis is [std], y-axis is pressure. [a] the shear modulus of gels before they swell. [b] the shear modulus of swollen gels.

In our experiment, the effective value of τ should be the difference between the deformed state and the initial state,

$$\delta\tau = \frac{\nu kT}{V}\left(\alpha_0 + \frac{2}{\alpha_0{}^2\alpha^3}\right)\delta\alpha. \tag{8.47}$$

When the number of the crosslinkers is changed, the total number and length of the chains is going to change. Assume the gelation efficiency of the crosslink molecules and the monomer units is β_B and β_I respectively, then intuitively we have the following relations,

$$\nu \sim bis\beta_B \tag{8.48}$$

$$r_0 \sim n^{3/5} \sim bis^{-3/5}(\beta_I/\beta_B)^{3/5} \tag{8.49}$$

$$r_1 \sim bis^{-1/3}\beta_B{}^{-1/3}. \tag{8.50}$$

So the α_0 can be written as

$$\alpha_0 \sim bis^{4/15}\beta_B{}^{4/15}. \tag{8.51}$$

Equate $\delta\tau$ and P in eq (8.25),

$$\begin{aligned} \mu &\sim \frac{\nu kT}{V}(\alpha_0 + \frac{1}{\alpha_0{}^2\alpha^3}) \\ &\sim bis(bis^{4/15} \; and \; bis^{-6/15}) \\ &\sim bis^{1.3} \; or \; bis^{0.5}. \end{aligned} \tag{8.52}$$

There are two possible exponents above. The experimental result is in between these two values. So what we have observed is the cross over between these tow exponents. In order for the cross-over to happen, α_0 must have the value of the order of unity. From the experimental recipe,

$$\nu = 8.6 \cdot 10^{-3} N_a \beta_B / liter = 5.2 \cdot 10^{-6} \beta_B / \mathring{A}^3, \tag{8.53}$$

$$n = \frac{700\beta_I}{2 * 8.6\beta_B} = 40.7\beta_I/\beta_B, \tag{8.54}$$

$$r = 29\beta_B{}^{-1/3}\mathring{A}, \tag{8.55}$$

$$r_0 = a\,n^3/5 = 6.4a(\beta_I/\beta_B)^{3/5}. \tag{8.56}$$

Where a is the length of a monomer unit. So we find

$$\alpha_0 = \frac{4.53(\mathring{A})}{a}(\beta_B{}^{4/15}/\beta_I)^{3/5}. \tag{8.57}$$

The length of a monomer unit is about $5\mathring{A}$. Our experimental values of β_B and β_I are close to one. So the value of α_0 is indeed of the order of one.

If the calculation above is valid, we can conclude that in most of the cases (bis: 0.1 - 1), our samples are nearly perfect networks. A general discussion on the possible imperfections of a network is given in appendix A.

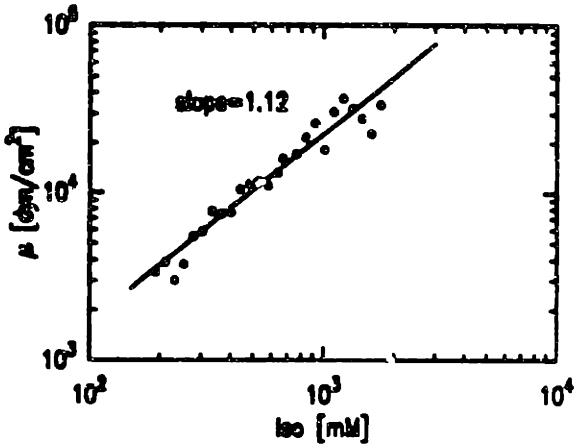

Figure 8.8: Shear modulus of acrylamide gel with different monomer molecules in the pre-gel solution. The unit of the x-axis is [std], y-axis is pressure.

8.4.3 Monomer Effect

The effect of the network concentration has been studied be several groups on the physically connected agrose gel networks (Nassal and Jolly 1988; Masayuki et al 1987; 1985) and chemically crosslinked networks (Richards and Davison 1985). A power law has been observed by the above groups. Depending upon the experimental condition, the exponent varies. In general, the phenomenological form of the concentration dependence can be written as

$$\mu = C_1\phi^x + C_2\phi^y \tag{8.58}$$

with the exponents x and y around 2 and 4, respectively.

Figure 8.8 is the shear modulus of gels with different monomer concentration. The monomer dependence of the shear modulus μ is similar to that of the cross-link molecules.

8.4.4 Ionization Effect

Figure 8.9 shows the ionizable group dependence of the shear modulus of acrylamide gels. The experiment were done on swollen gels. The gels with different swelling ratio

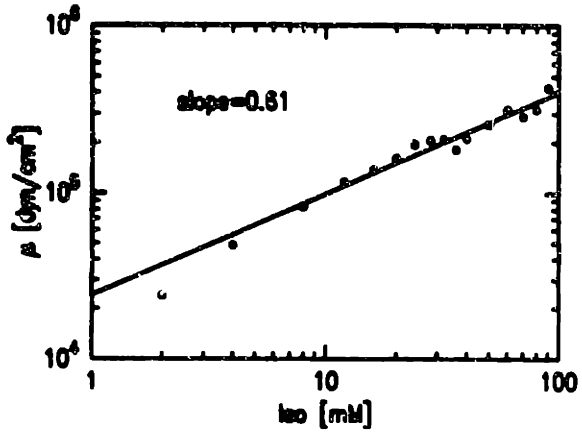

Figure 8.9: Shear modulus of acrylamide gel with different ionizable groups attached to the network. The unit of the x-axis is [std], y-axis is pressure.

are cut into short cylinders with the same size. The result in figure 8.9 is normalized shear modulus (modulus per unit network chains).

The shear modulus increases as the ion concentration increases in our case. This is just the opposite of what Ilavsky (1982) has reported.

For detailed explanation about this data, see chapter 9.

8.4.5 Pulling Experiment

All of the experiments we mentioned so far are related with the gels upper an compression pressure. In this and the next sections, we demonstrate another kind of experiment, i.e., the pulling experiment. The advantage of the pulling experiment is that the range of the deformation ratio is much larger, with a bigger linear region. The difficulty of it has always been finding a way of holding the gel. In our case, the gel was carefully dried first. Then a small piece of moistened towel paper were used to wrap the ends loosely. The use sewing string to tie the towel paper. After a short while, the ends of the gel become swollen. Now the ends of the gel are fairly tightly held by the paper. Next step is to pull the gel by holding the papers on the two ends. Figure 8.10a is a schematic sketch of the setup. The result is shown in figure 8.10b.

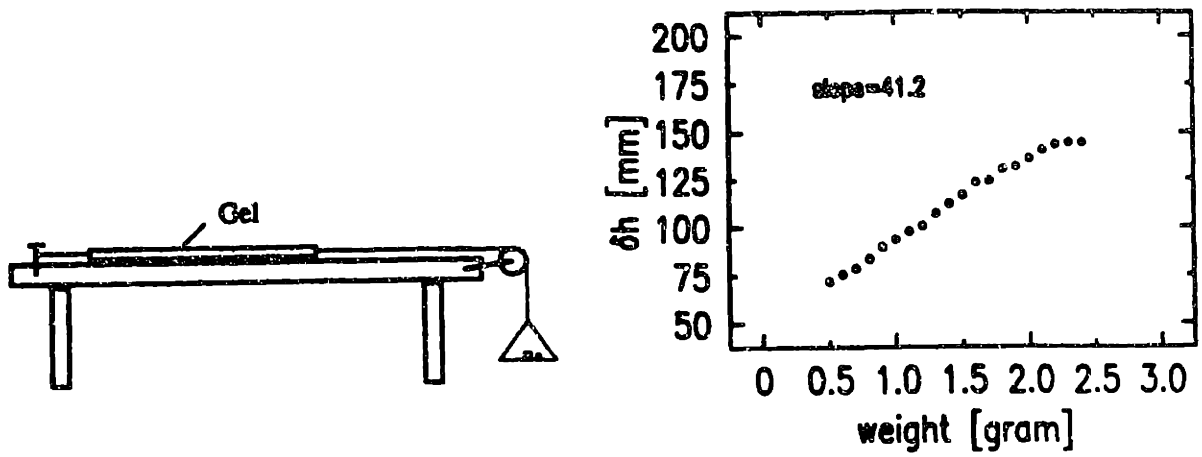

Figure 8.10: [a] A schematic sketch of the pulling experiment setup. [b] Elongation of a long cylindrical acrylamide gel under a pulling force.

The time dependence of the elongation in this experiment seemed to be small. From figure 8.10b, we find

$$\mu = 3.8 \times 10^4 \text{ dynes/cm}^2 \tag{8.59}$$

8.4.6 Fracturization

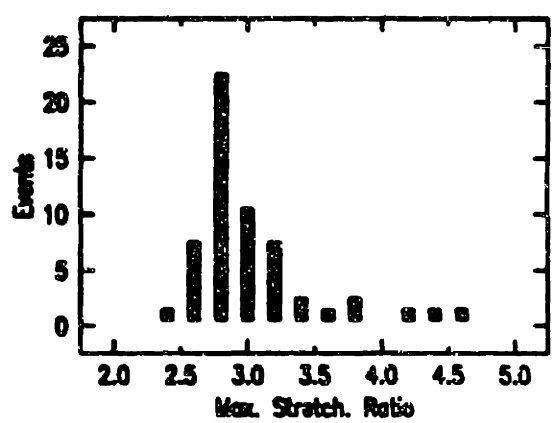

Figure 8.11: Fracturization of acrylamide gels. The gels were pulled by hands in water until they broke.

In this experiment, each sample was pulled slowly by hands in water until it broke. The initial and final length was measured. Figure 8.11 is the distribution of the maximum stretching ratio of the samples.

8.5 External Pressure Induced Phase Transition

8.5.1 Theoretical Consideration

This problem can be treated thermodynamically by writing down the free energy of the system,

$$F = F_g(\alpha, \beta, T) + F_w(\beta). \tag{8.60}$$

Where α and β are the expansion ratio on the radial and axial direction, respectively. The T is the temperature of the system. F_g is the Flory-Huggins mean-field free energy of the gel network system,

$$F_g = \nu kT \left\{ N_0 \frac{1-\phi}{\phi} \left[ln(1-\phi) + \frac{\Delta F}{kT}\phi \right] + \frac{1}{2}\left[2\alpha^2 + \beta^2 - 3 - (2f+1)ln(\alpha^2\beta) \right] \right\}. \tag{8.61}$$

F_w is the gravitation energy related with the introduction of the weight,

$$F_w = wgh_0(\beta - 1). \tag{8.62}$$

Minimize the free energy in eq. (6.1), we will find the thermodynamically stable states. This problem is mathematically identical with the one Tanaka et al solved for the ionic gel in electric field (Tanaka 1981, the explanation in this paper is not quite according to the private conversation with Tanaka) .

The result of Tanaka's calculation is plotted on Fig.8.12. According to their result, when the weight is sufficiently big, the phase transition will occur.

If carefully designed, this can be a more direct way of studying the critical behavior of the gel system.

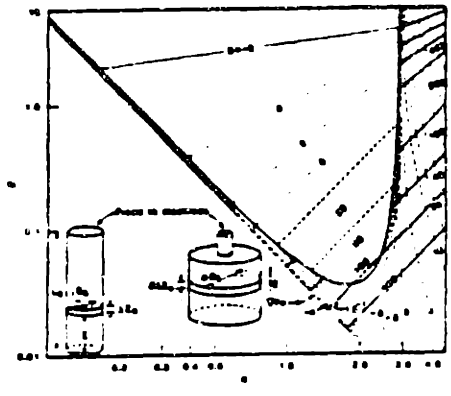

Figure 8.12: Phase diagram of a gel system under uniaxial external pressure.

8.5.2 Experimental Observations

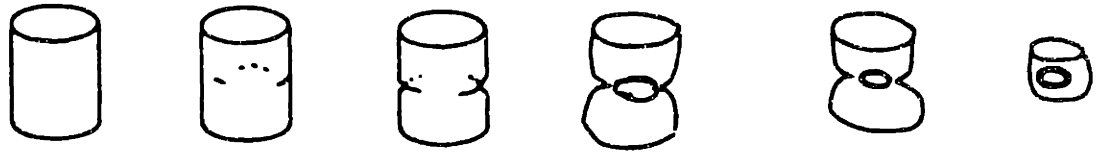

Figure 8.13: Sequence of the ring formation.

The samples used in this experiment are ionic gels with $32mM$ sodium-acrylate. The transition temperature of this sample is around 42 °C when freely immersed in water (figure 8.12). Since the size of the gels we used in this experiment are very large (7mm), the kinetics are very slow near the phase transition (more than a month). The results we present below are hence very preliminary. To increase the visibility of the network, we have added very small amount of blue dextran polymers (so the gels looked slightly blue).

We increased the temperature from below and waited at 40 °C for a month. First

we observed small lines (scratches) appeared on the surface of the gel. As the time goes, the lines eventually connected together and formed a ring. The ring became thicker and thicker and the diameter of the gel at the middle became smaller and smaller. Figure 8.13 represents the sequence of these observations. The lines and rings appeared on the gels are collapsed regions. So the gels were either in the coexistence states, or in the process of undergoing a phase transition.

We then increased the temperature to 40 °C. All the gels collapsed at this temperature after one month.

After all the gels had collapsed, the temperature was set to 39 °C. After another month, all the gels were swollen.

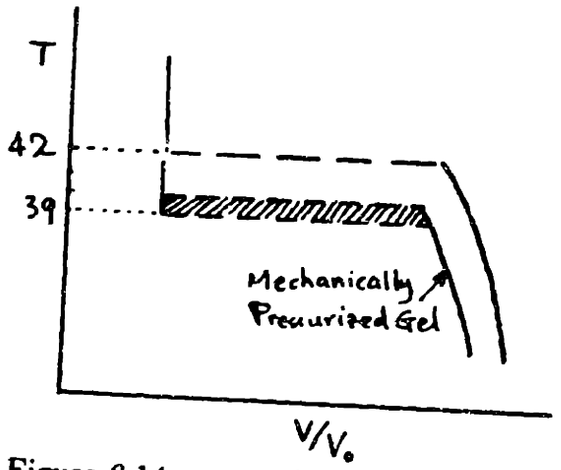

Figure 8.14: Comparison between the free gels and the mechanically pressurized gels. Notice the transition temperature difference.

Figure 8.14 summarize what we have observed on the phase transition aspect of the mechanical pressure effect. The transition temperature is apparently different. We noticed that the transition temperature of gels under different mechanical pressure (1mg to 17mg) falls in a region with the temperature span about 2 °C.

Chapter 9

Study of Polyelectrolyte Gels

In a polyelectrolyte system, several length scales presents (Witten and Pincus 1987). Upon the changes of the charge concentration, chain length, temperature, etc, these length scales can change as well. Due to the competition among these length scales, a polyelectrolyte system can exhibit very interesting behavior.

We studied the swelling ratio and mechanical property of polyelectrolyte gels. Our results can be explained by the competition among various length scales (Suzuki et al 1989). In this chapter, however, we will present a different theory to interpret some of the results we have obtained.

This chapter is organized as follows. Section 1 introduces the elasticity theory near the stretching limit of a polymer. Section 2 discusses the effect of the sodium acrylate on the gelation process. Section 3 and ıre the major sections related with the stretching limit observation. The last section discusses the effect of crosslink molecules on the exponent Suzuki et al observed.

9.1 Stretching Limit Elasticity

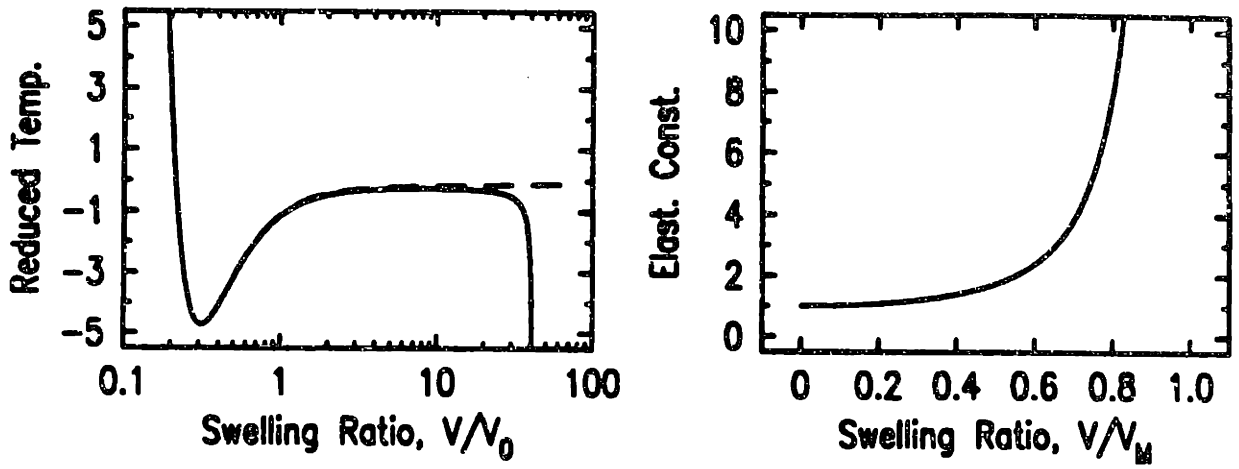

Figure 9.1: [a]. Comparison of the osmotic pressure obtained from Flory-Huggins free energy (dash line) and the free energy with the Langevin elastic term (solid line). [b] Expected elastic constant of a polymer chain as a function of swelling ratio.

Intuitively, the swelling of a unbreakable network system under positive pressure will eventually reach a limit at which the network is fully stretched. In this section, we will give a brief introduction to the elasticity of a highly stretched polymer chain. The detailed calculation can be found in appendix C.

For a flexible chain with no self-avoiding effect, the configuration distribution function with end-to-end distance r is a gaussian function with the variance $nb^2/3$. Where n is the total number of basic units with unit length b. The gaussian approximation is valid for $r \ll r_{max}$, with $r_{max} = nb$ been the length of the chain. The rigorous distribution that covers the whole possible range of r is the Langevin distribution function,

$$C(r)\,dr^3 = A\,exp\left[-n\int_0^{r/nb} L^*(\lambda)\,d\lambda\right]\,dr^3\,. \qquad (9.1)$$

Where $u = L^*(\lambda)$ is the inverse of the Langevin function $L(u)$

$$\lambda = L(u) = \coth(u) - \frac{1}{u}. \tag{9.2}$$

The λ is defined as r/nb. For small r, the Gaussian distribution is recovered. For large r, i.e., $\lambda \sim 1$, $L^*(\lambda)$ diverges, and r is bounded by an upper limit nb. Qualitatively speaking, the Gaussian form is recovered when $\lambda < 1/2$.

A comparison of the osmotic pressure obtained from Flory-Huggins free energy and the free energy with the Langevin elastic term is shown in figure 9.1a. Figure 9.1b is the expected elastic constant of a polymer chain as a function of swelling ratio.. When the network reaches the stretching limit, the curve diverges.

9.2 Gelation Analysis

In our experiment, the gel ionization is introduced by substituting certain amount of acrylamide molecules with sodium acrylate. Since sodium acrylate in water is dissociated into Na^+ and Ac^-, we expect the repulsion among these charged particles (Ac^-) will affect the network bond formation. The following studied were conducted to have a more quantitative understanding of this problem.

9.2.1 Dry-Gel Experiment

Gels of varying sodium acrylate with known swelling ratio (V/V_1) and weight (m_{gel}) were dried slowly in an oven at temperature $\sim 60°C$. Then the weight of the dried gel (m_{dry}) were measured. From these information, the network concentration ϕ_1 of the gel when the size of it is equal V_1 is

$$\phi_1 = \frac{m_{dry}}{m_{gel}} \frac{V}{V_1}. \tag{9.3}$$

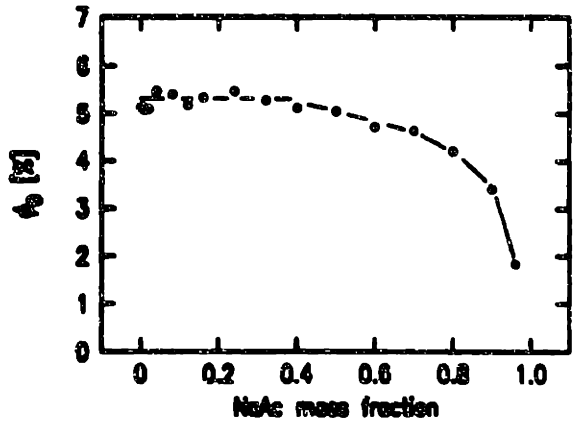

Figure 9.2: Normalized network concentration of acrylamide gel. The concentration of the network material in the pre-gel solution is 5%.

Where V_1 is the size of the gel when it was made. Fig.9.2 is our experimental result. At high sodium acrylamide concentration, ϕ_1 decreases dramatically. This indicate that in the high sodium acrylate region, the gelation process is much less effective, large amount of monomer chemicals did not become part of the network. When the gel was kept in water for several days, these monomers and short polymer chains were washed away, causing the decreasing in ϕ_1 in Fig.9.2. We should point out here that Fig.9.2 gives only the upper limit of ϕ_1, because there are branched long polymer chains and small networks trapped in the gel and could not be washed away. The real situation can be much worse than is indicated by Fig.9.2.

9.2.2 Light Scattering Study

In this experiment, we studied the pre-gel solution without the crosslinking molecules. So what we had was a polydisperse polymer solution. The purpose of this study is again to investigate the probability of forming chemical bonds between molecules. These probabilities should be related with the length distribution of the polymers. The solution concentration was 5%. The study on the diluted solution (1%) showed no significant difference.

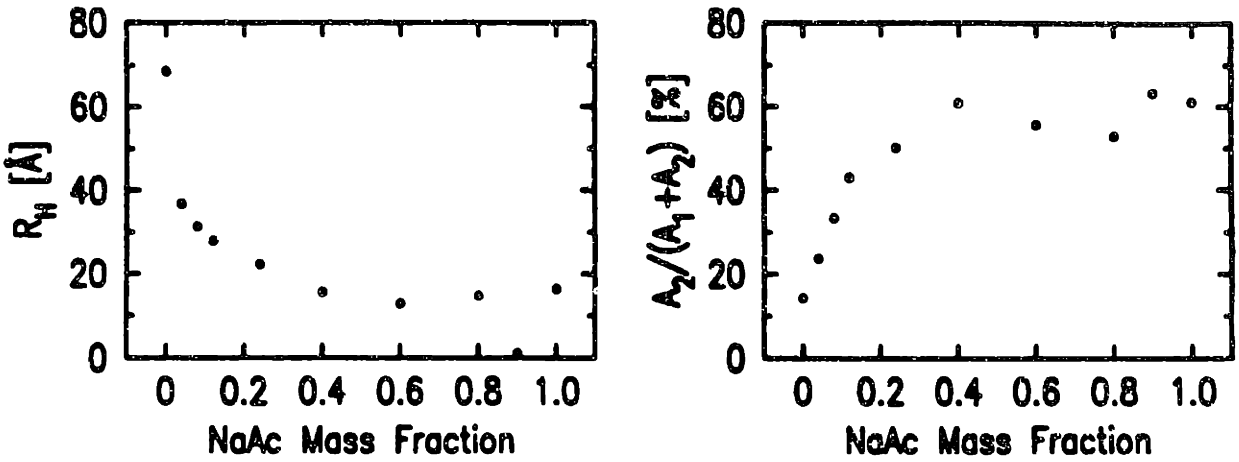

Figure 9.3: [a] Hydrodynamic radius of polymer solutions. [b] the amplitude weight of the slow component of the double exponential fit.

Figure 9.3a is the hydrodynamic radius of the polymers we measured. Figure 9.3b is the relative amplitude of the double exponential fit (slow/total) of the auto-correlation function. These results indicate that it is harder to form bonds between sodium acrylate molecules. At high sodium acrylate concentration , the polymers can not grow too long because the repulsion between sodium acrylate molecules. Also the system becomes more polydisperse.

9.3 Swelling Ratio

Figure 9.4 is the equilibrium swelling ration of acrylamide gels as a function of the concentration of sodium acrylate in preparation. It is clear from this figure that there exist three regions. For low sodium acrylate concentration (region I), the swelling ratio increases monotonically, then the curve enters a plateau region (region II), finally, at very high sodium acrylate concentration, the swelling ratio seems to diverge (region

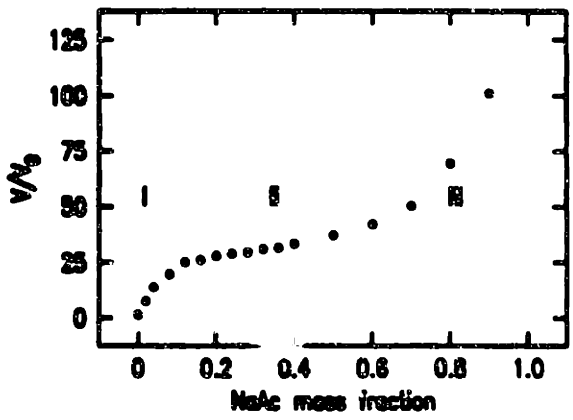

Figure 9.4: Swelling ratio of acrylamide gel as a function of the concentration of the sodium acrylate ionic groups. The gel is made by the standard recipe.

III).

Recently Y. Suzuki, et al pointed out that in the first region, the relation between the swelling ratio and the ion concentration obeys a scaling law. The exponent was interpreted as due to the charges on the network and the elasticity of the network. According to their theory, when the concentration of ions is beyond a critical value, they start to condensate on the network chain forming a charged shield (tube). The second region above can be explained as the condensation of the the ions on the network chain in their theory. In this chapter, we provide another possible explanation to this plateau.

Throughout this chapter, we assume that the stretching limit arrives before the charge condensation occurs (so we can neglect the charge condensation effect). As we have indicated in the Appendix C, in general, the energy needed to fully stretch a polymer chain is much less than the strength of the carbon-carbon bond. As the ion concentration increases, the osmotic pressure due to the ions (and counterions) increase as well. The network, forced by this pressure, swells larger and larger, until it reaches its stretching limit. Then the swelling ratio will become flat, as we have observed in the second region of Fig.9.4.

Figure 9.5: Schematic diagram of a loosely connected network. Many dangling bonds exist.

Based on the study of the gelation process in section 9.2, The third region can be explained as the following. To simplify the argument, we shall call the sodium acrylate A molecules, and call the acrylamide and bis molecules B molecules. Due to the electrostatic repulsion, bonds between two A particles are unfavored. Thus the maximum amount of A particles we can have without increase the overall bond energy is equal to the amount of B particles, and the -A-B-A-B- connection will be adapted to minimize the energy. When the amount of A is more than that of B, a good part of the excess amount of A may ended up been left alone and washed away later on. Indeed, from Fig.9.2, we find that the value of ϕ_1 starts to deviate from 5% at the sodium acrylate fractional concentration around 0.5. So as the concentration of sodium acrylate increases, the number of effective monomers decreases. When this value falls below the gelation threshold, we will not get a gel. Above this threshold, although we have a gel, but it has many cut bonds. The gel is a very loosely connected network (Fig.9.5). Effectively, we have a gel with very long chains and very few crosslinks. Due to the expansion pressure created by the ions, the network can swell to a very large degree.

9.4 Shear Modulus

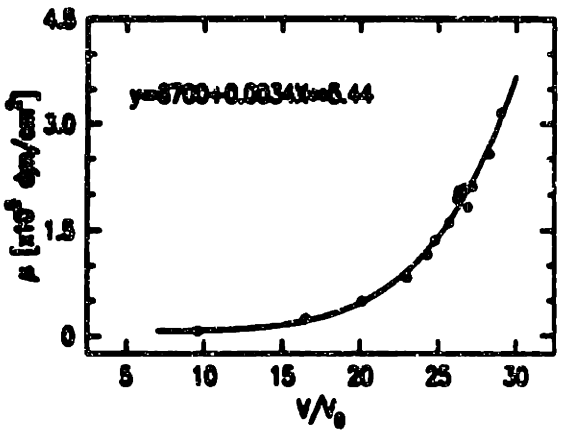

Figure 9.6: Shear modulus of polyelctrolyte network as a function of equilibrium swelling ratio (controlled by the concentration of the ions).

The experimental technique used here is the same as that described in chapter 8. The gels of different sodium acrylate were fully swollen in water. From each of these gels, a small cylindrical piece is cut out. The size of these small cylindrical pieces are the same for all the concentration of sodium acrylate. Then the instantaneous shear modulus is measured. This number is then normalized by the swelling ratio to take care of the network concentration difference. So the final value of the shear modulus is the shear modulus of unit network concentration.

Figure 9.6 is the shear modulus of polyelctrolyte network as a function of equilibrium swelling ratio (controlled by the concentration of the ions). This figure is similar to figure 9.1b. The shear modulus appears to diverge near $V/V_0 \sim 30$.

This can be explained by the stretching limit theory easily. Since in this experiment the volume is a constant, the shear deformation is related with the compression in the axial direction and the radial expansion. But near the stretching limit, it is very hard to expand the network in any direction any further. This yields the high shear modulus.

9.5 Crosslinking Molecules Effect

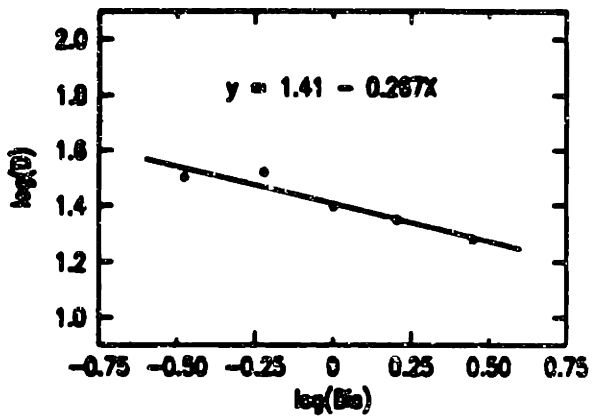

Figure 9.7: Scaling behavior of the swelling ratio versus crosslinking molecules for fixed amount of monomer units. The scaling power is ν_B.

It is very easy to show that for an ideal network, the swelling ratio is

$$\begin{aligned} \frac{V}{V_1} &= \frac{V_{net}}{V_1}\frac{V}{V_{net}} \\ &= \frac{\phi_1}{3}(\frac{b}{a})^2 n^2 \lambda^3 \\ &\sim \phi_1 ISO^{3\nu_I} BIS^{-3\nu_B}. \end{aligned} \tag{9.4}$$

where V_1 and V_{net} is the volume of the gel when it was made and the volume of the network when it was tightly packed. The a and b is the effective radius and length of the monomer unit (or persistent unit). The exponents ν_I and ν_B both are equal to 2/3 in the ideal situation.

Fig.9.7 demonstrates the scaling dependence of the swelling ration on the crosslink molecules. The power of the behavior is denoted by ν_B.

The relation between final diameter D and the BIS concentration is analyzed by fitting a line to the $log(D) - log(BIS)$ plot

$$log(D) = A(f) - \nu_B(f) log(BIS) \tag{9.5}$$

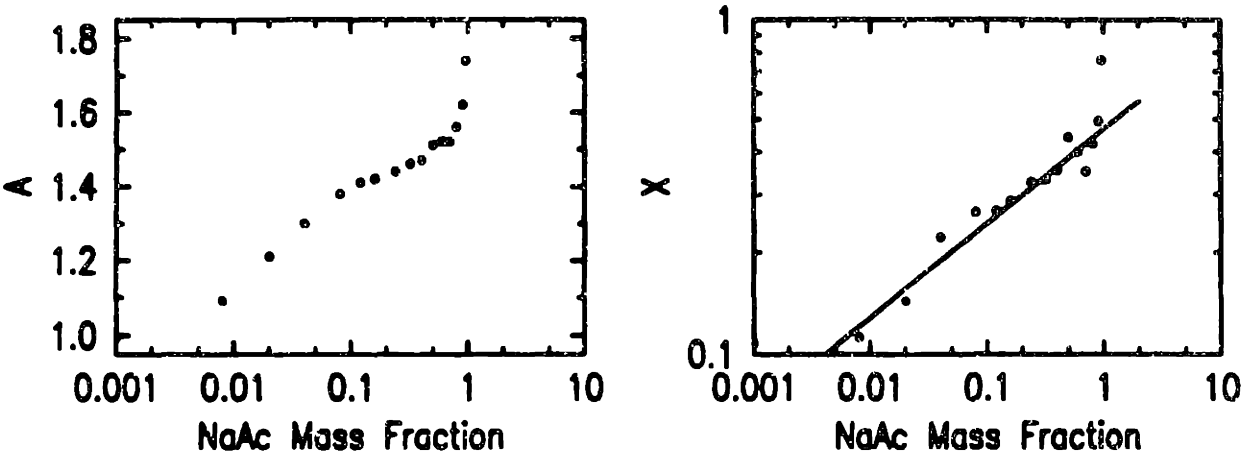

Figure 9.8: [a] Sodium acrylate dependence of the parameter A. [b] Sodium acrylate dependence of the power ν_B.

Where f is a short Land notation for sodium acrylate. Figure 9.8a and 9.8b is the parameter A and the exponent ν_B plotted against the sodium acrylate concentration, respectively. From our results, we can write down the following phenomenological relations

$$D(BIS = 1, f) = 10^{A(f)} \sim f^{\nu} \sim f^{0.3}, \tag{9.6}$$

$$\nu_B(f) \approx 0.1 \cdot f^{\nu'} = 0.1 \cdot f^{0.3}. \tag{9.7}$$

The first equation agrees with the result Dr. Suzuki had obtained recently. Combine everything together

$$D(f, BIS) = 10 f^{\nu} BIS^{-0.1 f^{\nu'}} \tag{9.8}$$

For $BIS \approx 1$, we can write

$$\begin{aligned} D(f, BIS) &= 10 f^{\nu} (1 + \delta B)^{-0.1 f^{\nu'}} \\ &= 10 f^{\nu} (1 - 0.1 f^{\nu'} \delta B). \end{aligned} \tag{9.9}$$

So there is an correction term. In general, the correction term is smaller than the first term.

From the discussion above, we find that the exponent ν is coupled with ν'. The coupling is weak for small ion concentration. This is clearly shown in figure 9.8b. If we fit all of these swelling ratio curves with

$$log(D) = A + \nu\, log(f)\,, \tag{9.10}$$

we will find that the value of the exponent changes

$$\delta\nu \sim 0.1\,. \tag{9.11}$$

A more general scaling form is

$$D \sim f^{\nu(B_0)} \left(\frac{B}{B_0}\right)^{-\varepsilon_0 f^{\nu'}}\,. \tag{9.12}$$

From the fact that D is independent of the reference value B_0, we can show that

$$\nu(B_0) \sim ln(B_0)\,. \tag{9.13}$$

Different reference concentration of bis will give different exponent ν. Dr. Suzuki's result happens to be the result with the reference bis concentration the standard recipe concentration.

Chapter 10

Surface Tension of Gels, Etc.

The interfacial energy is directly related with many phenomenon, including surface wetting, surface tension, liquid crystal, domain formation, etc. In this chapter, we mainly discuss the surface tension of gels both in solvent and in the saturated vapor of the solvent. We will show that when the gel size is of the order of several hundred microns (sub-millimeter), the surface tension is not negligible. We will also explain the observation first made by Dr. Hirokawa (private conversation) about the collapsing of gels in saturated solvent vapor.

We will also briefly discuss several other experimental results we obtained in the past several years. They all appear interesting to a greater or lesser extend.

10.1 Surface Tension Theory

Based on the consideration that the interfacial properties of a liquid-gas system are not independent quantities once the temperature and the pressure is given, Cahn and Hilliard (1958) derived a very successful theory of the interface between two co-existence phases. The surface tension of polymer melts has been studied both theoretically (Poser and Sanchez 1979; Rabin 1984) and experimentally (Wu 1969;

Bhatia et al 1985) with great success.

In this section, we will give a brief introduction to the basic theory of the surface tension. Then we will apply this theory to gel network system to relate the surface tension with the swelling ratio of the gels.

10.1.1 General Discussion

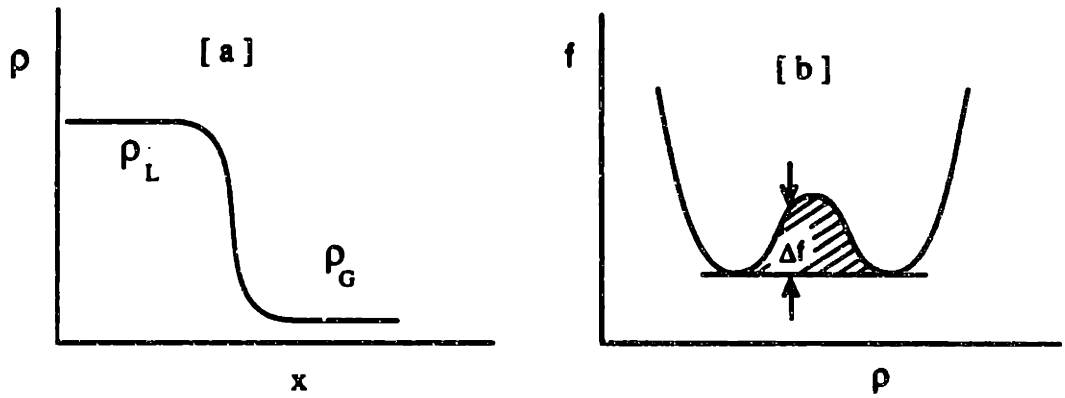

Figure 10.1: [a] Density profile of liquid-gas interface. The non-zero thickness of the interface gives rise of the surface energy and hence the surface tension. [b] Interface free energy as a function of density (hence distance x).

For a liquid-gas system below the critical point, liquid and gas coexist. Due to their different density, a definite Interface between them exist. The density profile varies from the value of liquid phase to the value of gas phase (Fig.10.1a). Related with this profile, there is a free energy increase. A typical Landau-type formula can be used to describe the surface energy (Cahn and Hillard 1958):

$$\gamma = \int_0^\infty \left[\Delta f + \kappa(d\rho/dx)^2\right] dx, \tag{10.1}$$

where $\rho(x)$ is the density profile, Δf is the free energy difference between the Interface molecules and the bulk ones (see Fig.10.1b). The system minimizes it's free energy

by adjusting the profile $\rho(x)$. The surface tension is the Interface free energy per unit surface area. For simplicity, we will use the symbol γ for both surface energy and the tension.

In the surface wetting case, there are two contributing factors to the surface energy, one is the density profile of the liquid film, the other is the wall-film (gel-film) interaction:

$$\gamma = \Phi(c_s) + \int_0^\infty \left[\Delta f + \kappa(dc/dx)^2\right] dx, \tag{10.2}$$

where the first term is the wall-film interaction and c_s is the film density at the surface, the second term is the film free energy. We have assumed that the wall-film interaction is a short range interaction. We are going to assume that our gel is totally wet.

10.1.2 Surface Tension of Gels

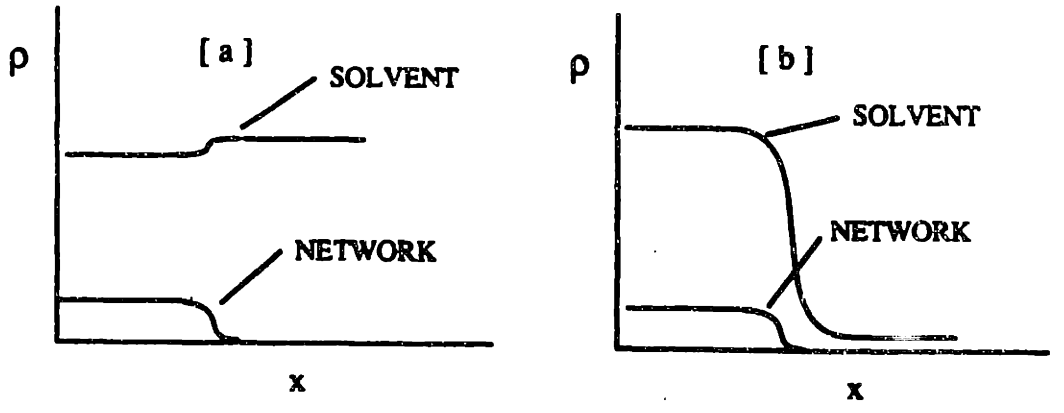

Figure 10.2: Density profile of a gel [a] in solvent, [b] in saturated vapor.

There are two cases that we are interested in the case of gel (figure 10.2). One is the gel immersed in solvent, the other is the gel surrounded by the solvent saturated

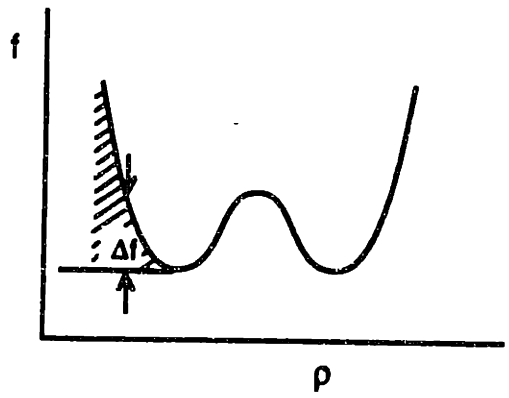

Figure 10.3: Surface tension contribution of the gel system.

vapor. There are two density profiles in each case, as shown in figure 10.2. One is the network density profile, the other is the solvent density profile. Our final goal is to estimate the surface tension of these profiles.

The surface tension contributed by the network density profile is different from that of a liquid-vapor interface. The contribution is shown by the shaded area in figure 10.3. From figure 10.3, we expect the surface tension of a gel system is much larger than the typical liquid-vapor system.

10.1.3 Effect on the Swelling Ratio

According to Flory-Huggins mean field theory, the osmotic pressure of a gel network can be written as:

$$\frac{\Pi}{kT} = \frac{N}{v}\left[\phi + ln(1-\phi) + \frac{\Delta F}{2kT}\phi^2\right] + \nu\left[(f+\frac{1}{2})\frac{\phi}{\phi_1} - \left(\frac{\phi}{\phi_1}\right)^{1/3}\right]. \qquad (10.3)$$

Where N is Avogadro's constant, v is the molar volume of the solvent, ν is the number of chains per unit volume at $\phi = \phi_1$, and f is the number of dissociated counterions per chain. For a swollen gel, the first term is eq. (10.3) is small and can be neglected

$$\frac{\Pi}{\nu kT} = (f+\frac{1}{2})\frac{\phi}{\phi_1} - \left(\frac{\phi}{\phi_1}\right)^{1/3}. \qquad (10.4)$$

In general, when the gel is small, the pressure due to the surface tension should be considered,

$$\Pi_s = \frac{\gamma}{r} = \frac{\gamma}{r_1}\left(\frac{\phi}{\phi_1}\right)^{1/3} . \tag{10.5}$$

Where γ is the surface tension of the gel, r_1 is the radius of the gel at $\phi = \phi_1$, and r is the equilibrium radius. For a liquid-gas system, the surface tension goes to zero as the system approaches the critical point. When the critical point of the solvent is far from the experiment region, the surface tension varies very slowly with temperature and can be treated as a constant. During our experiment, the temperature changes by several degrees, so in practice kT is a constant as well. Combine eq (10.5) and eq (10.4), at equilibrium ($\Pi_{total} = 0$)

$$\left(\frac{\phi}{\phi_1}\right)^{2/3} \equiv \left(\frac{r_1}{r}\right)^2 = \frac{2}{2f+1}\left(1 + \frac{\gamma}{\nu kT}\frac{1}{r_1}\right) . \tag{10.6}$$

If we plot $(r_1/r)^2$ vs r_1^{-1} for the same kind of gel, we expect to get a straight line. The slope of it will be proportional to the surface tension of it.

Define α as the relative linear size of the gel,

$$\alpha \equiv \left(\frac{V}{V_1}\right)^{1/3} = \left(\frac{\phi_1}{\phi}\right)^{1/3} . \tag{10.7}$$

$$\begin{aligned} \alpha^{-2} &= \frac{2}{2f+1}\left(1 + \frac{\gamma}{\nu kT}\frac{1}{r_1}\right) \\ &= A\left(1 + \frac{B}{r_1}\right) . \end{aligned} \tag{10.8}$$

So from a $\alpha^{-2} - 1/r_1$ plot, we can obtain information about the surface tension γ and gel structure parameter f or ν.

At equilibrium,

$$\alpha_e = \sqrt{f + \frac{1}{2}}\left(1 - \frac{\gamma}{2\nu kT r_1}\right) . \tag{10.9}$$

The fractional change of the gel size due to the surface tension can be estimated from the second term in the parentheses. A typical value of γ for polymer solution (CRC Handbook of Chemistry and Physics) is 60 dyne/cm, ν is $\sim$ 1 mM, take the initial radius r to be 0.1cm, we find that the correction term is about 1%.

10.2 Experimental Results

10.2.1 Gels in Solvent

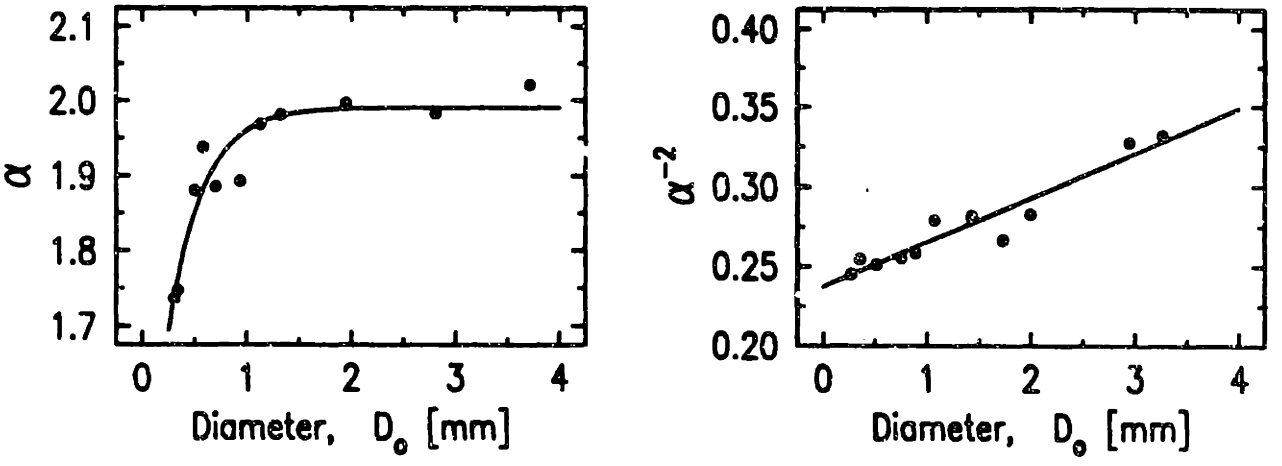

Figure 10.4: [a] Linear swelling ratio of acrylamide gels with different initial diameter (D_1) in water. These were ionic gels with 11mM sodium acrylate. [b] Replot of the figure 10.4a. The slope is proportional to the surface tension γ.

Figure 10.4a is a very typical result of our experiment. We noticed that the linear swelling ratio starts to decrease at $\sim 1.2mm$ as the gel size decreases. The swelling difference between a large gel and the smallest gel we had ($D_0 = 0.307mm$) is about 12%, or the volume swelling ratio is about 36% . This is a very large difference. This

means that when ever we are dealing with small gels (of the order of 1 mm), the surface tension can not be neglected.

From figure 10.4b, we find

$$A = \frac{2}{2f+1} = 0.24 \pm 0.01 \tag{10.10}$$

$$B = \frac{\gamma}{\nu} = 0.014 \pm 0.003\,, \tag{10.11}$$

or

$$f = 3.7 \pm 0.2 \tag{10.12}$$

$$\frac{\gamma}{\nu kT} = 0.014 \pm 0.003\,. \tag{10.13}$$

At room temperature (300K), $N_0kT = 2.5 \times 10^{10} ergs$, $\nu \leq 8.6 \times 10^{-6} N_0/\text{cc}$, so $\gamma \sim 300 dynes/cm$. This number is much larger than the the value of a typical liquid-gas interface. The surface tension for water-air interface is about 72 *dynes/cm*

10.2.2 Gels in Saturated Vapor

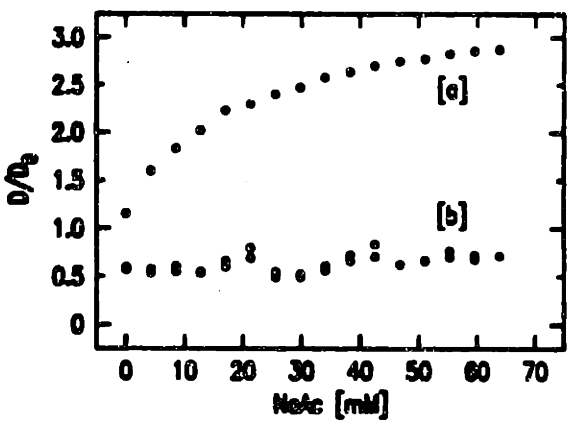

Figure 10.5: Linear swelling ratio of ionic acrylamide gels [a] in water, [b] in saturated water vapor. The initial diameter of the gels was 1.28mm.

The samples we used in this experiment were ionic acrylamide gels. In saturated vapor, all of the gels collapsed (figure 10.5). This indicates that the surface tension

of a gel in saturated vapor is tremendous

$$E_{surface} \gg E_{elast}. \tag{10.14}$$

Where $E_{surface} = 4\pi\gamma r^2$ and $E_{elast} = (K/2)(1 - V_f/V_i)^2$ is the surface energy and the elastic energy of the gels at the collapsed state. From chapter 8, we know that the bulk modulus of our gels are about $3 \times 10^4 dynes/cm^2$. Take $r \sim 1mm$ and $V_f/V_i \sim 0$ for the 33mM ionic gel, we find $\gamma \sim 10^5 dynes/cm$. This value again is much larger than the surface tension of a typical liquid-vapor system.

The only possible source of the large value of the surface tension of gels in solvent (10^2) and in vapor (10^5) is the density profile of the network at the boundary, as we have stated earlier.

10.3 Other Miscellaneous Experiments

10.3.1 Gels in Polymer Solutions

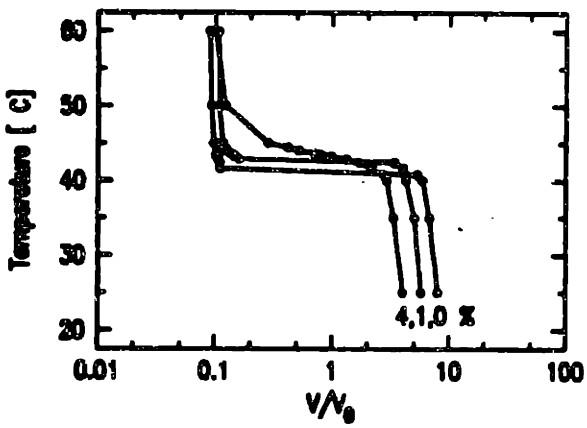

Figure 10.6: Swelling ratio of 32mM ionic Iso gels in Dextran solution. The molecular weight of the dextran is 200,000.

The basic procedure of this experiment is the following. First we make a gel in water, then put it in high molecular weight polymer solution. Because of the large size of

the polymers, they can not enter the gel network. The presence of these polymers decreases the chemical potential of the solvent outside the gel, providing an effective osmotic pressure to the network. This type of work has been done by several people (Hossian, Hirotsu, and the author of this thesis)

Figure 10.6 is our typical result. We expected at the beginning that the gel in higher polymer concentration solution should have a smaller volume due to the larger pressure. In out results, however, we find that there is a cross-over behavior among these curves. In the swollen state, higher polymer concentration corresponds to smaller gels, and vice versa. On the other hand, during the transition the cross-over occurs. The higher polymer concentration corresponds to larger gels instead.

We believe that this cross-over is caused by the absorption of the dextran polymer on the surface of the gel. The polymers absorbed onto the gel changes the surface property of the gel. Depending upon the sign of the effect, it can vary the behavior of the gels in many ways.

10.3.2 Gels in Water-Alcohol Mixture

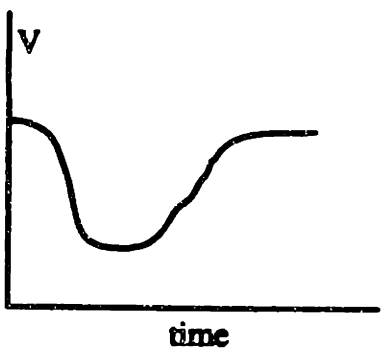

Figure 10.7: Time dependence of iso gel in water-alcohol mixture. The temperature of the gel was changed at time zero.

Hirotsu (Hirotsu, 1987) had studied the swelling ratio of the isopropylacrylamide gel water-alcohol mixture. In this subsection, we discuss the stability of the gels in water-alcohol mixture. Figure 10.7 illustrate time dependence of the size of a gel after the

temperature had been changed at time zero. In this figure, after the temperature had been changed, the gel collapsed first, then swelled back to the swollen state again. This may be the result of the temperature dependent preferential absorption of the solute molecules on the network.

10.3.3 Gravitational Effect

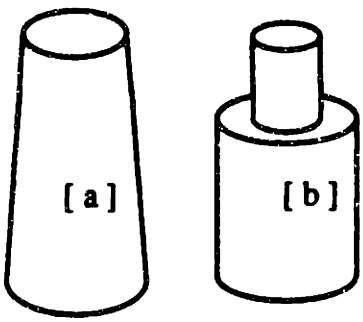

Figure 10.8: [a] Cylindrical gel in saturated vapor. The gravitational effect is z-dependent. [b] Expected transition behavior due to the gravity.

What will happen to a large (can neglect surface tension) upright cylindrical gel in saturated vapor? What is the effect of the gravity on the swelling ratio of this gel? These are the questions we raise in this subsection.

The chemical potential of solvent molecules In the gravitation field varies along the z-axis. The osmotic pressure due to the gravity will eventually be balanced by the elasticity of the network. Since the osmotic pressure is linear in z (proportional to the chemical potential), this problem can be treated in the way we have described in section 8.5 about the phase transition of gels induced by the external pressure. The only difference is that now the pressure is z position dependent. (Actually now Tanaka's (1981) result can be used without any modification). We will not go into the theoretical calculation here.

Appendix A

Experimental Details

A.1 Gel Recipes

There are many ways to form a network (Mark and Erman 1988). The common way is tostart from monomers by using the radical copolymerization technique. Another way is to start from polymers. To chemically link polymers in to a network, we can use vocanization (sulfer cure), peroxide cure (radical process), and high energy radiations (e, γ, UV). A network can also be made by physically connect polymers together. Some common ways are, addition of glue like filling particles, monomers (links formed by the negatively charged polymer side groups been attracted to the same positively charged particles), microcrystalization of polymers, hydrogen bonds, etc. We usually use the copolymerization method to make gels. Here are the two recipes referred as the standard (std) recipes in this thesis.

A.1.1 Acrylamide Gel

A. TEMED(240μl), Bis(133mg), Acrylamide(5g) in deionized, distilled water(100ml).

B. Amonium Persulfate(400mg) in deionized, distilled water(10ml).

C. Use N_2 gas to bubble the solution [A] and [B] for several minutes.

D. Mix a portion of [A] with 1% (by weight) of [B], quickly transfer the mixture into the container in which the gel is going to be made.

E. The gelation process will be completed in about ten hours.

The interaction parameter, χ, of the polyacrylamide-water system is 0.45, mentioned by Weiss, N., Van Vliet, T. and Silberberg, A., (1979). The reduced temperature appears as $1/2 - \chi$, so the acrylamide gel is temperature insensitive in the room temperature region. A convenient parameter is the solvent concentration (for instance, aceton-water mixture).

A.1.2 Isopropylacrylamide Gel

A. TEMED($240\mu l$), Bis(133mg), Isopropylacrylamide(7.8g) in deionized, distilled water(100ml).

B. Amonium Persulfate(400mg) in deionized, distilled water(10ml).

C. Use N_2 gas to bubble the solution [A] and [B] for several minutes.

D. Mix a portion of [A] with 1% (by weight) of [B], quickly transfer the mixture into the container in which the gel is going to be made.

E. The gelation process will be completed in about ten hours.

Isopropylacrylamide gel is very sensitive to the change of the temperature in the 25-35 °C region. This region becomes higher for ionic gels.

A.1.3 Purification of N-isopropylacrylamide

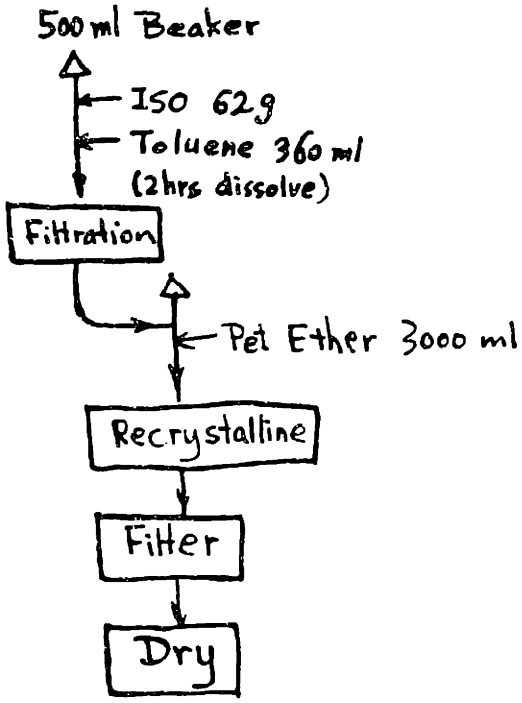

Figure A.1: Purification of Iso monomers.
The N-isopropylacrylamide was bought from Kodak Chemical Labs and purified according to this diagram.

A.1.4 Related Molecular (Formular) Weights

Molecule	MW (FW)	Handy Conversions
Acrylamide	71.08	700mM = 5g/100cc
Amonium Persulfate	228.2	1.69mM = 400mg/10cc/100
N,N'-methylenebisacrylamide	154.17	8.6mM = 133mg/100cc
N-isopropylacrylamide	113.16	640mM = 7.8g/100cc
Sodium Acrylate	94.04	1mM = 9.40mg/100cc
TEMED	116.12	(2.4*d/116.21)mM = 240μl/100cc

note: To suppress the spontaneous hydrolysis caused by TEMED, 20mg/100cc sodium pyrosulfite can be used (M. Ilavsky, Macromolecules **15**, 782(1982)).

The structure of a polymer network is, in general, quite complex. Fig.A.2 includes some of the non-ideal features of a real network. There are chains that are entangled

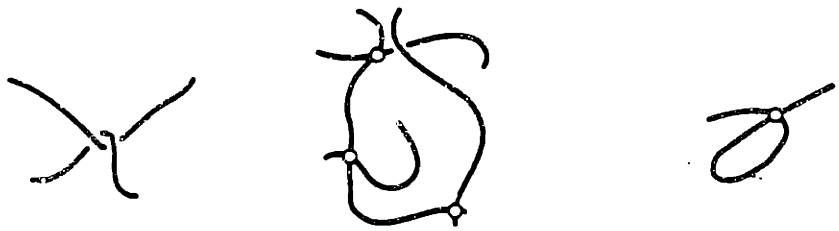

Figure A.2: Deviation of a real network from a phantom network. (a) Entanglement. (b) Dangling chains. (c) Intramolecular cross-linking.

together, making contribution to the elasticity of the network. Also there are some unfinished chains that dangling around. There are also intra-cross links that makes a chain shorter. The length of a chain between two crosslinkers is not a constant. Some places have more cross-lionkers than others. All of these makes the network system harder to model theoretically.

A.2 Temperature Control

In many of the experiments mentioned in this thesis, the temperature was controlled for various purposes. There are two type of temperature controls we have used. One is rough control by using conmercially avilable water circulator, which usually has a stability ±50mK. The other is precision control, which uses the water circulator to control the ambient temperature as the first stage. Here we will only discuss the basic principle of the precision temperature controller.

A.2.1 Sample Holder

All of out sample holders are alike as far as the temperature regulating mechanisim is concerned. Figure A.3 is a schematic description of our sample holders. Some of the

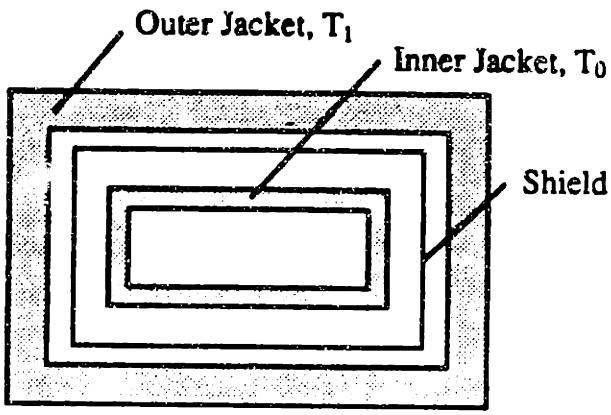

Figure A.3: Schematic sample holder with Precision temperature control.

general priciples we had kept in mind when we were designing these sample holders are listed below.

- The setup shoud be two-stage temperature controlled.
- In general, the sample holder should have three pieces, the inner container, shield, and an outer container.
- The inner container should be thermally massive to have a long temperature relaxation, hence to stablize the temperature. Its temperature will be directely controlled be a heater connected to an electronic system with feed-back featuer.
- The shield is need to decrease the temperature gradient effect and uniformize the temperature. It should be thermally light weight.
- The temperature of the outer container will be controlled by a rough temperature regulator to provide a stable enviorment for the inner container.

A.2.2 Electronics

We have used several temperature controllers. Figure A.4 is a schematic diagram of one of them. The electronic circuit is more or less standard, so we will not go into

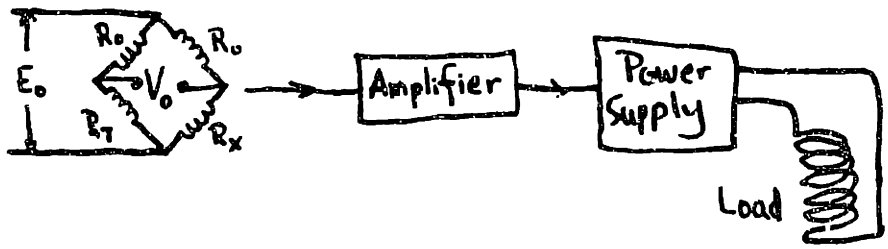

Figure A.4: Schematics of the electronic circuit diagram.

the details of it.

A.3 Some Cells

Many cells had been made to contain the samples. We will discuss some of the cells we have used for various experiemnts. Figure A.5 below shows the two cells we have used in the critical isobar and the heat capacity experiment.

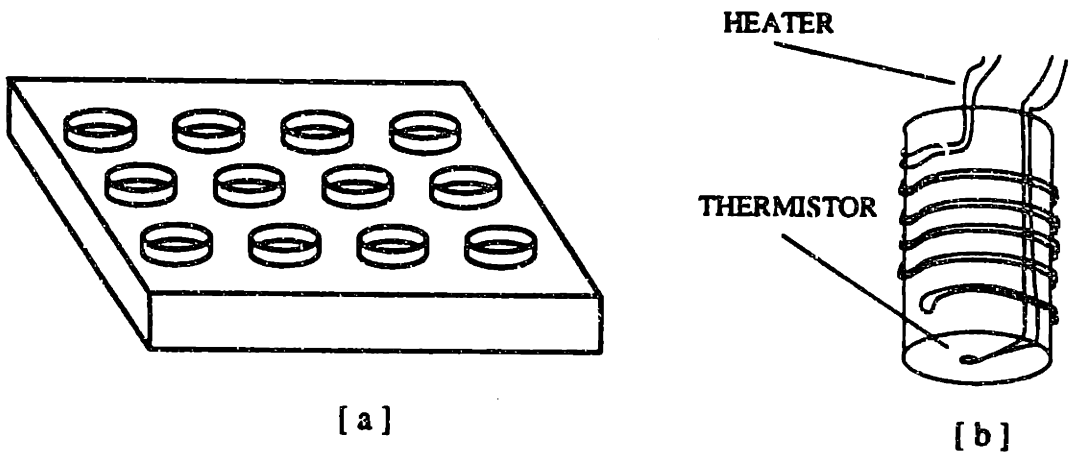

Figure A.5: [a]. Isobar sample cells. It can hold 64 samples. [b] cell of the heat capacity experiment.

Appendix B

Criticality of Flory-Huggins' Mean-Field Theory

This note is intended to be a handy reference and a confirmation to the people who is interested in the polymer coil-global and gel network phase transition. The criticality of Flory-Huggins theory is calculated and discussed. The exponents are found to be the same as that of a typical mean-field theory. Relations of some experimentally more accessible quantities and the quantities of the most theoretical interest are discussed. Some results are compared with the existing experimental data.

B.1 Some General Thermodynamic Relations

For a gel network system, the external pressure, in general, is zero. The convenient parameter is f, the total number of free ions trapped inside the gel. But in order to relate the experimentally measured quantities of a gel system with more recognizable thermodynamic quantities that is related with the external pressure, in this section we consider the more general case, i.e, leave the external pressure as a function of

other variables. The most general free energy can be written as

$$F = F(t,V,f), \tag{B.1}$$

$$dF = -Sdt - PdV + \mu df, \tag{B.2}$$

where t, V, and f are the temperature, volume and the total number of particles of one component. From eq. (B.2), we get:

$$S = -\frac{\partial F}{\partial t}, \tag{B.3}$$

$$P = -\frac{\partial F}{\partial V}, \tag{B.4}$$

$$\mu = \frac{\partial F}{\partial f}. \tag{B.5}$$

And the Maxwell's relations:

$$\begin{cases} \left(\frac{\partial S}{\partial V}\right)_{tf} = \left(\frac{\partial P}{\partial t}\right)_{vf}, \\ \left(\frac{\partial S}{\partial f}\right)_{tv} = -\left(\frac{\partial \mu}{\partial t}\right)_{vf}, \\ \left(\frac{\partial P}{\partial f}\right)_{tv} = -\left(\frac{\partial \mu}{\partial t}\right)_{tf}. \end{cases} \tag{B.6}$$

Define the following quantities:

$$\chi_{tf} = -\frac{1}{V}\left(\frac{\partial V}{\partial P}\right)_{tf}, \quad \text{(isotherm compressibility)} \tag{B.7}$$

$$K_{tp} = \frac{1}{V}\left(\frac{\partial V}{\partial f}\right)_{tp}, \quad \text{(isotherm expandability)} \tag{B.8}$$

$$\alpha_{pf} = \frac{1}{V}\left(\frac{\partial V}{\partial t}\right)_{pf}, \quad \text{(isotherm expansion)} \tag{B.9}$$

and heat capacities:

$$C_{pf} = t\left(\frac{\partial S}{\partial t}\right)_{pf}, \tag{B.10}$$

$$C_{pv} = t\left(\frac{\partial S}{\partial t}\right)_{pv}, \tag{B.11}$$

$$C_{vf} = t\left(\frac{\partial S}{\partial t}\right)_{vf}, \tag{B.12}$$

By using the Maxwell's relations and the mathematical identities

$$\left(\frac{\partial x}{\partial y}\right)_z \left(\frac{\partial z}{\partial x}\right)_y \left(\frac{\partial y}{\partial z}\right)_x = -1 \tag{B.13}$$

and

$$\left(\frac{\partial x}{\partial y}\right)_z = \left(\frac{\partial x}{\partial y}\right)_s + \left(\frac{\partial x}{\partial s}\right)_y \left(\frac{\partial s}{\partial y}\right)_z, \tag{B.14}$$

we can obtain the following relations,

$$\chi_{tf} = K_{tp}\left(\frac{\partial f}{\partial P}\right)_{tv}, \tag{B.15}$$

$$\chi_{tf} = \alpha_{pf}\left(\frac{\partial t}{\partial P}\right)_{fv}, \tag{B.16}$$

$$C_{pf} - C_{vf} = tV\left(\frac{\partial P}{\partial t}\right)_{fv} \alpha_{pf}, \tag{B.17}$$

$$C_{pv} - C_{fv} = -t\left(\frac{\partial \mu}{\partial t}\right)_{fv}\left(\frac{\partial f}{\partial t}\right)_{pv}. \tag{B.18}$$

B.2 General Discussion of the Flory-Huggins Mean-Field Theory

The Flory-Huggins mean-field free energy of a gel network system is

$$F(t,\phi,f) = \frac{t}{2}\left[2n\frac{1-\phi}{\phi}ln(1-\phi) + 3\phi_0^{2/3}\phi^{-2/3} + (2f+1)ln\phi\right] - \frac{n}{2}\phi \tag{B.19}$$

with

$$\frac{\phi}{\phi_0} = \frac{V_0}{V} \tag{B.20}$$

Where $F(t,\phi,f)$ is the free energy per chain of a network in the unit of Flory's effective polymer-polymer interaction energy ΔF, $t = kT/\Delta F$ is the reduced temperature, f is the total number of free ion particles (free gas) of a chain, n is the effective

number of monomer units in a chain, ϕ is the volume fraction of the network , ϕ_0 is a reference concentration of the system. From eq. (B.19), we have:

$$S = -\frac{1}{2}\left[2n\frac{1-\phi}{\phi}ln(1-\phi) + 3\phi_0{}^{2/3}\phi^{-2/3} + (2f+1)ln\phi\right], \tag{B.21}$$

$$P = \frac{t}{2V_0}\left[-\frac{2n}{\phi_0}ln(1-\phi) - 2n\frac{\phi}{\phi_0} + (2f+1)\frac{\phi}{\phi_0} - 2(\frac{\phi}{\phi_0})^{1/3}\right] - \frac{n}{2V_0\phi_0}\phi^2, \tag{B.22}$$

$$\mu = tln\phi. \tag{B.23}$$

From the renormalization-group (RG) theory point of view, when the external pressure is fixed, there are only two relevant parameters t and f. So the system has two degrees of freedom. This tells us that there can exist only two independent critical exponents. Here we will only concentrate on the relations (B.15)-(B.18). From (B.22)

$$\left(\frac{\partial f}{\partial P}\right)_{tv} = \frac{V}{t}, \tag{B.24}$$

$$\left(\frac{\partial t}{\partial P}\right)_{fv} = \frac{2V_0\phi_c t}{n\phi^2}. \tag{B.25}$$

Both (B.24) and (B.25) are finite and non-singular functions around the critical point. So we know immediately that the critical behavior of the isotherm compressibility χ_{tf}, isotherm expandability K_{tp} and the thermal expansion α_{pf} are the same, they all have the same exponent. This critical exponent of χ_{tf}, by definition, is γ.

Since the entropy depends only on V and f explicitly, we have

$$C_{vf} = 0, \tag{B.26}$$

$$C_{pf} = tV\left(\frac{\partial P}{\partial t}\right)_{fv}\alpha_{pf}, \tag{B.27}$$

$$C_{pv} = -t\left(\frac{\partial \mu}{\partial t}\right)_{fv}\left(\frac{\partial f}{\partial t}\right)_{pv}. \tag{B.28}$$

From (B.22) and (B.23)

$$\left(\frac{\partial \mu}{\partial t}\right)_{fv} = ln\phi, \tag{B.29}$$

$$\left(\frac{\partial f}{\partial t}\right)_{pv} = -\left(\frac{\partial P}{\partial t}\right)_{fv}\left(\frac{\partial P}{\partial f}\right)_{tv} \tag{B.30}$$

$$= -\frac{n\phi}{2t^2},$$

$$C_{pv} = \frac{n\phi}{2t} ln\phi. \tag{B.31}$$

Both (B.29) and (B.30) are finite at the critical point. From (B.27) we know that C_{pf} has the same critical exponent as χ_{tf}. The quantity C_{pv} is finite. The exponent of it is zero. By definition, this exponent is α

$$\alpha = 0 \tag{B.32}$$

Since there are only two independent exponents, there are relations among different critical exponents. Two of them are

$$\alpha + 2\beta + \gamma = 2, \tag{B.33}$$

$$d\nu = 2 - \alpha, \tag{B.34}$$

where d is the dimensionality of the system, ν is the exponent of the correlation length. In general, mean-field predicts

$$\begin{cases} \alpha = 0, \\ \beta = \frac{1}{2}, \\ \gamma = 1. \end{cases} \tag{B.35}$$

We should point out that in many ways, the variable f behaves as the external pressure. Since in gel experiment, usually P = 0, we can drop the subscript p for the experimentally measured, e.g., C_{pf}, C_{pv}, K_{tp}, etc. In the liquid-gas transition, P = P(V, T) is the equation of the state, in the gel transition, we can write $f = f(\phi, t)$ from (B.22).

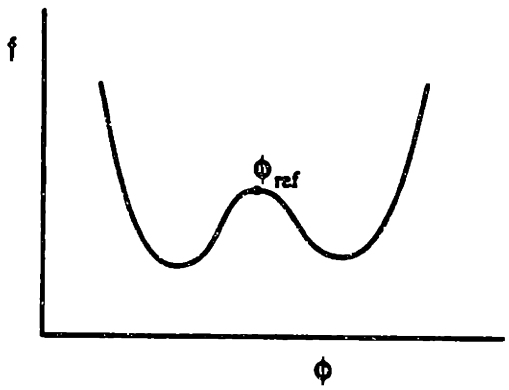

Figure B.1: Flory-Huggins free energy. The local maximum point has been choosen as the reference point.

B.3 Phase Diagram

In general, the equilibrium of a gel network system is reached when the osmotic pressure is zero:

$$P = \frac{t}{2V_0}\left[-\frac{2n}{\varphi_0}ln(1-\phi) - 2n\frac{\phi}{\phi_0} + (2f+1)\frac{\phi}{\phi_0} - 2(\frac{\phi}{\phi_0})^{1/3}\right] - \frac{n}{2V_0\phi_0}\phi^2 = 0 \quad \text{(B.36)}$$

In the following part of this note, we will assume P = 0 unless otherwise mentioned. The critical behavior of the system is independent of the value of the pressure. For fixed t and f, the gel adjusts its density ϕ so that at equilibrium, the free energy is a global minimum. For a specific sample, the f value is fixed, when we change t, depends on the value of f, we may get either a continuous or a discontinuous change in ϕ. The critical point of the system is determined by the equation of the state (B.36) and :

$$F^{(2)}(c) \equiv \left(\frac{\partial^2 F}{\partial \phi^2}\right)_{tf} = 0, \quad \text{(B.37)}$$

$$F^{(3)}(c) \equiv \left(\frac{\partial^3 F}{\partial \phi^3}\right)_{tf} = 0. \quad \text{(B.38)}$$

Where $F^{(n)}(c)$ is the n-th derivative of the free energy evaluated at the critical point. For n = 40 and $\phi_0 = 0.05$ (the same as $S_0 = 10$), the numerical value of the critical

point is:

$$\begin{cases} t_c = & 0.74723, \\ \phi_c = & 0.12798, \\ f_c = & 0.65851. \end{cases} \tag{B.39}$$

For $t < t_c$ and $f > f_c$, the free energy has two minima and one maximum (figure B.1). At certain value of t = t(f), the free energy of the two minima have the same value, the two states (corresponds to the two minima) co-exist, and the first order phase transition occurs. Let's choose the density at which the free energy is maximum to be a reference density, ϕ_r. Expand the free energy around this point, we have

$$F(t,\phi,f) = F(r) + F^{(1)}(r)\delta\phi + \frac{F^{(2)}(r)}{2}\delta\phi_r{}^2 + \frac{F^{(3)}(r)}{3!}\delta\phi_r{}^3 + \frac{F^{(4)}(r)}{4!}\delta\phi_r{}^4 + \ldots \tag{B.40}$$

Where $\delta\varphi_r = \phi - \phi_r$, and $F^{(n)}(r)$ is the n-th derivative of F evaluated at the reference point.

$$F^{(1)}(r) = \frac{nt}{\phi^2}\left[-ln(1-\phi) - \phi + \frac{(2f+1)}{2n}\phi - \frac{1}{n}\phi_0{}^{2/3}\phi^{1/3}\right] - \frac{n}{2}. \tag{B.41}$$

$$F^{(2)}(r) = \frac{nt}{\phi^3}\left[2ln(1-\phi) + \frac{\phi}{1-\phi} + \phi - \frac{(2f+1)}{2n}\phi + \frac{5}{3n}\phi_0{}^{2/3}\phi^{1/3}\right]. \tag{B.42}$$

$$F^{(3)}(r) = \frac{nt}{\phi^4}\left[-6ln(1-\phi) - 4\frac{\phi}{1-\phi} + (\frac{\phi}{1-\phi})^2 - 2\phi + \frac{(2f+1)}{n}\phi - \frac{40}{9n}\phi_0{}^{2/3}\phi^{1/3}\right]. \tag{B.43}$$

$$F^{(4)}(r) = \frac{nt}{\phi^5}\left[24ln(1-\phi) + 18\frac{\phi}{1-\phi} - 6(\frac{\phi}{1-\phi})^2 + 2(\frac{\phi}{1-\phi})^3 + 6\phi - 3\frac{(2f+1)}{n}\phi + \frac{440}{27n}\phi_0{}^{2/3}\phi^{1/3}\right]. \tag{B.44}$$

Where F(r) means that the function F is evaluated at the reference point (t, ϕ_r, f). $F^{(1)}(r) = 0$ by (B.36). Under the condition $t \sim t_c$ and $f \sim f_c$, we will have $\phi_r \sim \phi_c$, and $\delta\phi_r$ will be a small number. Up to the fourth power of $\delta\phi_r$, when $F^{(3)}(r)$ is zero, eq. (B.40) is symmetric about ϕ_r, and the two minima of F are the same. So the

co-existence condition is determined by eq (B.36) and

$$F^{(3)}(r) = 0. \tag{B.45}$$

Notice that the reference point under the co-existence condition is uniquely determined. Let us treat first order transition point (t_t, f_t) as functions of the reference density ϕ_r:

$$\delta t \equiv t_t - t_c = \delta t(\phi_r), \tag{B.46}$$

$$\delta f \equiv f_t - f_c = \delta f(\phi_r). \tag{B.47}$$

Then these two functions can be linearized around the critical point:

$$\delta f = \frac{\partial f_t}{\partial \phi_r}(\delta \phi_{rc}), \tag{B.48}$$

$$\delta t = \frac{\partial t_t}{\partial \phi_r}(\delta \phi_{rc}), \tag{B.49}$$

with $\delta\phi_{rc} \equiv \phi_r - \phi_c$. From eq. (B.45) and (B.36), we get:

$$f_0 \equiv \frac{\partial f_t}{\partial \phi_r} = \frac{n}{\phi^2}\left[-3ln(1-\phi) - 3\frac{\phi}{1-\phi} + \frac{3}{2}(\frac{\phi}{1-\phi})^2 - \frac{40}{27n}\phi_0{}^{2/3}\phi^{1/3}\right]. \tag{B.50}$$

$$t_0 \equiv \frac{\partial t_t}{\partial \phi_r} = -\frac{2t_c{}^2}{n\phi_c} f_0. \tag{B.51}$$

The numerical value in the case of $\phi_0 = 0.05$ and n = 40 is:

$$\begin{cases} t_0 = \ \ 3.30832, \\ f_0 = -6.94707. \end{cases} \tag{B.52}$$

Under the co-existence condition, eq. (B.40) becomes

$$F - F(r) = \frac{1}{2}F^{(2)}(\delta\phi_r)^2 + \frac{1}{4!}F^{(4)}(\delta\phi_r)^4. \tag{B.53}$$

This is nothing other than Landau-type free energy. Following the conventional definition, we define

$$a = F^{(2)}(r), \tag{B.54}$$

$$u = \frac{1}{4!}F^{(4)}(r), \tag{B.55}$$

then,

$$F - F(r) = \frac{a}{2}(\delta\phi_r)^2 + u(\delta\phi_r)^4, \tag{B.56}$$

Minimize the free energy of (B.56) with respect to $\delta\phi$, we get the very familiar equation

$$\delta\phi_{r\pm}\left(a + 4u(\delta\phi_r)^2\right) = 0. \tag{B.57}$$

The solutions of (B.57) are

$$\delta\phi_{r\pm} = \pm\left(-\frac{a}{4u}\right)^{1/2}, \tag{B.58}$$

$$\delta\phi_r = 0. \tag{B.59}$$

Expand $F^{(2)}(r)$ around the critical point, by using eq. (B.58) , we have

$$F^{(2)}(t_t, \phi_r, f_t) = \frac{n}{2\phi_c t_c}\delta t \equiv a_0\delta t \tag{B.60}$$

or

$$a = a_0\delta t. \tag{B.61}$$

Where $a_0 = n/2\phi_c t_c$ is a constant. The parameter $u = F^{(4)}(r)$ can be replaced by $F^{(4)}(c)$ directly. In general, a_0 and u are constants, and the stability requires that $F^{(4)}(r)$ been a positive number. When $t > t_c, a > 0$. There is one solution to (B.57), i.e, $\delta\phi = 0$. On the other hand, when $T < 0, a < 0$, there are two non-zero solutions to (B.57). These two solutions are the two co-existence states. In the case of $\phi_0 = 0.05$ and n = 40,

$$\begin{cases} a_0 = 209.13297, \\ u = 206.35814. \end{cases} \tag{B.62}$$

From (B.56), we realize that $\delta\phi_r$ serves as the order parameter of the system. But in practice, what we can measure is ϕ and ϕ_c, not ϕ_r. The conventional definition of the order parameter is

$$\delta\phi \equiv \phi - \phi_c. \tag{B.63}$$

Using (B.49) and (B.51), we find

$$\delta\phi_{\pm} = \delta\phi_{r\pm} + \delta\phi_{rc} = \pm\left(\frac{a_0}{4u}\right)^{1/2}(-\delta t)^{1/2} - \frac{1}{t_0}(-\delta t). \tag{B.64}$$

Eq. (B.64) can be re-written as

$$\delta\phi_{+} = B(-\delta t)^{\beta}\left[1 - B_1(-\delta t)^{\Delta}\right], \tag{B.65}$$

$$\delta\phi_{-} = -B(-\delta t)^{\beta}\left[1 + B_1(-\delta t)^{\Delta}\right]. \tag{B.66}$$

where

$$B = \left(\frac{a_0}{4u}\right)^{1/2}, \tag{B.67}$$

$$B_1 = \frac{1}{t_0 B} \tag{B.68}$$

with the critical exponent β and the correction-to-scaling exponent Δ been

$$\beta = \frac{1}{2}, \tag{B.69}$$

$$\Delta = \frac{1}{2}. \tag{B.70}$$

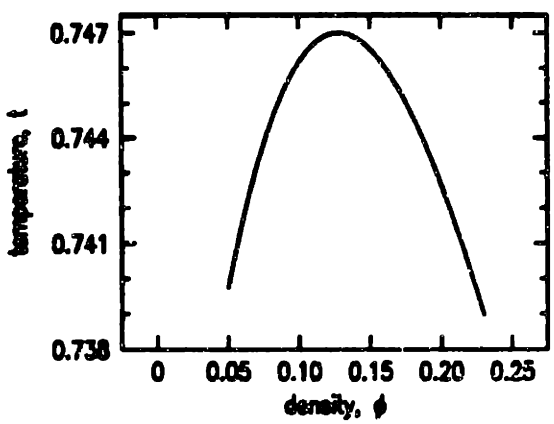

Figure B.2: Co-existence curve of Flory-Huggins network mean field theory.

The co-existence curve can be solved from (B.65) and (B.66)

$$-\delta t = B^{-2}\delta\phi^2\left(1 + \frac{B_1}{B}\delta\phi\right)^2. \tag{B.71}$$

The result of eq (B.71) is plotted in figure B.2. Finally, using (B.71), let us re-write (B.53) in a scaling form

$$F = \delta t^2 g\left(\frac{\delta\phi}{\delta t^{1/2}}\right). \tag{B.72}$$

Where g is some nice analytic function with g(0) finite and $g(0)\delta t^2$ coming from F(r). Here, We have dropped the trivial constant term and linear in δt term of F(r). The linear term contribute a trivial constant to the entropy only. Now we assume (B.72) is the scaling form of the free energy around the vicinity of the critical point for $t < t_c$. Compare (4.34) with the well known scaling form of free energy

$$F_{singular} = \delta t^{2-\alpha} g\left(\frac{\delta\phi}{\delta t^{\beta}}\right) \tag{B.73}$$

we find immediately that for the Flory-Huggings theory,

$$\begin{cases} \alpha &= 0 \\ \beta &= \frac{1}{2}. \end{cases} \tag{B.74}$$

B.4 Calculation of χ_{tf} and C_{tv} for $t > t_c$

Since χ_{tf}, K_{tp} and C_{pf} all have the same critical behavior, we need to calculate only one of them. Now let's evaluate the inverse of χ_{tf},

$$\begin{aligned} {\chi_{tf}}^{-1} &= -V\left(\frac{\partial P}{\partial V}\right)_{tf} \\ &= -V\left(\frac{\partial\phi}{\partial V}\right)^2\left(\frac{\partial^2 F}{\partial\phi^2}\right)_{tf} \\ &= \frac{\phi^3}{\phi_0 V_0} F^{(2)}(\phi, t, f). \end{aligned} \tag{B.75}$$

Assume we approach the critical point from some path $\phi = \phi(t)$ and $f = f(t)$. Expand $F^{(2)}$ near the critical point, (B.76) becomes

$${\chi_{tf}}^{-1} = \frac{{\phi_c}^3}{\phi_0 V_0}\left\{F^{(2)}(c) + \left[\frac{\partial F^{(2)}}{\partial\phi}\frac{d\phi}{dt} + \frac{\partial F^{(2)}}{\partial f}\frac{df}{dt} + \frac{\partial F^{(2)}}{\partial t}\right]\delta t\right\}. \tag{B.76}$$

All the derivatives are evaluated at the critical point. The first and the last terms are zero. The second term should be treated with care. Although $\partial F^{(2)}/\partial\phi = F^{(3)}$ goes to zero at the critical point, $\partial\phi/\partial t$ may go to infinity. From (B.42)

$$\frac{\partial F^{(2)}(c)}{\partial f} = -\frac{t_c}{{\phi_c}^2}. \tag{B.77}$$

Re-write (B.76) by using (B.77)

$$\chi_{tf}{}^{-1} = \frac{{\phi_c}^3}{\phi_0 V_0}\left[F^{(3)}\frac{d\phi}{dt} - \frac{t_c}{{\phi_c}^2}\frac{df}{dt}\right]\delta t. \tag{B.78}$$

Along the isocore, $\phi = \phi_c$, the first term does not exist. using (B.30), we get

$$\chi_{tf}^{-1} = \frac{n{\phi_c}^2}{2\phi_0 V_0 t_c}(t - t_c), \tag{B.79}$$

$$\chi_{tf} = \frac{2\phi_0 V_0 {t_c}^2}{\phi_c}(t - t_c)^{-1}. \tag{B.80}$$

So, just as expected, we get

$$\gamma = 1. \tag{B.81}$$

Expand eq (B.31) around the critical point From eq (B.31), the heat capacity at the critical point is

$$C_{pv} = C_0. \tag{B.82}$$

Where C_0 is

$$C_0 = \frac{n\phi_c}{2t_c} ln(\phi_c). \tag{B.83}$$

B.5 Calculation of χ_{tf} and C_{pv} for $t < t_c$

The critical exponents are defined along the co-existence curve. Along this curve, ϕ and f are functions of t. From (B.71) and (B.50), (B.51), we have

$$\delta\phi = B\delta t^{1/2}, \tag{B.84}$$

$$\delta f = -\frac{n\phi_c}{2{t_c}^2}\delta t. \tag{B.85}$$

From (B.76), we notice that the first term has to be carefully treated.

$$F^{(3)} = F(3)(c) + \left[F^{(4)}(c)\frac{d\phi}{dt} + \frac{\partial F^{(3)}(c)}{\partial f}\frac{df}{dt}\right]\delta t. \tag{B.86}$$

The first term in the bracket diverges and the second term is finite, so we can neglect the second term.

$$F^{(3)} = 4!u\frac{d\phi}{dt}\delta t. \tag{B.87}$$

Using (B.45), (B.50), (B.51) and (B.71), we have

$$\chi_{tf}^{-1} = -2\frac{n{\phi_c}^2}{2\phi_0 V_0 t_c}(t - t_c), \tag{B.88}$$

$$\chi_{tf} = \frac{\phi_0 V_0 t_c}{n{\phi_c}^2}(t_c - t)^{-1}. \tag{B.89}$$

Notice that the amplitude of the compressibility for $T < t_c$ is only half of the value for $T > t_c$. This is a very well known result. This can be explained by the amplitude of the fluctuation of the system. Expand eq (B.31) around the critical point using the free energy in eq (B.53)

$$C_{pv} = C_0 + 2uB^4. \tag{B.90}$$

Compare (B.90) and (B.82), we find that there is a jump in the heat capacity. This is again standard mean field theory result.

Appendix C

Highly Stretched Polymer Chains

A long flexiable chain is defined as a mathematical string. In this model, we do not consider the excluded volume effect. This configuration of the chain can be simulated by random walk with the number of steps n equal the total number of the monomer (persistent) units in the chain and the size of each step a equal the length of the monomer unit. For a long chain, when the end-to-end distance r is small compared with the totsl chain length na, the distribution of the end-to-end distance of the chain is (Flory 1953)

$$W(r) = Const \cdot exp\,[-G_G(n,r)]\,4\pi r^2 dr. \tag{C.1}$$

Where n is the total number of the steps, $G_G(n,r)$ is

$$G_G(n,r) = \frac{3r^2}{2na^2} \equiv 3\alpha^2. \tag{C.2}$$

Notice that $-kTG_G$ is part of the fiee energy of the system. Take derivative of this term with respect to r, we get

$$\tau \equiv \frac{\partial(kTG_G)}{\partial r} = \frac{3kT}{na^2} r \sim \alpha. \tag{C.3}$$

Here τ is defined as the retractive force . It is well known (James and Guth ?) that for any $r < na$, the exact solution to this problem is

$$W(r) = Const \cdot exp\,[-G_L(n,r)]\,4\pi r^2 dr, \tag{C.4}$$

and

$$G_L(n,r) = \frac{1}{a}\int_0^r L^*(\lambda)dr \qquad (C.5)$$
$$= n\int_0^\lambda L^*(\lambda)d\lambda.$$

Where $\lambda \equiv r/na$ is the scaled chain length, the function $L^*(\lambda)$ is defined as the inverse of the Langevin function $L(u)$

$$L(u) = coth(u) - \frac{1}{u} \equiv \lambda, \qquad (C.6)$$

and

$$u = L^*(\lambda) = 3\lambda + \frac{9}{5}\lambda^3 + \frac{297}{175}\lambda^5 + \cdots. \qquad (C.7)$$

The relation between u and τ is

$$u = \frac{a}{kT}\tau. \qquad (C.8)$$

So we can write

$$G_L(n,r) = \frac{3}{2}\frac{r^2}{na^2} + n\left[\frac{9}{20}\lambda^4 + \frac{297}{1050}\lambda^6 + \cdots\right]. \qquad (C.9)$$
$$= G_G(n,r) + higher\ order\ terms.$$

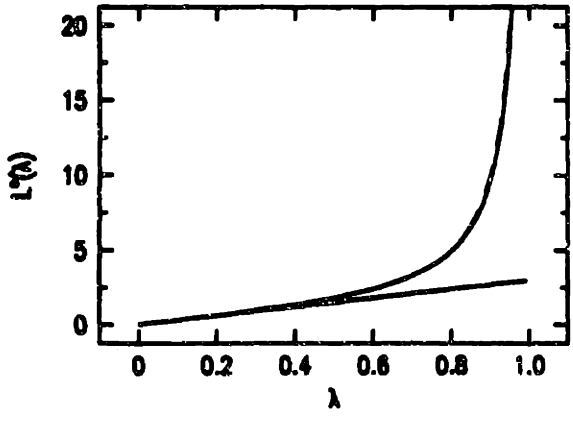

Figure C.1: Comparision between the retraction force of Gaussian distribution and the Langevin distribution. The striaght line is from Gaussian distribution. The solid curve is from Langevin distributio. The dotted curve is the justified Padé approximation.

From this equation we see immediately that the Gaussian distribution function (C.1) is just the small r limit approximaiton of the Langevin distribution. This is clearly shown in Fig. C.1.

When r is comparable with the total length of the chain, $L^*(\lambda)$ diverge, the Taylor expansion no longer valid. A justified Padé approximation was found to be very satisfactory(see Fig.C.1)

$$u = \frac{3\lambda - \frac{6}{5}\lambda^3}{1-\lambda^2}. \tag{C.10}$$

This equation can also be written as the Gaussian term and the correction to Gaussian term

$$u = 3\lambda + \frac{9}{5}\frac{\lambda^3}{1-\lambda^2}. \tag{C.11}$$

The retractive force is

$$\begin{aligned} \tau \equiv \frac{\partial(kTG_L)}{\partial r} &= \frac{kT}{a}L^*(\lambda) \\ &= \frac{kT}{a}\frac{3\lambda - \frac{6}{5}\lambda^3}{1-\lambda^2} \end{aligned} \tag{C.12}$$

So when we increase τ, λ increases linearly first but then becomes nonlinear and will eventually saturate around $\lambda \leq 1$. The impact of this is shown in Fig.B.2, which is a plot of $\pi - V$ curves with end-to-end distance obey Gaussian and Langevian distribution, respectively.

Now let us do some numerical estimation. The energy neened to stretch the chain from $r = 0$ to $r = na(1-\epsilon)$ is

$$\begin{aligned} E_S(\epsilon) &\equiv \int_0^{na(1-\epsilon)} \tau(r)dr \\ &= nkT\int_0^{(1-\epsilon)} \frac{3\lambda - \frac{6}{5}\lambda^3}{1-\lambda^2}d\lambda \\ &= \frac{3}{5}nkT\left[-\frac{9}{2}ln(2\epsilon) + 3\right]. \end{aligned} \tag{C.13}$$

If we try $\epsilon = 0.1$, we get

$$E_S \sim 6nkT, \tag{C.14}$$

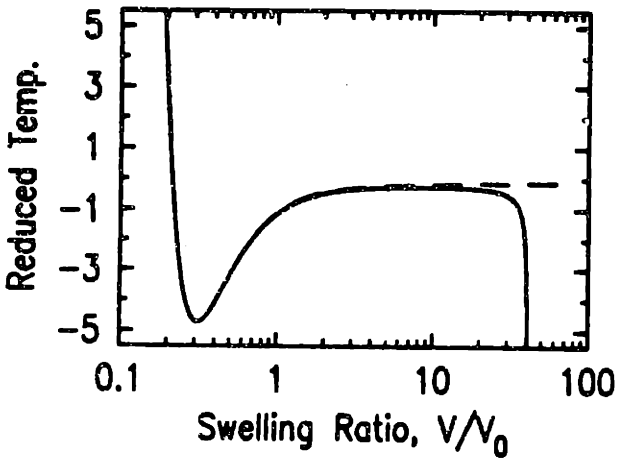

Figure C.2: Flory-Huggins $\pi - V$ curve (dotted) and Langevian modified curve (solid).

or, the stretch energy per bond

$$\frac{E_S}{2n} \sim 3kT, \tag{C.15}$$

We know from the text book (for instance, Kemp-Vellaccio 1980) that the strength E_B of a carbon-carbon bond is around $82kcal/mol$, which is roughly around $150kT$ at room temperature. So the strength of the polymer chain in general, is much stronger than the force needed to stretch a polymer to its full length. In practice, we can assume that a polymer chain in infinitely strong.

In the case of gel under elogational deformation, τ is defined as the force per initial cross section area. For a Gaussian chain

$$\tau = \frac{\nu kT}{V}\left(\alpha - \frac{1}{\alpha^2}\right). \tag{C.16}$$

The second term comes from the geommetrical consideration. For a Langevin chain

$$\tau = \frac{\nu kT}{V}\left(\frac{\sqrt{n}}{3}L^*(\lambda) - \frac{1}{\alpha^2}\right). \tag{C.17}$$

From this equation, we find that the limit exist for gel as well. In another words, the swelling ratio of a network system has an upper limit.

Appendix D

Kinetics of Gels

In this appendix, we will calculate the kinetics of the swelling and shrinking process of free gels of a long cylinder and a large disc. We will choose the final equilibrium state of the sample to be the reference state.

The free energy related with a strained media is

$$F(\mathbf{r}) = \frac{1}{2}K\left(\nabla\cdot\mathbf{u}\right)^2 + \frac{1}{2}\mu\left(u_{ik} - \frac{1}{3}\nabla\cdot\mathbf{u}\ \delta_{ik}\right)^2. \tag{D.1}$$

Where K and μ is the bulk and shear modulus, respectively. The strain tensor u_{ik} is defined as

$$u_{ik} \equiv \frac{1}{2}\left(\frac{\partial u_k}{\partial x_i} + \frac{\partial u_i}{\partial x_k}\right), \tag{D.2}$$

with $\mathbf{u}$ the displacement vector, represents the displacement of a point in the network from its reference position.

The stress tensor σ_{ik} is defined as

$$\begin{aligned}\sigma_{ik} &\equiv \frac{\partial F}{\partial u_{ik}}, \\ &= K\nabla\cdot\mathbf{u}\ \delta_{ik} + 2\mu\left(u_{ik} - \frac{1}{3}\nabla\cdot\mathbf{u}\ \delta_{ik}\right),\end{aligned} \tag{D.3}$$

The equation of motion of the gel network is

$$f\frac{\partial\mathbf{u}}{\partial t} = \nabla\cdot\tilde{\sigma}. \tag{D.4}$$

The f is the friction coefficient between the network and the solvent. We have neglected the acceleration term $\rho\partial^2\mathbf{u}/\partial t^2$, which is much smaller than other terms.

By using eq (D.2)-(D.4), and the relation

$$\nabla \times (\nabla \times \mathbf{u}) = \nabla(\nabla \cdot \mathbf{u}) - \nabla^2\mathbf{u}, \tag{D.5}$$

eq (D.4) can be written as

$$\frac{\partial \mathbf{u}}{\partial t} = \frac{K + \frac{1}{3}\mu}{f}\nabla(\nabla \cdot \mathbf{u}) + \frac{\mu}{f}\nabla^2\mathbf{u}. \tag{D.6}$$

$$= D\nabla(\nabla \cdot \mathbf{u}) - \frac{\mu}{f}\nabla \times (\nabla \times \mathbf{u}) \tag{D.7}$$

Where

$$D = \frac{K + 4\mu/3}{f}. \tag{D.8}$$

Now let us consider a very long cylindrical gel. In a cylindrical coordinate system, we expect the radial swelling ratio is independent of the z-coordinate as the length of the gel approaches infinity. In another word, the displacement vector $\mathbf{u}$ can be approximated as

$$\mathbf{u} = u_r(r,t)\hat{r} + u_z(z,t)\hat{z}. \tag{D.9}$$

With this approximation, the second term in eq (D.2) is zero,

$$\frac{\partial \mathbf{u}}{\partial t} = D\nabla(\nabla \cdot \mathbf{u}) \tag{D.10}$$

Using a similar argument, we can show that eq (D.9) and (D.10) hold for large disc gels as well.

D.1 Long Cylinder Gel

We will assume that the swelling ratio of the gel is isotropic. This assumption will be justified by the experimental result which will be discussed later. Below is a

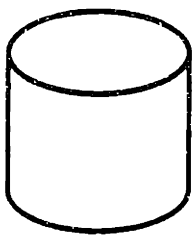

Figure D.1: A small segment of gel with the height and the diameter about the same. In a swelling process, the amount of solvent entered the gel through any portion of the surface is approximately proportional to the area of the portion.

We will assume that the swelling ratio of the gel is isotropic. This assumption will be justified by the experimental result which will be discussed later. Below is a hand waving argument, we believe it gives a very good accuracy even quantitatively. Without losing any generality, we will assume the process is a swelling process with the linear swelling ratio $(1+\epsilon)$.

Now we consider a small gel with height l and the diameter d (figure D.1). Assume $l \sim d$. The amount of the solvent molecules entered the gel through the side and ends are $A(1+\epsilon)^2 \sim (1+2\epsilon)$ and $A(1+\epsilon)$, respectively (A is the proportionality constant).

Now let's consider the gel in figure D.1 been a portion of a long cylindrical gel. During the swelling process, the ends effect of a long gel can be neglected. So inside the gel, there is no relative motion between the network and the solvent molecules in the z-direction. The solvent molecules can only enter (relative to the network) the gel through the cylinder side. So the total amount of solvent entered through the side is $A(1+\epsilon)^3 \sim (1+3\epsilon)$. Or the amount of solvent molecules entered the gel through the side in this case is 3/2 times larger than that of a small gel with open ends.

This means that in order to achieve the same degree of swelling ratio, the long cylinder gel network has to feel 3/2 times more frictional force than that of a small gel. In other words, the effective friction coefficient is $3f/2$.

For a long gel, the radial component u_r of the displacement vector is determined

by

$$\frac{1}{D_e}\frac{\partial u_r}{\partial t} = \left[\frac{\partial^2 u_r}{\partial r^2} + \frac{1}{r}\frac{\partial u_r}{\partial r} - \frac{u_r}{r^2}\right] = -q^2, \tag{D.12}$$

with the condition $u_r(0,t) = 0$ for all t. The effective diffusion constant is denoted by D_e, which is equal $2D/3$.

The solution of this equation is

$$u_r(r,t) = \sum_n B_n e^{-D_e q_n^2 t} J_1(\alpha_n r/a), \tag{D.13}$$

where α_n is the eigenvalue of the problem, $q_n = \alpha_n/a$, and a the final radius of the cylindrical gel.

The swelling ratio along z-axis is independent of z,

$$u_z(t,z) = A(t)z. \tag{D.14}$$

Following our isotropic swelling assumption, we get

$$A(t) = \frac{1}{a}u_r(a,t) = \frac{1}{a}\sum_n B_n e^{-D_e q_n^2 t} J_1(\alpha_n) \tag{D.15}$$

The boundary condition of this problem is

$$\sigma_{rr} = M\left[\frac{\partial u_r}{\partial r} + (1 - \frac{2\mu}{M})(\frac{u_r}{r} + A)\right] = 0, \tag{D.16}$$

or,

$$\alpha_n J_1'(\alpha_n) + 2\left(1 - \frac{2\mu}{M}\right) J_1(\alpha_n) = 0. \tag{D.17}$$

or,

$$\alpha_n J_0(\alpha_n) + \frac{1+\sigma}{1-\sigma} J_1(\alpha_n) = 0. \tag{D.18}$$

where $M = K + 4\mu/3$ is the longitudinal modulus. When then gel is fixed at the two ends, $A(t)$ will be zero. Then we recover Peters and Candau's (1988) result.

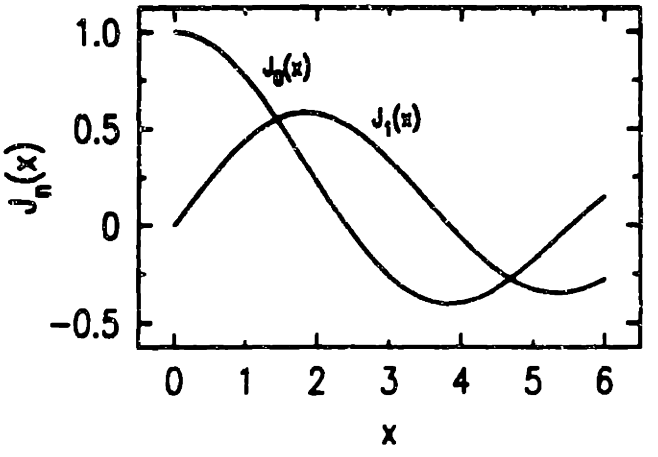

Figure D.2: Bessel function $J_0(x)$ and $J_1(x)$.

D.1.1 Special Cases

$2\mu/M = 1$ **case**

In chapter 8, we obtained the Poisson's ratio $\sigma = 0.40$, this corresponds exactly to $2\mu/M = 1$. In this case, eq (D.18) becomes

$$J_1'(\alpha_n) = 0. \tag{D.19}$$

From figure D.2, we find $\alpha_1 \sim 1.6$ and $\alpha_2 \sim 5.3$. The relaxation time is

$$\begin{aligned} \tau_{long} &= \frac{a^2}{D_e \alpha_1^2} \\ &= 0.29 \frac{a^2}{\mu} f\,. \end{aligned} \tag{D.20}$$

$\mu = 0$ **case**

In this case, eq (D.18) becomes

$$\alpha_n J_0(\alpha_n) + 3J_1(\alpha_n) = 0. \tag{D.21}$$

In the above we have used the identity $xJ_1' = J_1 + xJ_0$.

From figure D.3, we find $\alpha_1 \sim 2.9$ and $\alpha_2 \sim 5.8$.

The first solution $\alpha_1 \sim 2.9$ is close to the number Tanaka and Fillmore got for a spherical gel, which is $\alpha_1 = \pi$. It is the pre-factor 3/2 in front of the friction coefficient that makes the relaxation time longer.

$$\begin{aligned} \tau_{long} &= \frac{a^2}{D_e \alpha_n^2} \\ &= 0.18 \frac{a^2}{K} f \,. \end{aligned} \tag{D.22}$$

D.2 Large Disc

Following the same argument, we will find that in this case, the effective friction coefficient is three times larger than that of a small gel. So the relaxation time is expected to be three times longer.

D.2.1 Experimental Result

Figure D.3 is our experimental result on the swelling ratio of long and short gels. The relaxation time of the diameter and the length of the long gel are the same within our experimental error. This justifies our basic assumption that the swelling is isotropic. The ratio of the relaxation times of the short gel and the long gel is 0.7, which agrees very well with our theory.

D.3 Summary

We have calculated the kinetics of the gel relaxation process. We believe that the results given by Peters and Candau are not realistic. Our experimental result verifies our theory.

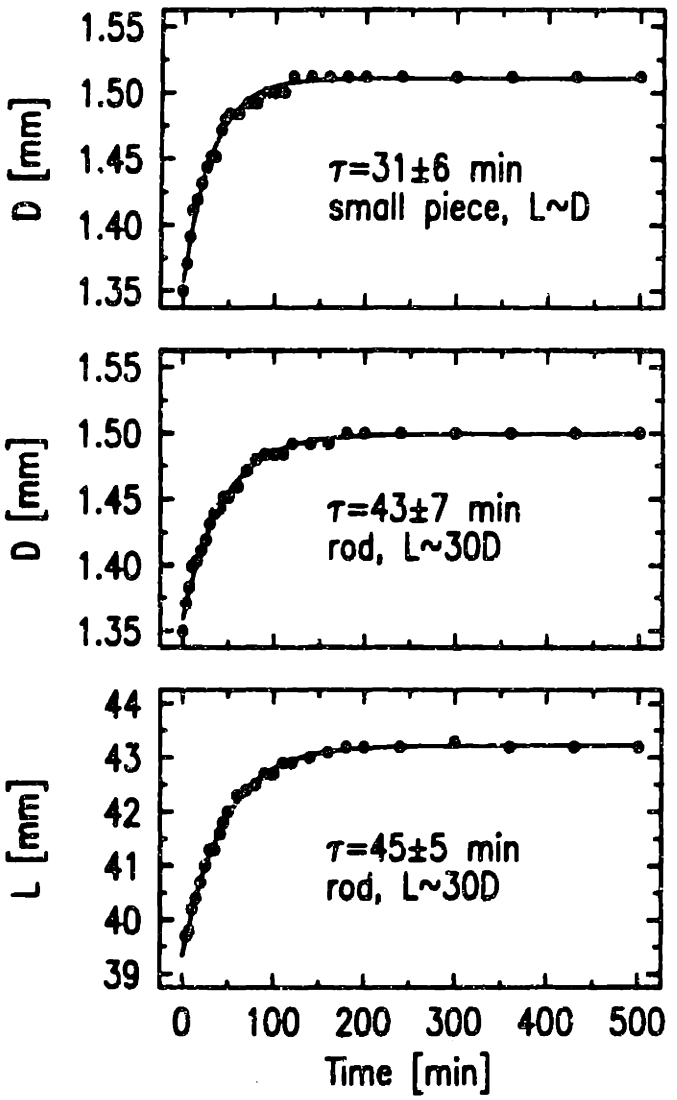

Figure D.3: Relaxation of short ($l \sim d$) and long ($l \sim 30d$) gels. The samples were made in a micropipette with inner diameter equal 1.35mm. The swelling process was monitored by a microscope. The samples were acrylamide gels.

Bibliography

[1] Aharony, A. and Hohenberg, P. C., (1976) Phys. Rev. B **13** 3081. [3]

[2] Aharony, A. and Ahlers, G., (1980) Phys. Rev. Lett. **44** 782. [3]

[3] Aharony, A. and Fisher, M., (1983) Phys. Rev. B **27** 4394. [3]

[4] Amiya, T and Tanaka, T. (1987) Macromolecules **20**, 1162. [1]

[5] Amiya, T., et al, (1987) J. Chem. Phys. 86, 2375.

[6] Anderson, P. W., (1981) "Some General Thoughts about Broken Symmetry" in *Symmetries and Broken Symmetries*, N. Bocarro, ed. (Idset, Paris). [1]

[7] Bagnuls, C. and Bervillier, C., (1985a) Phys. Rev. B **32** 7209. [3]

[8] Bagnuls, C. and Bervillier, C., (1985b) Phys. Lett. **107A** 299. [3]

[9] Bagnuls, C., Bervillier, C., Meiron, D. I. and Nickel, B. G., (1987) Phys. Rev. B **35** 3585. [3]

[10] Bhatia, Q. S., Chen, J., Koberstein, J. T., Sohn, J. E. and Emerson, J. A., (1985) J. Colloid and Interface Science **106**(2), 353. [10]

[11] Bansil, R. and Gupta, M. K., (1980) Ferroelectics bf 30, 64. [6]

[12] Barmatz, M., Hohenberg, P. C. and Kornlit, A., (1975) Phys. Rev. B **12** 1947. [3]

[13] Benedek, G. B. (1966) *Critical Phenomena*, N.B.S. MICS. Pub. 273. [1]

[14] Berne, B. J. and Pecora, R. *Dynamic Light Scattering*, A Wiley-Interscience Publication, JhonWiley & sons, 1976.

[15] Bervillier, C., (1986) Phys. Rev. B **34**, 8141 and the references cited therein.[3]

[16] Beysens, D. and Bourgou, A., (1979) Phys. Rev. A **19**, 2407.[3]

[17] Bourgou, A. and Beysens, D., (1981) Phys. Rev. Lett. **47**, 257.[3]

[18] Brenner, S. L., Gelman, R. A. and Nossal, R., (1978) Macromolecules **11**(1), 202. [7] [8].

[19] Brilliuon, L., (1914) C. R. Acad. Sci. **158**, 1331.[1]

[20] Brilliuon, L., (1922) Ann. Phys. (Paris) **17**, 88.[1]

[21] Brout, R., (1965) *Phase Transition*, W. A. Benjamin, Inc., New York.

[22] Cahn, J. W. and Hillard, J. E., (1958) J. Chem. Phys. **28**(2), 258. [10]

[23] Chang, M-C. and Houghton, A. (1980a) Phys. Rev. B **21**, 1881. [3]

[24] Chang, M-C. and Houghton, A. (1980b) Phys. Rev. Lett. **44**, 785. [3]

[25] Chase, S. I. and Kaufman, M., (1986) Phys. Rev. B **33**, 239 and the references cited therein.[3]

[26] de Gennes, P. G., (1976) J. Phys. (Paris) Lett. **37L**, 1. [8]

[27] de Gennes, P. G., (1978), J. Phys. (*Paris*) Lett. **39L**, 299. [3]

[28] de Gennes, P. G., (1979), *Scaling Concepts in Polymer Physics*, Cornell Univ. Press.

[29] Dušek, K. and Patterson, D., (1968) J. Polym. Sci. **6** 1209.[1]

[30] Edwords, S. F. (1965) Proc. Phys. Soc. **85** 613. [1]

[31] Edwords, S. F. (1966a) *Critical Phenomena*, N.B.S. MICS. Pub. 273. [1]

[32] Edwords, S. F. (1966b) Proc. Phys. Soc. **88** 265. [1]

[33] Fisher, M. E., (1967) Rept. Progr. Phys. **30**, 731.

[34] Fisher, M. E., Phys. Rev. **176**, 257 (1968). [3]

[35] Fisher, M. E. and Scesney, P. E., (1970) Phys. Rev. A **2**, 825.[3]

[36] Fisher, M. E., (1983) "Scaling, Universality, and Renormalization Group Theory," in *Critical Phenomena* (Springer-Verlag, New York), J. W. Hahne, ed.

[37] Flory, P. J., (1942) J. Chem. Phys. **10**, 51. [1]

[38] Flory, P. J., (1983) *Principles of Polymer Chemistry*, Cornell University Press, 1953. [1]

[39] Funke, W., (1983) *Plastic and Rubber Processing and Applications* **3**, 243. [6]

[40] Ginzburg, V. L., 1960. Soviet Phys. Solid State **2**, 1824. [1,A]

[41] Gross, E., (1930) Nature **126**, 201. [1]

[42] Gross, E., (1932) Nature **129**, 722.

[43] Heller, P and Beneked, G. B. (1962) Phys. Rev. Lett. **8**, 428. [1]

[44] Heller, P. (1967) Rept. Prog. Phys., 731. [1]

[45] Hirotsu, S., (1987) J. Phys. Soc. Japan **56** 233.

[46] Hirotsu,S., Hirokawa, Y. and Tanaka, T., (1987) J. Chem. Phys. **87**, 1932. [1]

[47] Hochberg, A. and Tanaka, T., (1979) Phys. Rev. Lett. **43** 217. [1]

[48] Hsu, T. P., Ma, D. S. and Cohen, C., (1983) Polymer **24** 1273.

[49] Huang, K., (1965) *Statistics Mechanics*, John Wiley & Sons, Inc., New York.

[50] Huggins, J. Chem. Phys. **9**, 440(1941). [1]

[51] Huster, M. E., Stine, K. J. and Garland, C. W., (1987) Phys. Rev. A **36**, 2364. [3]

[52] Hwa, T. and Kardar M., (1988) Phys. Rev. Lett. **61** 106.

[53] Ilavsky, M. (1982) Macromolecules, **15**, 782.[1, 8]

[54] James, H. M. (1947) J. Chen. Phys. **15** 651. [1]

[55] James, H. M. and Guth, E., (1943) J. Chen. Phys. **11** 455. [1]

[56] James, H. M. and Guth, E., (1947) J. Chen. Phys. **15** 669. [1]

[57] James, H. M. and Guth, E., (1949) J. Pol. Sci. **4** 153. [1]

[58] Kadanoff, L. P., (1966) Physics **2**, 263. [2]

[59] Kadanoff, L. P. et al (1967) Rev. Modern Phys **39**, 395. [1]

[60] Kadanoff, L. P. and Martin, P. C., (1963) Ann. Phys., N.Y. **24**, 419. [4]

[61] Kemp, D. S. and Vellaccio, F., (1980) *Organic Chemistry*, Worth Publishers, Inc..

[62] Landau and Lifshitz, *Theory of Elasticity*, (1986) Pergamon Press.

[63] Landau, L. D. and Placzek, G., (1934) Phys. Z. Sowjetunion **5**, 197.

[64] Lipa, B. J. and Buc! ngham, M. J., (1968) Phys. Lett. **26A**, 643. [3]

[65] Lee, T. D. and Yang, C. N., (1952) Phys. Rev. **87**, 410.

[66] Le Guillou, J. C., and Zinn-Justin, J. (1977) Phys. Rev. Lett. **39**, 95. [3]

[67] Lindsey, C. P. and Patterson, G. D., (1980) J. Chem. Phys **73**, 3348.

[68] Ma, Shang-Keng, (1976), *Modern Theory of Critical Phenomena*, the Benjamin/Cummings Publishing Company, Inc. [1]

[69] Mark, J. E. and Erman, B., (1988) *Rubberlike Elasticity / A Molecular Primer*, John Wiley & Sons.

[70] J. E. Martin and J. P. Wilcoxon, (1989),Phys. Rev. A **39** 252. [6]

[71] Mooney, M., (1940) J. Appl. Phys., **11** 582. [8]

[72] Moore, M. A., (1977), J. Phys. (*Paris*) **A10**, 305. [3]

[73] Mountain, R. D. (1966) Rev. Mod. Phys. **38** 205. [4]

[74] Mountain, R. D. and Zwanzig, R. V. (1968) J. Chem. Phys. **48** 1451. [4]

[75] Nicoll, J. F. and Albright, P. C., (1986),Phys. Rev. B **34** 1991. [3]

[76] Nossal, R. and Brenner, S. L., (1978) Macromolecules **11**(1) 207. [7] [8]

[77] Nossal, R. and Jolly, M. (1982) J. Appl. Phys. **53** 5518. [7] [8]

[78] Onsager, L., (1944),Phys. Rev. **65** 117.

[79] Palmer, R. G., Stein, D. L., Abrahams, E. and Anderson, P. W., (1984) Phys. Rev. Lett **53**, 958.

[80] Poser, C. I. and Sanchez, I. C., (1979) J. Colloid and Interface Science **69**(3) 539. [10]

[81] Rabin, Y., (1984) J. Polymer Science: Polymer Letters Ed. **22**, 335. [10]

[82] Richards, E. G. and Temple, C. J., (1971) Natural Physical Science, **230** 92. [6]

[83] Richards, R. W. and Davison, N. S., (1986) Macromolecules **19** 1381. [8]

[84] Rivlin, R. S., (1947) J. Appl. Phys. **18** 444. [8]

[85] Rouch, C., Safonane, A., Tartaglia, P. and Chen, S. H., (1988) Phys. Rev. A **37**, 4995. [3]

[86] Sanchez, G., Meichle, M. and Garland, C. W., (1983) Phys. Rev. A **B28**, 1647.[3]

[87] Sanchez, I. C., (1983) J. Chem. Phys. **79**(1), 405.[10]

[88] Saul, D. M., Wortis, M. and Jasnow, D., (1975),Phys. Rev. B **11** 2571. [3]

[89] Smith, T. L., (1975), Polym. Prepr. **22** 169. [8]

[90] Standford, J. L. and Stepto, R. F. T., (1981) Polym. Prepr. **22**(2) 165. [6]

[91] Stanley, H. E., (1971) *Introduction to Phase Transitions and Critical Phenomena*, Oxford University Press.

[92] Staudinger, H., (1920). Berichte d. D. Chem. Gesellschaft, **53** 1073. [1]

[93] Sun, S-T., Li, Y., Sato-mustuo, E. and Tanaka, T. , (to be published in J. Chem. Phys.).

[94] Suzuki, Y. et al, (to be published).

[95] Tanaka, T., Hocker, L. O. and Benedek, G. B. (1973) J. Chem. Phys **59**, 5151. [5]

[96] Tanaka, T., Ishiwada, S. and Ishimoto, C., (1977) Phys. Rev. Lett. **38** 771. [1]

[97] Tanaka, T. (1978a) Phys. Rev. A **17** 763. [1]

[98] Tanaka, T. (1978b) Phys. Rev. Lett. **40** , 820.

[99] Tanaka, T. (1979a) Polymer **20** 1404. [1]

[100] Tanaka, T. and Fillmore, D. (1979b) J. Chem. Phys. **70**, 1214. [5]

[101] Tanaka, T. et al, (1980) Phys. Rev. Lett. **45** , 1636.

[102] Tanaka, T., Sun, S-T. and Nishio, I. (1981a) *Scattering Technique Applied to Supramolecular and Nonequillibrium Systems.* [1]

[103] Tanaka, T. et al, (1981b) Scientific American 244, 124.

[104] Tanaka, T., Nishio, I., Sun, S-T., and Ueno-Hisho, S., (1982) Science 218, 467.

[105] Tanaka, T, (1985) "Light Scattering from Polymer Gels", *Dynamic Light Scattering*, ed. Robert Pecora, 1985 Plenum Press, New York.

[106] Tokita, M., Niki, R. and Hikichi, K., (1985) J. Chem. Phys. **83**(5) 2583. [8]

[107] Tokita, M. and Hikichi, K., (1987) Phys. Rev. A **35** 4329. [8]

[108] Uhlenbeck, G. E., (1966) *Critical Phenomena*, N.B.S. [illegible] Pub. 273. [1]

[109] Weiss, N and Silberberg, A., (1975) Polym Prepr. Am. Chem. Soc., Div. Polym. Chem. **16**, 289. [6]

[110] Weiss, N and Silberberg, A., (1977) Br. Polym. J. **9**, 144. [8]

[111] Weiss, N., van Vliet, T. and Silberberg, A., (1979) J. Polym. Sci., Phys. edition **17**, 2229. [6]

[112] same as before, to be published (when saw 1977), (inhomo theory).

[113] Wilson, K. G. (1971) Phys. Rev. B **4**, 3174, 3184. [2]

[114] Wilson, K. G. (1983) Rev. Mod. Phys. **55**, 583. [2]

[115] Witten, T. A. and Pincus, P. (1987) Europhys. Lett. **3**(3), 315. [9]

[116] Wu, S. (1969) J. Colloid and Interface Science **31**(2), 153. [10]

[117] Call Number List

J. Chem. Phys. QC .J841

Phys. Rev. Lett. QC .P581

Phys. Rev. QC .P578-579

Rev. Mod. Phys. QC .R455

Sci. Am. T .S416

Science Q .S399

J. Phys (paris) and J. Phys. (Paris) Lett. QC .J831

J. Phys. Soc, Jpn QC .P582

Polymer QD .P782

Phys. Lett. QC .P586

J. Phys. A & B QC .8462